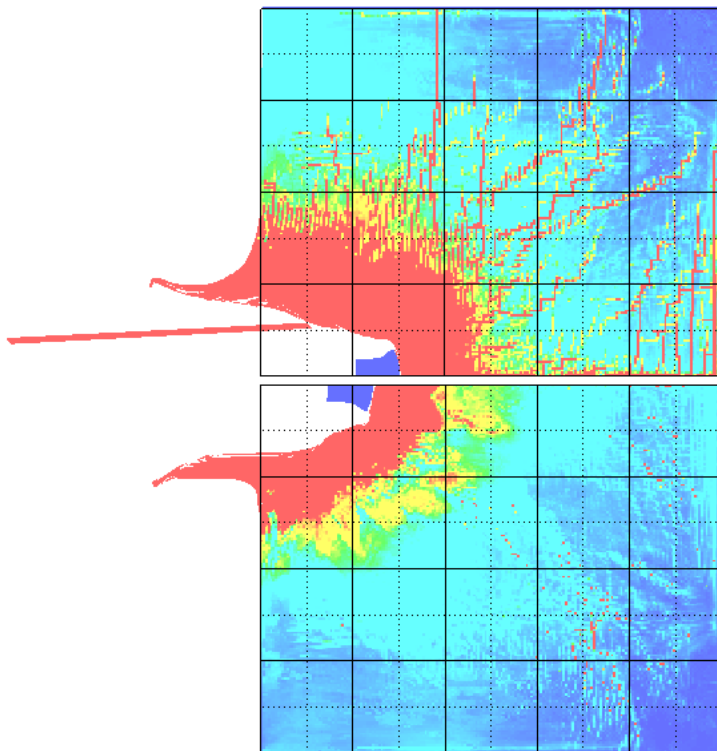


CHALMERS



Modelling of Concrete Structures Subjected to Blast and Fragment Loading

ULRIKA NYSTRÖM

*Department of Civil and Environmental Engineering
Division of Structural Engineering, Concrete Structures*
CHALMERS UNIVERSITY OF TECHNOLOGY
Göteborg, Sweden 2013

THESIS FOR THE DEGREE OF DOCTOR OF PHILOSOPHY

Modelling of Concrete Structures Subjected to Blast and Fragment Loading

ULRIKA NYSTRÖM

Department of Civil and Environmental Engineering
Division of Structural Engineering, Concrete Structures
CHALMERS UNIVERSITY OF TECHNOLOGY

Göteborg, Sweden 2013

Modelling of Concrete Structures Subjected to Blast and Fragment Loading

ULRIKA NYSTRÖM

ISBN 978-91-7385-805-2

© ULRIKA NYSTRÖM, 2013

Doktorsavhandlingar vid Chalmers tekniska högskola

Ny serie nr 3486

ISSN 0346-718X

Department of Civil and Environmental Engineering

Division of Structural Engineering, Concrete Structures

Chalmers University of Technology

SE-412 96 Göteborg

Sweden

Telephone: + 46 (0)31-772 1000

Cover:

Results from numerical simulations of plain (upper) and fibre-reinforced (lower) concrete cylinders subjected to projectile impact.

Chalmers Reproservice

Göteborg, Sweden 2013

Modelling of Concrete Structures Subjected to Blast and Fragment Loading

ULRIKA NYSTRÖM

Department of Civil and Environmental Engineering

Division of Structural Engineering, Concrete Structures

Chalmers University of Technology

ABSTRACT

Reinforced concrete is one of the most widely used building materials in modern civil infrastructure primarily thanks to its low cost and wide field of applications. Because of its ductile material response under high pressure levels and when properly reinforced, high structural energy-absorbing capacity, it is also suitable for use within protective design. However, the response of concrete structures exposed to blast and fragment loading, originating from accidental or intentional explosions, is fraught with high complexity. Even though extensive efforts have been undertaken worldwide within this area of research, the phenomena involved are not fully understood yet.

With the aim of further increasing the knowledge of the dynamic response of concrete structures subjected to blast and fragment loadings, literature reviews, theoretical reasoning and numerical simulations have been used in an iterative manner. In this thesis, the theoretical bases of concrete material response relevant in case of high dynamic loading, blast and fragment load characteristics and the dynamic effects of wave propagation are treated. In addition two numerical studies on the structural response are presented. The first numerical study was a comparative investigation of the relative effect on the impact resistance when adding steel fibres to concrete. It was concluded that the depth of penetration of the striking projectile was only slightly influenced by the addition of fibres, while the size of the front- and rear-face craters was decreased. The second numerical study involved combined blast and fragment loading of a reinforced concrete wall strip, and was conducted to investigate the synergistic effect and the cause thereof. It was observed that the total damage of the wall strip subjected to the combined loads was highly related to the damage caused by the fragment impact alone, and the synergetic effect of the two loads was confirmed. A third numerical study of the effect of reinforcement on the projectile impact resistance was conducted within the scope of the work presented. In this study, it was found that the presence of reinforcement improved the impact resistance of the concrete if a suitable reinforcement detailing was used.

Further, also presented is the new material model, denoted CDPM2, which has been developed. This model combines the theories of plasticity and damage mechanics to describe the dynamic failure of concrete. It has been shown that the model is able to describe the behaviour of concrete for a wide range of loading conditions, static as well as dynamic. Nevertheless, it was also found that the model should be modified to further improve its capability. Even though some principles for possible modification have been presented, implementation and further evaluation of such modification have not been part of the work presented in this thesis.

Key words: Concrete, fibre-reinforced concrete, numerical simulation, material modelling, dynamic loading, blast load, fragment impact

Modellering av stötvågs- och splitterbelastade betongkonstruktioner

ULRIKA NYSTRÖM

Institutionen för bygg- och miljöteknik

Avdelningen för konstruktionsteknik, Betongbyggnad

Chalmers tekniska högskola

SAMMANFATTNING

Betong är tack vare sin låga kostnad och sitt stora användningsområde ett av de mest använda byggmaterialen i modern tid. Dess stora energiabsorberande förmåga vid höga tryck, samt det sega beteende betongkonstruktioner har vid väl utformad armering, gör betongen också lämplig i skyddande konstruktioner. Responsen hos konstruktioner utsatta för extrem dynamisk belastning, så som stötvågs- och splitterbelastning, är dock förknippad med hög komplexitet och trots många år av forskning världen över är de fenomen som uppstår ännu inte helt klarlagda.

Med målsättningen att öka kunskapen om betongkonstruktioners respons vid stötvågs- och splitterbelastning har litteraturstudier, teoretiska analyser och numeriska simuleringar använts på ett iterativt sätt. Den teoretiska grunden för betongmaterialets beteende, karaktärisering av stötvågs- och splitterlast, lasternas verkan på betongkonstruktioner och dynamiska aspekter på vågpropagering behandlas i sammanlaggningsdelen i denna avhandling. Därtill presenteras två numeriska studier. Den första numeriska studien var en jämförande studie av vilken relativ inverkan som tillsättning av stålfibrer i betong har på dess motståndsförmåga mot projektilinträning. Det kunde konstateras att inträngningsdjupet var relativt opåverkat av fibertillsättningen medan kraterstorleken, på både fram och baksidan av den beskjutna kroppen, minskade. I den andra studien undersöktes responsen hos en armerad betongväggsstrimla vid kombinerad belastning av stötvåg och splitter. Det kunde konstateras att den totala skadan i väggelementet var starkt relaterat till skadan orsakad av enbart splitterbelastningen. Vidare framgick att väggstrimlans mittnedböjning var större för det kombinerade lastfallet än för den sammanlagda nedböjningen orsakad av stötvågs- respektive splitterbelastningarna separat. Detta tyder på en synergieffekt för de kombinerade lasterna. En tredje numerisk studie har utförts inom ramen för det presenterade arbetet. I denna studie har armeringens inverkan på betongens motståndsförmåga vid projektilbeskjutning undersökts. Slutsatsen drogs att armering kan ha viss betydelse för detta motstånd förutsatt att armeringen är lämpligt inlagd.

I avhandlingen presenteras även en ny materialmodell (CDPM2) för dynamiskt belastad betong. Modellen har visat god förmåga att beskriva responsen vid ett stort antal lastfall, statiska så väl som dynamiska. I utvärdering av modellen har det visats att genom vissa modifieringar skulle modellens förmåga att beskriva responsen vid stora dynamiska laster kunna förbättras. Vissa riktlinjer för möjliga modifieringar har presenterats, men implementeringen och den vidare utvärderingen av dessa är inte en del av det presenterade arbetet.

Nyckelord: Betong, fiberarmerad betong, numeriska studier, materialmodellering, dynamisk belastning, stötvåg, splitter

LIST OF PUBLICATIONS

This thesis is based on the work contained in the following papers, referred to by Roman numerals in the text.

- I. Nyström, U. and Gylltoft, K. (2011): Comparative Numerical Studies of projectile impacts on plain and steel-fibre reinforced concrete. *International Journal of Impact Engineering*, Vol. 38, pp. 95-105.
- II. Nyström, U. and Gylltoft, K. (2009): Numerical studies of the combined effects of blast and fragment loading. *International Journal of Impact Engineering*, Vol. 36, pp. 995-1005.
- III. Grassl, P., Dimitris, X., Nyström, U., Rempling, R., and Gylltoft, K. (2012): CDPM2: A damage-plastic approach to modelling of the failure of concrete. Submitted to *International Journal of Solids and Structures*, August, 2012.
- IV. Nyström, U. (2013): CDPM2: Evaluation of the concrete material model behaviour for high dynamic loading. Submitted to *International Journal of Solids and Structures*, January, 2013.

AUTHOR'S CONTRIBUTION TO JOINTLY PUBLISHED PAPERS

The contributions of the present author to the appended papers are described here:

- I. Responsible for the planning and performance of the numerical studies and planning and writing of the paper.
- II. Responsible for the planning and performance of the numerical studies and planning and writing of the paper.
- III. Defining the requirements for the presented model and contributed with comments on the paper.

OTHER PUBLICATIONS BY THE AUTHOR

Licentiate Thesis

Nyström, U. (2008): *Concrete structures subjected to blast and fragment impacts: Numerical simulations of reinforced and fibre-reinforced concrete*. Licentiate Thesis. Department of Civil and Environmental Engineering, Division of Structural Engineering, Concrete Structures, Chalmers University of Technology, Publication no. Lic 2008:4, Göteborg, Sweden.

Conference Papers

Nyström, U. and Leppänen, J. (2006): Numerical studies of projectile impacts on reinforced concrete. *Proceedings of the 2nd International Conference on Design and Analysis of Protective Structures 2006*, 13-15 November, 2006, Singapore, pp. 310-319.

Nyström, U. and Gylltoft, K. (2008): Comparative numerical studies of projectile impacts on plain and steel-fibre reinforced concrete. *Proceedings of the Nordic Concrete Research & Development Symposium*, 8-11 June, 2008, Båstad, Sweden, pp. 198-199.

Nyström, U. and Gylltoft, K. (2008): Simulations of blast and fragment impacts on reinforced concrete. *Proceedings of the 20th International Symposium on Military Aspects of Blast and Shock, MABS 20*, 1-5 September, 2008, Oslo, Norway.

Pascualena, F., Vantomme, J., Ndambi, JM., and Nyström, U. (2010): A comparative numerical simulation study on blast response of reinforced concrete slabs subjected to fire. *Proceedings of the Final Conference on Cost Action C26 - Urban Habitat Constructions under Catastrophic Events*, 16-18 September, 2010, Naples, Italy, CRC Press, Taylor & Francis Group, London, UK, pp. 277-282.

Grassl, P., Nyström, U., Rempling, R. and Gylltoft, K. (2011): A damage-plasticity model for the dynamic failure of concrete. *Proceedings of the 8th International Conference on Structural Dynamics, EURO-DYN 2011*, 4-6 June, 2011, Leuven, Belgium, pp. 3287-3294.

Other Publications:

Nyström, U., Ekengren, B., Gylltoft, K., Johansson, M. and Leppänen, J. (2008): Stötvågs- och splitterbelastade betongkonstruktioner. *Bygg & Teknik*, Vol. 7/08, pp. 46-49.

Nyström, U. and Gylltoft, K. (2012): Explosionsbelastad betong: Dynamiska aspekter av materialets respons i numeriska simuleringar. *Bygg & Teknik*, Vol. 7/12, pp. 42-47.

Preface

The work in this thesis was carried out between March 2006 and January 2013 in the Department of Civil and Environmental Engineering, Division of Structural Engineering, Concrete Structures at Chalmers University of Technology. The work was performed within the “Dynamic behaviour of concrete structures subjected to blast and fragments” research project and is a continuation of earlier work on concrete structures subjected to severe dynamic loading conducted at Chalmers by Morgan Johansson and Joosef Leppänen. The project is financially sponsored by the Swedish Civil Contingencies Agency.

I would like to thank my supervisor and examiner, Professor Kent Gylltoft, for his guidance, flexibility, and kind heart. Further, I would like to thank my assistant supervisors PhD Morgan Johansson, Reinertsen Sverige AB, Senior Lecturer Joosef Leppänen, and Assistant Professor Rasmus Rempling for sharing of their knowledge and energy. I would also like to express my appreciation to MScEng Björn Ekengren, the Swedish Civil Contingencies Agency and MScEng Rolf Dalenius, the Swedish Fortifications Agency, for their valuable contributions to the work, and for their support. My colleagues at Structural Engineering are thanked for their kindness and willingness to help; I want to especially mention Associate Professor Mario Plos, and PhD student Jonas Ekström.

I would also like to thank Professor John Vantomme, and the rest of the staff at the Civil and Material Engineering Department of the Polytechnical Faculty of the Royal Military Academy, Brussels, for their hospitality.

Further, Senior Lecturer Peter Grassl, University of Glasgow, and PhD Tobias Olsson, DYNAMore Nordic AB, are thanked for their contributions to the work of developing and implementing the new material model, respectively, and for their great patience to answer questions related to their work. Gunilla Ramell, your language editing work is highly appreciated.

I thank my family; my parents and sisters for always being there, Philip for his patience, Aurélie for her ease, Erik for his great understanding, and Astrid for her never ending smiles.

Finally, I would like to express my gratitude to all the others who have contributed to the work, and supported me during this time.

Dilbeek, January 2013

Ulrika Nyström

Contents

ABSTRACT	I
SAMMANFATTNING	II
LIST OF PUBLICATIONS	III
PREFACE	V
CONTENTS	VI
NOTATIONS	VIII
1 INTRODUCTION	1
1.1 Background	1
1.2 Aim and objectives	1
1.3 Scientific approach	2
1.4 Methodology	3
1.5 Limitations	5
1.6 Research significance	7
1.7 Outline of the thesis	8
2 CONCRETE MATERIAL BEHAVIOUR	9
2.1 Material testing	9
2.2 Uniaxial tension and compression	9
2.2.1 Static behaviour	9
2.2.2 Dynamic behaviour	12
2.3 Influence of confining pressure	14
2.3.1 Static behaviour	14
2.3.2 Dynamic behaviour	17
3 BLAST AND FRAGMENT LOADS AND THEIR EFFECT ON CONCRETE STRUCTURES	19
3.1 General	19
3.2 Load characteristics at target	20
3.2.1 Blast load	20
3.2.2 Fragment load	22
3.2.3 Combined loading	23
3.3 Load effect on reinforced concrete structures	24
3.3.1 General	24
3.3.2 Modes of failure	25
3.3.3 Effect of reinforcement	26
3.3.4 Effect of steel fibres in concrete on local response	28
3.3.5 Effects of combined loading	29

4	DYNAMIC ASPECTS OF WAVE PROPAGATION	32
4.1	General	32
4.2	Inertia and wave propagation effects	33
4.3	Shock waves	34
4.3.1	Introduction	34
4.3.2	Shock wave formation	34
4.3.3	Shock transition – a thermodynamic processes	38
4.3.4	Rankine-Hugoniot jump conditions	40
4.3.5	Release from shocked state	41
5	NUMERICAL MODELLING AT HIGH DYNAMIC LOADING	43
5.1	Introduction	43
5.2	Solution techniques	44
5.2.1	Numerical solution	44
5.2.2	Lagrange solver	45
5.2.3	Material modelling	46
5.2.4	Large strain and stress theory	49
5.3	Material models for concrete	49
5.3.1	Background	49
5.3.2	RHT model	51
6	THE CONCRETE DAMAGE PLASTICITY MODEL 2	59
6.1	Development process	59
6.2	Needs and requirements	61
6.3	Theoretical description	63
6.4	Implementation	64
6.5	Verification	69
6.6	Validation	70
6.7	Evaluation	71
7	CONCLUSIONS	74
7.1	General conclusions	74
7.2	Suggestions for future research	75
8	REFERENCES	77

APPENDIX A EQUATION OF STATES FOR SOLIDS

APPENDIX B CONVERSION TO TRUE STRAINS AND STRESSES

Notations

Roman upper case letters

A	Shape factor for failure surface in RHT model
A_h	Hardening ductility measure in CDPM2
A_s	Damage ductility measure in CDPM2
B	Shape factor for residual strength surface in RHT model
B_0, B_1	Factors for internal-energy dependence in Polynomial Equation of State
B_h	Hardening ductility measure in CDPM2
B_Q	Brittle to ductile transition parameter in RHT model
C_h	Hardening ductility measure in CDPM2
D	Damage parameter
D_1, D_2	Material parameters in expression for plastic failure strain in RHT model
\mathbf{D}_e	Elastic stiffness matrix
D_f	Dilation constant in CDPM2
D_h	Hardening ductility measure in CDPM2
E	Young's modulus
F_{cap}	Cap function in RHT model
F_{elastic}	Pre-peak elastic stress to peak stress ratio in RHT model
F_{rate}	Describing strain-rate dependence in RHT model
G	Shear modulus
$G_{\text{elasto-plastic}}$	Shear modulus in pre-peak hardening regime in RHT model
G_F	Fracture energy
H_p	Hardening modulus in CDPM2
HTL'	Intersection point of Y_{TXC} and hydrostatic axis in RHT model
I_1	First invariant of the stress tensor
J_2, J_3	Second and third invariants of the deviatoric stress tensor
K	Bulk modulus
K_0	Bulk modulus of pore free material in $P-\alpha$ Equation of State
K_1, K_2, K_3	Factors describing shape of curve in Polynomial Equation of State
L	Length of test specimen or structural element
M	Shape factor for residual strength surface in RHT model
N	Shape factor for failure surface in RHT model
Q_1	Shear to compressive meridian ratio in RHT model
Q_2	Tensile to compressive meridian ratio in RHT model
$Q_{2.0}$	Reference value of tensile to compressive meridian ratio in RHT model
$R_3(\theta)$	Rubin function in deviatoric section in RHT model
S_d	Saturation degree
T	Temperature
T_0	Temperature in initial material state
U_p	Speed of piston
U_s	Shock wave propagation speed

u_p	Particle velocity
Y_{elastic}	Elastic limit surface in RHT model
Y_{fail}	Failure surface in RHT model
Y_{fric}	Residual strength surface in RHT model
Y_{TXC}	Compressive meridian in RHT model

Roman lower case letters

c	Speed of sound (wave speed)
c_e	Bulk sound speed in virgin porous material, in $P-\alpha$ Equation of State
c_0	Bulk sound speed in solid material, in $P-\alpha$ Equation of State
c_p	Specific heat capacity at constant pressure
e	Specific internal energy, or in CDPM2 the eccentricity factor
e_0	Specific internal energy in initial material state
e_H	Reference specific internal energy for Hugoniot curve
e_{ref}	Specific internal energy for reference state
$efmin$	Minimum value of equivalent plastic failure strain in RHT model
f_{c0}	Reference value of compressive uniaxial strength
f_c	Concrete compressive strength
$f_{c,\text{elastic}}$	Pre-peak elastic stress for uniaxial compression in RHT model
f_p	Yield function
f_s	Concrete shear strength
f_t	Concrete tensile strength
$f_{t,\text{elastic}}$	Pre-peak elastic stress for uniaxial tension in RHT model
f_{tl}	Damage stress threshold in bilinear softening curve used in CDPM2
g_p	Plastic potential
\mathbf{m}	Gradient of plastic potential in CDPM2
m_D, m_V	Invariants of \mathbf{m} (volumetric and deviatoric) in CDPM2
p	Pressure
p_{cold}	Cold compression curve
p_{el}	Elastic limit in hydrostatic compression
p_H	Hugoniot curve
p_{ref}	Pressure for reference state
p_s	Pressure in non-porous material
q	Hardening parameter function
q_{h0}	Initial hardening parameter in CDPM2
\mathbf{s}	Deviatoric Stress tensor
s_1, s_2, s_3	Principal deviatoric stresses
t	Time
x_h	Hardening ductility measure in CDPM2
x_s	Damage ductility measure in CDPM2

v	Specific volume
v_s	Specific volume of non-porous material in $P-\alpha$ Equation of State
v_0	Specific volume of initial material state
w	Crack opening
w_f	Ultimate crack opening
w_{fl}	Crack opening threshold in bilinear softening curve used in CDPM2

Greek letters

α_c	Variable distinguishing tensile and compressive stresses in CDPM2
α_{por}	Scale parameter for porosity in $P-\alpha$ Equation of State
$\alpha_{por,init}$	Initial value of porosity factor in $P-\alpha$ Equation of State
$\alpha_{por,e}, \alpha_{por,p}$	Elastic and plastic parts of α_{por}
α_r	Rate factor in CDPM2
α_{rc}	Compressive measure of the rate factor in CDPM2
α_{RHT}	Compressive strain-rate exponent used in RHT model
α_{rt}	Tensile measure of the rate factor in CDPM2
α_{therm}	Thermal volume expansion coefficient
β_c	Factor providing smooth transition of softening in CDPM2
δ	Kronecker delta
δ_{RHT}	Tensile strain-rate exponent used in RHT model
ε	Strain
$\dot{\varepsilon}$	Strain rate
$\tilde{\varepsilon}$	Equivalent strain measure in CDPM2
ε_0	Measure of the elastic strain at peak uniaxial tensile strength in CDPM2
$\varepsilon_1, \varepsilon_2, \varepsilon_3$	Principal strains
$\tilde{\varepsilon}_c$	Compressive measure of the equivalent strain in CDPM2
$\varepsilon_{engineering}$	Engineering strain
ε_{eq}^{pl}	Equivalent plastic strain
$\varepsilon_{eq}^{pl,fail}$	Equivalent plastic failure strain
$\varepsilon_{eq}^{pl,hard}$	Equivalent plastic strain at peak strength
$\tilde{\varepsilon}_t$	Tensile measure of the equivalent strain in CDPM2
$\mathbf{\varepsilon}_p$	Plastic strain tensor
ε_{true}	True strain
ε_v	Volumetric strain
Γ	Grüneisen parameter
μ	Compaction
ν	Poisson's ratio
$\kappa_{dc}, \kappa_{dc1}, \kappa_{dc2}$	Compressive damage history variables in CDPM2
$\kappa_{dt}, \kappa_{dt1}, \kappa_{dt2}$	Tensile damage history variables in CDPM2

κ_p	Plastic hardening variable
λ	Plastic multiplier
ω	Damage parameter in CDPM2
ω_c, ω_t	Compressive and tensile measures of the damage parameter in CDPM2
ρ	Density, or in CDPM2 the norm of deviatoric stress
ρ_0	Density of initial material state
ρ_s	Density of non-porous material in $P-\alpha$ Equation of State
σ	Stress
$\boldsymbol{\sigma}$	Stress tensor
$\sigma_1, \sigma_2, \sigma_3$	Principal stresses
$\sigma_{\text{engineering}}$	Engineering stress
σ_{eq}	Equivalent stress
$\sigma_{\text{eq,residual}}$	Equivalent residual stress capacity in RHT model
σ_{HEL}	Stress at Hugoniot elastic limit
$\boldsymbol{\sigma}_p$	Principal stress tensor
$\boldsymbol{\sigma}_{pc}, \boldsymbol{\sigma}_{pt}$	Compressive and tensile parts of principal stress tensor defined in CDPM2
σ_r	Radial stress
σ_{true}	True stress
σ_v	Volumetric stress
θ	Lode angle

Abbreviations

ALE	Arbitrary Lagrange Euler
CDPM1	Concrete damage plasticity model version 1
CDPM2	Concrete damage plasticity model version 2
DIF	Dynamic increase factor
GP	General purpose
HEL	Hugoniot elastic limit
SPH	Smooth particle hydrodynamics
TXC	Triaxial compression

Other notations

$\overline{\langle \cdot \rangle}$	Effective value of quantity $\langle \cdot \rangle$
$\langle \cdot \rangle^{tr}$	Trial value of quantity $\langle \cdot \rangle$
${}^t \langle \cdot \rangle$	Quantity $\langle \cdot \rangle$ evaluated at time t
${}^{t+\Delta t} \langle \cdot \rangle$	Quantity $\langle \cdot \rangle$ evaluated at time $t + \Delta t$

1 Introduction

1.1 Background

Blast and fragment loads are characterised by their fast transient and high magnitude nature and may cause a response in the exposed concrete structure which may differ substantially from that of static loads. Besides the changed behaviour at the structural level, the dynamic effects also highly influence the response at the material level. The fast rate of loading and the influence of material inertia lead to a local build-up of high confining pressure levels. The behaviour of concrete is highly pressure and strain-rate sensitive in which the fast nature of the loads leads to increased strength and ductility. However, the high pressure levels cause large deformations and highly non-linear material behaviour. For high enough pressure levels and short load durations, wave propagation effects may cause the formation and further propagation of so-called shock waves in the material, which also affects the material response. Thus, the response of concrete exposed to blast and fragment loading is very complex, and despite decades of research within the area, the phenomena involved are not well understood yet.

Different approaches have been used in order to characterise and examine the response of concrete structures subjected to blast and/or fragment impacts. Traditionally, this type of research has been mainly experimental. However, in recent years the use of numerical simulation techniques has been more common and constitutes nowadays an important addition to physical testing. The use of numerical approaches has several advantages, of which the opportunities to reduce cost, especially in the case of parameter studies, and the possibility of observing the response in slower motion, are a two. However, validation of the numerical model is required, and the numerical approach can thus not entirely replace physical testing.

1.2 Aim and objectives

The work presented in this thesis has been carried out as part of a long-term research project conducted at the Chalmers University of Technology which is financially sponsored by the Swedish Civil Contingencies Agency (MSB). The aim of this project is to increase the knowledge of the dynamic response of reinforced concrete structures subjected to blast and fragment loading.

The objectives of the work presented in this thesis are to:

- Observe and understand different phenomena involved in the blast and fragment loading of reinforced concrete structures.
- Examine the effect of different designs on the target response, relevant to protective purposes, e.g effects of reinforcement detailing and the adding of steel fibres into the concrete.

As further described in Sections 1.3 and 1.4, numerical simulations were used to examine the behaviour of concrete under blast and fragment loading. Therefore, an accompanying objective of the work was to:

- Evaluate, and if needed improve, the numerical model to be applicable in general cases of blast and fragment loading of reinforced concrete.

The “numerical model” in this case refers to different assumptions, techniques and descriptions used in the numerical simulations, e.g. the material models, contact algorithms, element types, etc.

1.3 Scientific approach

The scientific approach chosen was to combine literature reviews, theoretical investigations and numerical studies in an iterative manner, where the numerical simulations provide an approximated description of the real behaviour. This is schematically shown in Figure 1.1, in which the “Physical problem description” refers to the theories important to define the behaviour of concrete exposed to blast and fragment loading, including the theory describing dynamic effects such as inertia and wave propagation. “Theories in solution method” in this case refers to the theory applied when the numerical solution method is used, i.e. in the idealisation and discretisation of the physical problem and in the numerical integration. “Application of theories” refers to the applied numerical simulations performed in order to observe, examine and understand the phenomena involved in blast and fragment loading of concrete structures.

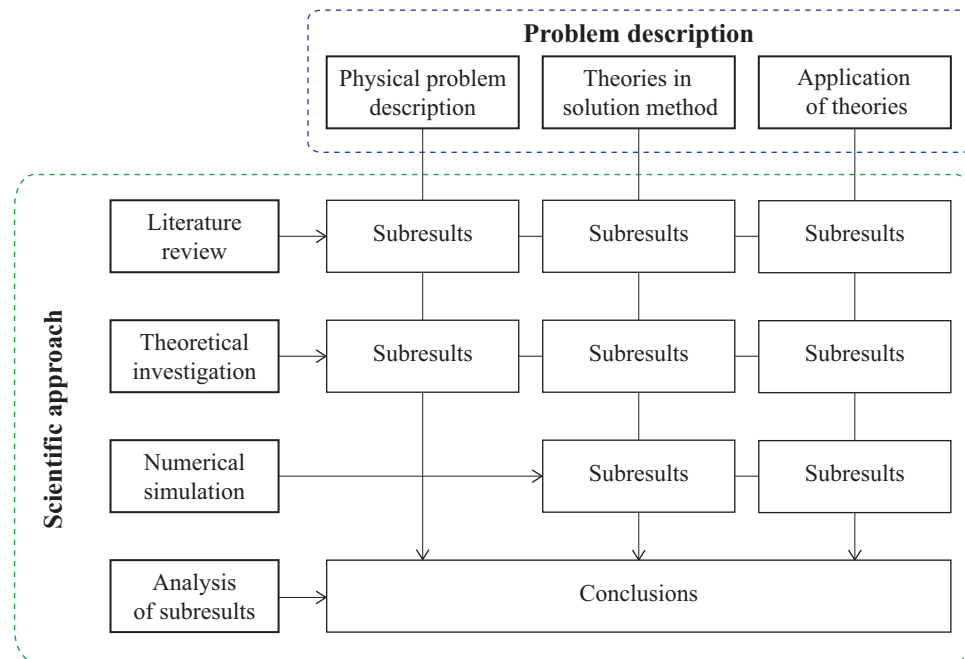


Figure 1.1 Schematic illustration of the scientific approach.

Literature reviews of the current knowledge within fields of interest are important to place the scientific question into relevant frames of references. The use of numerical simulations to solve problems involving fast transient nonlinear phenomena is motivated by the relatively low cost compared to experimental investigations. Further, a numerical simulation is a useful tool since it allows for comprehensive parameter

studies, idealised cases with reduced complexity and slow motion observations of the fast-paced phenomena involved. The discipline of numerical modelling is extensive and includes numerous theories and techniques applicable to the modelling of severe dynamic loading of concrete structures. A Lagrangian solver for the simulations was selected. This was motivated by e.g. the possibility of following history dependent material behaviour using this solver technique. Since the scale of view in the applied simulations is on a structural level, the material models used are formulated on a macroscopic scale where the concrete constituents, i.e. the aggregates, the cement matrix and the pores, are not modelled discretely. Further, the numerical modelling requires validation by means of experimental results. However, since no experiments are performed within the scope of this project, experimental data are taken from the literature.

1.4 Methodology

As described in Section 1.3 and shown in , the methodology used to meet the objectives involved are: reviews of the existing literature, theoretical investigations, and the performance of applied numerical simulations of blast and/or fragment loading of concrete structures. However, in order to increase the understanding of the methodology used, it is described in greater detail.

Literature studies has been conducted to define and understand important factors involved in blast and fragment loading of reinforced concrete structures, including:

- blast and fragment load characteristics
- blast and fragment load effects on reinforced concrete structures
- the influence of dynamics on the response at material, as well as, structural levels, and underlying phenomena
- concrete material behaviour under fast loading and high compressive pressures

Since the scientific approach involves numerical simulations, the literature reviews also entailed:

- numerical solution techniques used in simulations of fast transient, high pressure loading involving material and geometrical nonlinearity
- theories used in constitutive modelling of material behaviour in general, and of concrete behaviour in particular

Based on these literature reviews, theoretical reasoning was used to investigate the applicability of the different theories in case of blast and fragment loading of concrete structures.

Numerical simulations were used in applied studies to examine:

- the effect of reinforcement on local damage in concrete
- the effect on local damage by adding (steel) fibres to concrete in case of projectile impact

- the effect of combined blast and fragment loading on the response of a reinforced concrete structure

In the first numerical study, the amount, size and position of reinforcement was varied to evaluate its effect on local damage. The effect of fibres in the concrete was studied by varying material model input data to correspond to different amounts of fibres in the concrete. In order to study the effect of combined blast and fragment loading, the results of a simulation of combined loading was compared to results of simulations where the loads had been treated separately. Thus, these numerical investigations had a parameter-study character.

The methodology used in the numerical studies is schematically shown in Figure 1.2. Each of the numerical studies were based on observations from earlier studies (experimental, theoretical or numerical), reported in the literature or studies (theoretical or numerical) made within the framework of this project. Based on these observations, theoretical reasoning was used to formulate a hypothesis. The numerical studies were then used to test this hypothesis. However, before the numerical study was initiated, the hypothesis had to be deduced into predictions from which the scope of the study had to be defined, i.e. material properties, type of structure and load characteristics were specified. Since numerical simulations are mathematical predictions of real behaviour, limited by assumptions and idealisations, a validation process of the numerical model was essential. This was performed by comparing results from reference simulations of experiments with the observations reported from those experiments. It was required that the basic experimental conditions, e.g. material properties, geometries and loading conditions, were close to those used in the numerical study. Since no experiments have been performed within the scope of this project, the experiments used within the validation process were derived from the literature. When found necessary the validation process did also involve the calibration and modifications of the numerical model. Once the numerical model was validated and its limitations surveyed, parametric variations were used to study their influence on the behaviour. The results were then interpreted and general conclusions drawn. If further investigations were required, the definition of the study was modified and additional numerical simulations performed.

The use of numerical simulations introduces limitations such that the results from these studies can never be better than the numerical model itself. Therefore, the capability of the numerical model was under constant observation throughout the project. Even though the numerical models used in the studies were able to yield results used to extract generic conclusions about real behaviour, the limited possibility of modifying the material model used to describe the concrete behaviour became an issue. The need to modify the model arose from its limited ability of describing certain material behaviours and the limited possibility of modifying the model input variables to take into account the effect of for example adding fibres to the concrete mix which influences such factors as the tensile softening behaviour.

A decision to develop and implement a 'new' material model (called the Concrete Damage Plasticity Model 2, CDPM2) was taken after the consideration of different possibilities of advancement. The process of developing this model involved the following elements: setting up requirements for the model, making the theoretical build-up, implementing the model in a program, verifying implementation, validating the model and evaluating this response.

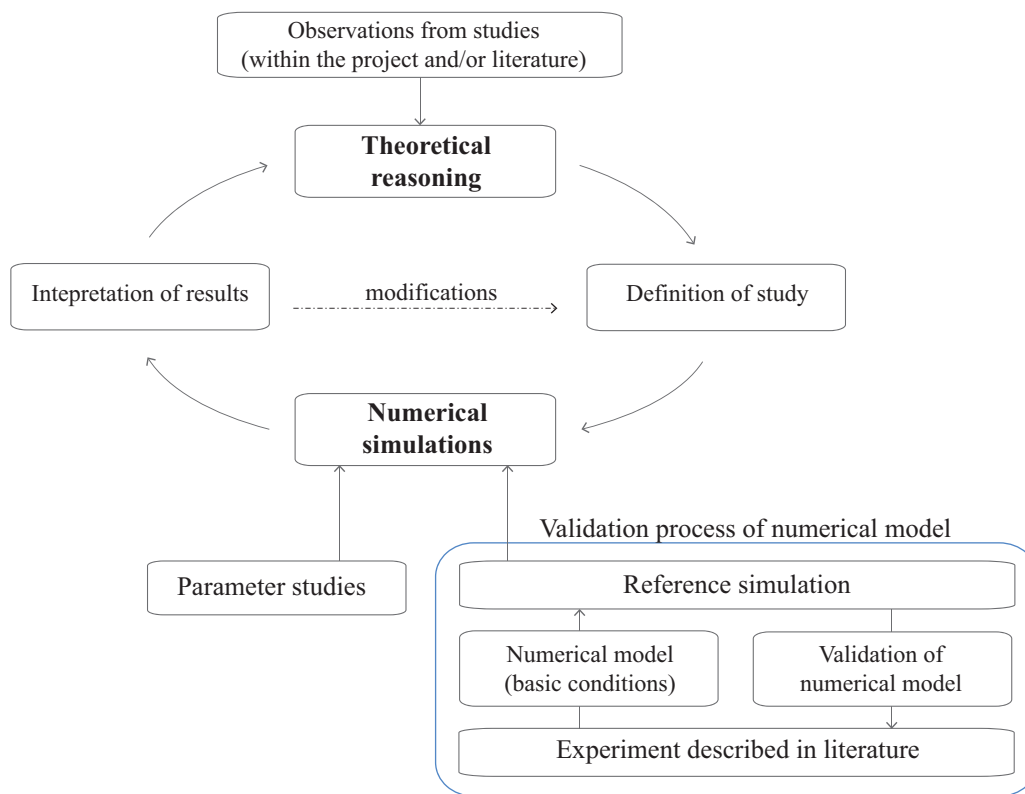


Figure 1.2 Schematic illustration of the methodology used in the numerical studies.

1.5 Limitations

This work is limited to the study of normal strength concrete as well as normal strength concrete with the addition of moderate dosages of steel fibres (where specifically noted). Further, the concrete structures studied within this work are limited to structures of low complexity and rather represent structural members than entire structures.

In the work presented within this thesis, the focus was kept on the effect of an explosion on a reinforced concrete structure; see Figure 1.3. The explosion process, including e.g. initiation of detonation, decomposition of explosive material, casing breakup, fragment ejection, release of shock wave and propagation of shock wave and fragments in the air, has been paid no or very limited attention. Further, the loads are considered as a blast load and fragments, but secondary loads such as debris from surrounding structures are disregarded. The penetration of projectiles has, however, been included in the studies as these can be viewed as special cases of fragment impacts.

Methods used to characterise blast and fragment loads caused by the detonation of cased charges involve idealisations and simplifications, often necessary in order to make them sufficiently generic. This approach limits the effectiveness of the methods,

thereby also limiting the results attained. The fragments used when simulating fragment cluster impacts are of the same geometrical shape, size, velocity and mass and are all assumed to move in a general direction perpendicular to the target surface of the same velocity. In reality, all these parameters would normally vary among fragments, but in order to simplify the numerical model and be able to draw general conclusions from the results, these simplifications were necessary.

The applied numerical simulations conducted are based on fictive cases. Thus, no experiments performed correspond to these simulations which limits the possibility of validating the results of the simulations. However, as described in Section 1.4, the validation of the numerical model in these cases was approached by comparing numerical results with experimental results for similar conditions during which relevant findings were used to identify limitations of the case studied.

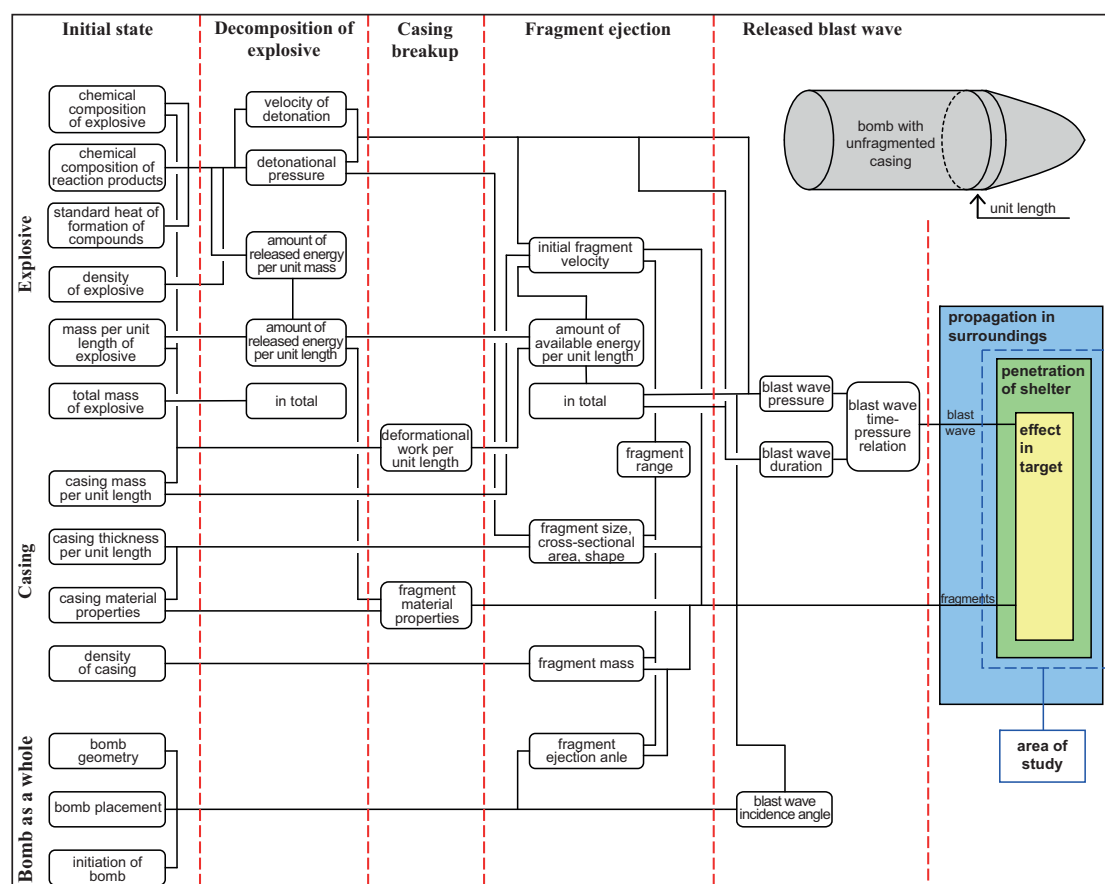


Figure 1.3 Schematic illustration of the course of events and factors impacted in the process from initiation of bomb to its effect on the exposed structure (target). The area of interest in the present study is marked.

1.6 Research significance

The area of research regarding blast and fragment loading of concrete has been paid attention for many decades. Traditionally, this research was mainly experimental. However, the fast nature of the response and complexity of the phenomena involved both regarding loading and material behaviour complicate the analyses of test results and limit the opportunity of drawing conclusions. Further, since the response is depending on material factors as well as test conditions, the conclusions drawn are often case sensitive and lack generality. In more recent years, analysing the response of concrete exposed to blast and fragment loading by means of numerical simulations have grown more common. This allows for cost effective parameter studies and the possibility of following the response in slower motion.

Experimental studies of the effect of fibres in concrete reported in the literature have shown a significant improvement of the resistance to local damage compared to plain concrete; see Paper I. However, due to the limitations involved in drawing generic conclusions from such studies, as discussed above, a numerical study of the effect of adding fibres into concrete has been conducted. This study has allowed for parameter studies and generic conclusions to be drawn.

Combined blast and fragment loading is considered to be synergetic in the sense that the combined loading results in greater damage than the combined damage caused by the blast and fragment loading separately. This effect is pointed out in some literature and design manuals within the area of protective design; see Paper II. However, due to the complex nature of the effect, the high parameter dependence and limited number of documentations and comparable experiments, the design manuals often disregard the synergy effect or treat it in a very simplified manner. In order to increase the understanding of the combined effects of blast and fragment loading, a numerical investigation was conducted. This investigation allowed for idealised loading conditions and generic conclusions of the effect of the combined blast and fragment loading on the damage evolution and structural response.

Even if numerical simulations are effective tools to study the behaviour of blast and fragment loaded concrete structures, the method involves limitations. One crucial factor affecting the ability to model concrete behaviour accurately is the constitutive laws used to mathematically describe the material response. In the numerical studies referred to above, the RHT model was used. Even though this model is reported to describe the response of concrete accurately in several applications of projectile penetration (Hansson, 2002; Leppänen, 2003; Schuler, 2004; Tham, 2006), it suffers from limited accuracy in loading cases involving tensile cracking (Leppänen, 2006; Magnusson and Hansson, 2005; Nyström, 2008). Further, it lacks the versatility to take into account effects of for example fibres in the concrete. Since also other material models developed for concrete exposed to high transient loadings often suffer from limitations and lack of versatility, and pointing out the limited possibility of overcoming these weaknesses by employing user subroutines, the need for a “new” model to be implemented in a suitable numerical simulation tool arose. With the combination of stress-based plasticity and isotropic damage mechanics the constitutive model CDPM2 for the rate dependent failure of concrete was developed characterized by its numerical stability and flexibility to adapt to newly developed concrete based materials, such as fibre reinforced concrete.

The model has shown good agreement with experimental results under various load conditions, from uniaxial tension to hydrostatic compression and shock wave loading. Nevertheless, the current version of the CDPM2 has a limited capability of describing the behaviour of concrete at pressure levels higher than about five GPa and accumulation of damage at high strain rates. However, upon modification it is believed that use of the model would increase the opportunities of studying the behaviour of concrete structures exposed to combined blast and fragment loading and the effects of different designs of the concrete target in future research.

These papers are not enclosed
to the thesis available online.



1.7 Outline of the thesis

This thesis is composed of an introductory part and four enclosed papers published or submitted for publication in reviewed scientific journals. The introductory part aims at giving some background on the subjects treated in the enclosed papers, while also including information complementary to these papers.

Chapters 2 to 4 present the theory relevant for understanding the physical problem. In *Chapter 2*, the behaviour of concrete under various loading conditions relevant to describing the material response to high dynamic loading is presented. *Chapter 3* is divided into two parts corresponding to the characterisation of blast and fragment loading and their effect on reinforced concrete structures, respectively. In the latter part, common modes of failure in reinforced concrete structures exposed to blast and fragment loadings are presented together with findings from the applied numerical studies performed within the scope of the work presented in this thesis. Two of the numerical studies are presented in appended Papers I and II. In *Chapter 4*, the dynamic effects caused by highly transient loads are presented. Simplified, these can be divided into inertia and wave propagation effects. However, the theory of shock wave formation, propagation and material transformation is paid special attention.

Chapter 5 presents the theory used for the numerical solution method, with special emphasis on constitutive modelling. A brief review of the evolution of material models used to describe the behaviour of concrete under high dynamic loading and a more comprehensive description of the RHT model (Riedel, Hiermaier and Thoma; developed by Riedel, 2000) are also presented. The RHT model was used to describe the concrete material behaviour in the applied numerical studies. Clearly, many existing material models for concrete provide good results for the loading cases for which they were developed. Nevertheless, their lack of versatility call for a constitutive model to account for the dynamic failure of concrete, which is easy to extend and is based on input parameters with physical meaning. The development of such a material model denoted “Concrete Damage Plasticity Model 2” (CDPM2), is the topic of *Chapter 6*.

Major conclusions and suggestions for future research are presented in *Chapter 7*, and references used in the introductory part of this thesis are presented in *Chapter 8*.

2 Concrete material behaviour

2.1 Material testing

In order to understand and model the behaviour of concrete under blast and fragment loading, its behaviour under these conditions must be known. As further described in Chapters 3 and 4, blast and fragment loadings may cause high strain rates and the built-up of high confining pressures in the exposed material. Further, the high intensity of the loads and the subsequent high pressure levels may lead to the formation and propagation of shock waves, which are compressive waves causing almost instantaneous jumps in the material state, i.e. its stress state, density and temperature. However, as the intensity of the load decreases and the structure is released, the concrete is exposed to lower stress levels. This is also the case for parts of the structures which are relatively far from the load. Thus, the behaviour of concrete must be characterised for a wide range of stress conditions. In order to discern the phenomena involved during loading, the complexity has to be kept low during the testing of concrete. In practice, this means that comprehensive testing is performed under quasi-static loading, which are complemented by dynamic testing for cases with well-defined uniaxial stress conditions.

However, due to limitations in test facilities the maximum confining pressure levels reachable during quasi-static loading often seems to be limited to less than 1 GPa, most often in the range of 0.5 to 0.7 GPa; see Bažant *et al.* (1996), Gabet (2006) and Williams *et al.* (2006). Dynamic testing involving detonation or high velocity impact is used to characterise the behaviour under higher confining pressure levels. These tests are then evaluated under the assumption of one-dimensional shock wave propagation but the effects of temperature and strain rate cannot be distinguished from the material strength in these tests.

2.2 Uniaxial tension and compression

2.2.1 Static behaviour

Concrete is one of the most widely used building materials, among other things thanks to its high compressive strength, (f_c). However, one of its most pronounced disadvantages is its low tensile strength (f_t), which for normal concrete is in the order of 6 to 12 % of compressive strength. Despite this difference in absolute terms, the general behaviour of initial elasticity, pre-peak stress softening and post-peak strain softening may be observed in both uniaxial tensile and compressive tests. Figure 2.1 schematically shows the general behaviour of concrete under uniaxial tension and compression. Even though the strain at failure may be relatively large compared to elastic strain, due to the low values of failure strain (on the order of 1 % or less; Lubliner, 2008), concrete is regarded as brittle. This brittleness is especially pronounced in tension.

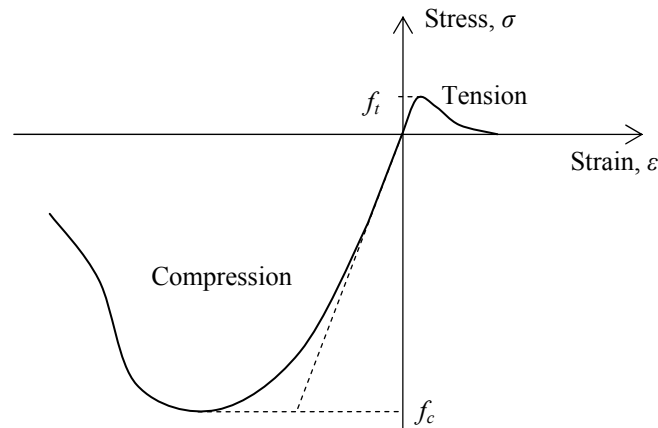


Figure 2.1 Stress-strain relation for uniaxial tension and compression.

The fracture process of concrete can in a mesoscopic view to a large extent be explained by the initiation, propagation and bridging of microcracks. Due to settlements, shrinkage and thermal expansion of the mortar, microcracks exist in concrete already before any load is applied. These microcracks are mainly concentrated to interfaces between the mortar and aggregates, which are referred to as “bond cracks” below.

In the initial phase of loading, the microcracks are nearly unchanged and the behaviour may be approximated as linear-elastic. At levels of about 30 and 60 % of the compressive and tensile ultimate strength, respectively, stable growth of the bond cracks is initiated and the material response becomes nonlinear; Chen (2007). For increased load levels, bond cracks start to extend in a stable manner. Even though the amount of microcracks in the mortar is initially limited and their effect on the response is negligible, the amount increases with the load level and their propagation causes the bridging of bond cracks for nearby aggregates. At stress levels of about 75 and 80 % of the compressive and tensile strength, respectively (Chen, 2007 and Weerheijm, 1992), the microcracking in the mortar becomes significant and the fracture process becomes unstable. The ultimate strength of the concrete is approached. After the failure strength has been reached, concrete shows strain-softening behaviour in both compression and tension. Due to the localisation of damage and subsequent growth of macrocracks, concrete gradually decreases in strength with increasing deformation.

Due to the inhomogeneity of damage in the concrete sample, testing and evaluating the results of crack softening is not evident. The damage process under uniaxial tension may be divided into two phases: a homogenous phase and an inhomogeneous phase. In the homogenous phase the damage, which consists of initiation and growth of microcracks, is evenly distributed over the sample volume. In the inhomogeneous phase, damage localises to fracture process zones in which the macrocracks develop while the rest of the sample is unloaded with the closure of the microcracks. In tension, where the general direction of macro-crack propagation is perpendicular to the load axis, after the formation of macrocracks, the measure of global strain is no

longer sufficient to characterise the local behaviour. Thus, the behaviour due to uniaxial tensile loading is often represented by two curves; a stress-strain relation during the homogenous damage phase, and a stress-crack opening phase to characterise the behaviour during the inhomogeneous damage phase; see Figure 2.2. Even though the transition point from global to local damage behaviour follows the ultimate stress point, it is often approximated to coincide with the point of ultimate strength; Bai *et al.* (2012). The area beneath the stress-crack opening relation in Figure 2.2 represents the tensile fracture energy, G_F . However, due to the difficulties related to measurements of the stress softening behaviour during the inhomogeneous phase, other test methods than uniaxial tension is often used to characterise the concrete response during this phase. An example of such a test method is the three-point bending test of a notched beam, often referred to as the “work-of-fracture” method, which was originally proposed by Hillerborg (1985).

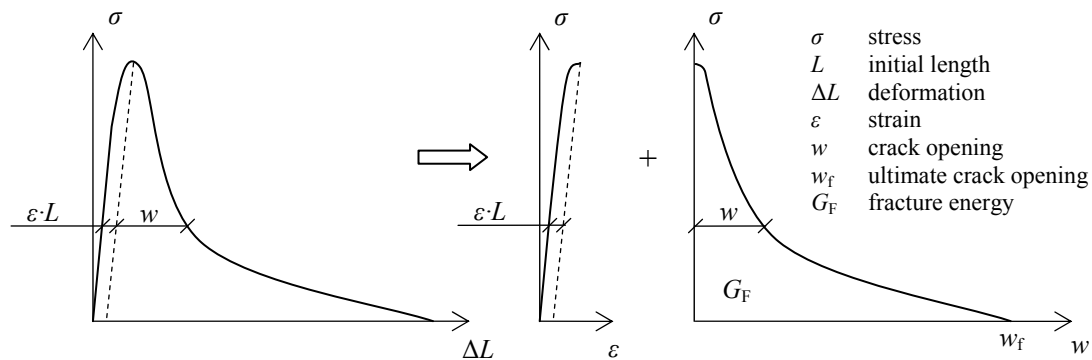


Figure 2.2 Stress-deformation relation for concrete in uniaxial tension, and separation into a stress-strain and a stress-crack opening relation.

In concrete compressed under no or low lateral confinement, a phenomenon referred to as dilation is observed. Even though the load is compressive, at a certain stage of loading, the lateral deformations become so large that the volume increases. This phenomenon is observed when the relation between the axial stress and the volumetric strain ($\varepsilon_v = \varepsilon_1 + \varepsilon_2 + \varepsilon_3$) is plotted; see Figure 2.3. This volume increase results from the formation of cracks parallel to the direction of the greatest compressive stress.

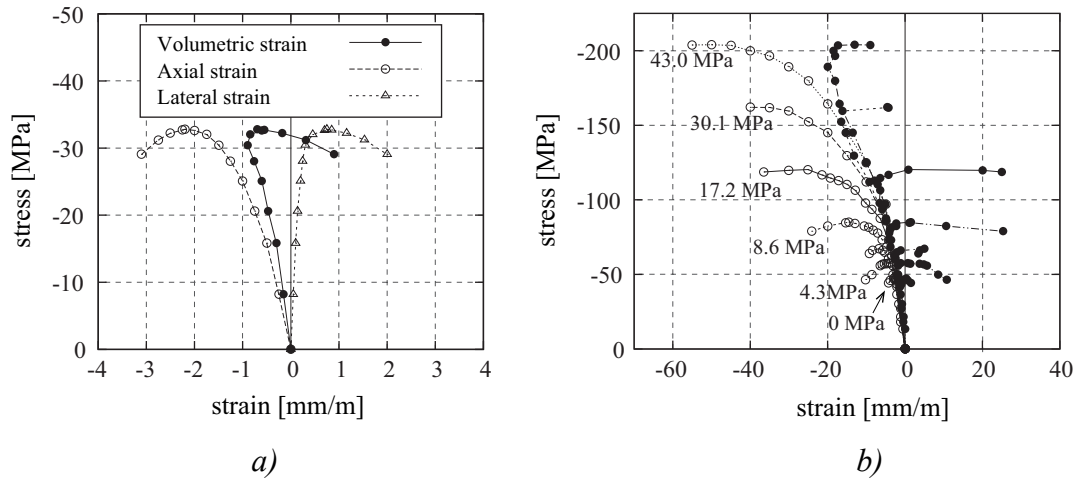


Figure 2.3 Dilation for compression under a) no or b) low, confining pressure, experimental data from Kupfer et al. (1969) and Imran and Pantazopoulou (1996), respectively.

2.2.2 Dynamic behaviour

As with most materials, the behaviour of concrete changes as the strain rate increases. The increase of the compressive and tensile strength is often characterised by a dynamic increase factor (DIF), describing the ratio between the dynamic and static strengths. As seen in Figure 2.4a, in which Malvar and Ross (1998) have compiled the results of experiments conducted by several researchers, the dynamic tensile strength of concrete may be as much as five to seven times higher than static ultimate strength. As seen in Figure 2.4b, the strain-rate effect is less significant on compressive strength but may still be more than doubled; Bischoff and Perry (1991).

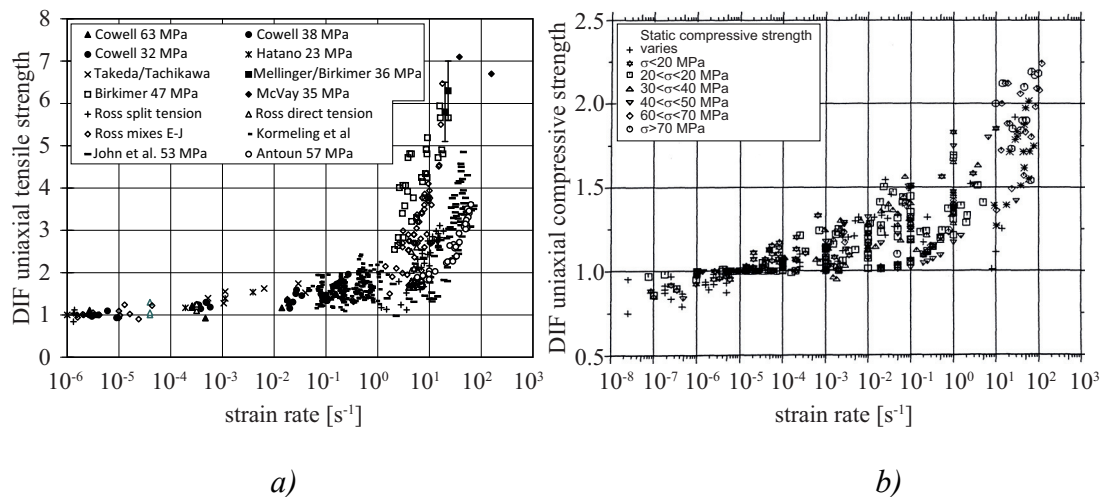


Figure 2.4 Dynamic increase factors (DIF) for concrete a) uniaxial tensile strength and b) uniaxial compressive strength, based on Malvar and Ross (1998) and Bischoff and Perry (1991), respectively.

As seen in Figure 2.4, there is a moderate increase of strength up to a strain rate of about 1 s^{-1} and 30 s^{-1} for tension and compression, respectively. Thereafter, the strength increases rapidly with increasing strain rate. According to Johansson (2000), who reviewed research on strain rate effects on concrete strength up to that date, the moderate increase can be explained by viscous effects leading to changed crack propagation and even multiple crack planes. This is a material effect which seems to be enhanced in the presence of water in concrete pores; Rossi *et al.* (1994). The more pronounced increase of strength is due to structural effects attributed to inertia. In compression, inertia causes delayed lateral deformation which leads to lateral confining pressures and since the strength in concrete is pressure dependent (see Section 2.3), a higher strength is attained than in static loading. In tension, though, inertia affects the material state around the crack tips and reduces the rate of crack propagation; Weerheijm (1992).

Young's modulus is reported to be strain rate sensitive as well but to smaller extent than the strength; Yan and Lin (2006). Figure 2.5 shows the relations for the strain rate dependence of the Young's modulus for uniaxial compression and uniaxial tension, respectively, calculated according to CEB (1993).

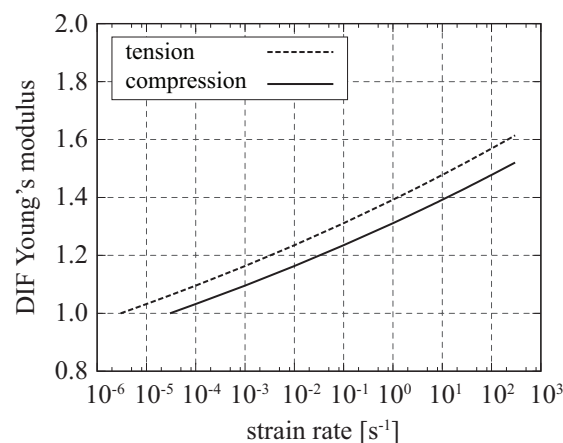


Figure 2.5 Strain rate dependence of Young's modulus in uniaxial compression and uniaxial tension, calculated according to CEB (1993).

Due to the lack of reliable test methods, it was previously unclear whether the fracture energy is strain-rate dependent as well, more recent studies (e.g. Schuler, 2004; Brara and Klepaczko, 2007; Weerheijm and van Doormaal 2007) indicate that this is the case for high strain rates. In Figure 2.6, data on the dynamic increase factor for fracture energy (i.e. the ratio of static and dynamic fracture energies) presented in Schuler (2004) and Weerheijm van Doormaal (2007) are shown in relation to the strain rate. These measurements correspond to the specific fracture energy, i.e. total fracture energy divided by fracture surface area and is not dependent on the number of crack planes. Thus, in the case of formation of multiple fracture zones, the total fracture energy in a specimen would increase further. The physical phenomena involved are not yet well understood, but Weerheijm and van Doormaal (2007) explain the increased fracture energy as similar to the strong increase of tensile strength for high strain rates; inertia effects at crack tips. According to Weerheijm and van Doormaal (2007), this phenomenon would lead to more extensive micro-cracking

but would not affect the ultimate crack opening measure for which no more stresses may be transported over the fracture zone, thus, producing an increased fracture energy.

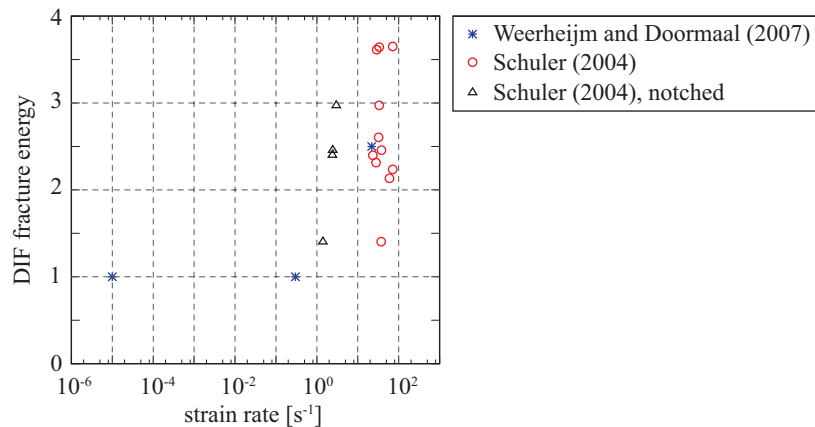


Figure 2.6 Dynamic increase factor (DIF) for specific fracture energy of concrete.

2.3 Influence of confining pressure

2.3.1 Static behaviour

Concrete is a pressure sensitive material, i.e. the strength changes with changing pressure levels. In order to characterise pressure sensitivity, the ultimate strength under different loading conditions are often plotted as a measure of the principal stress difference versus the hydrostatic pressure component; see Figure 2.7. As observed, the principal stress difference $\sigma_1 - \sigma_3$ (which is related to the shear strength of concrete) increases from a few MPa in uniaxial tension to several hundred MPa for very high confining pressures. Further, the observed difference between the tensile and compressive meridians may be explained by the fact that concrete fails at a lower principal stress difference value when undergoing triaxial extension test than under triaxial compression. However, for high pressure levels, the limit state data are scattered.

Vu *et al.* (2009) studied the effect the initial saturation degree of concrete on shear limit states and showed how an increased degree of saturation (S_d) reduced shear resistance for high confinement levels. The behaviour was explained by a combination of two phenomena: the loss of cohesion as the concrete underwent plastic compaction, and the reduced friction between grains due to presence of free water. As the concrete approached full compaction, the pore pressure due to water became sizable and increased volumetric stiffness and limited shear strength, which finally became insensitive to pressure. The lower the initial saturation degree, the higher compressive volumetric stresses may be reached before pore pressures produce this effect. In fact, the experimental data for “dry” concrete (S_d 11%) in Vu *et al.* (2009) and data from Gabet (2006) derive from the same test series using identical concrete. Gabet (2006) studied for example the effect of the loading path on limit

states and concluded that even if the compaction behaviour depended on the loading path, the limit state did not.

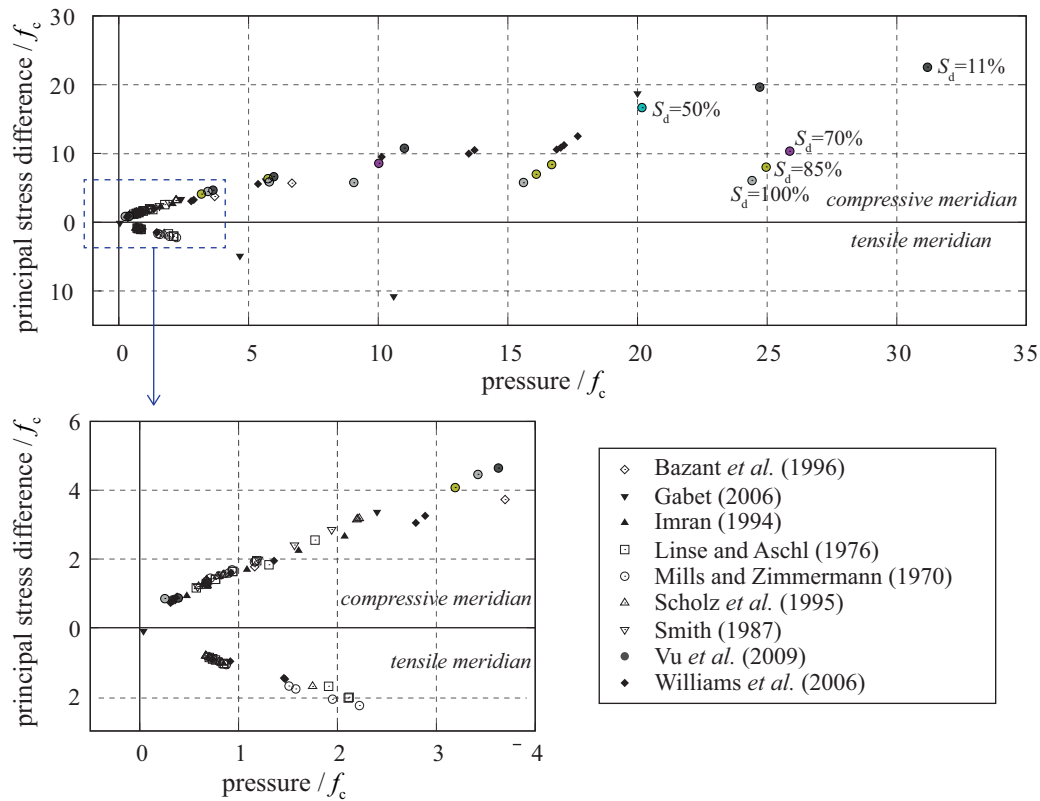


Figure 2.7 Normalised strength limit states as a function of pressure (compressive and tensile meridians).

Higher pressure levels also yielded a stiffer and more ductile behaviour which may be seen in Figure 2.8a, showing experimental results from triaxial compressive loading under different levels of confinement (50, 100, 200, 500 and 650 MPa, respectively), presented in Gabet (2006). The uniaxial compression strength of the concrete was 34 MPa. For confining pressures of 100 and 200 MPa the stress-strain curve seemed to reach a plateau, i.e. no strain softening behaviour was observed. For 500 and 650 MPa confinement, the ultimate strength was not reached during testing. However, these results showed a very ductile behaviour featuring large irreversible deformations. In Figure 2.8b, the hydrostatic part of the triaxial compression tests are shown together with a cyclic hydrostatic compression test on the same concrete, from Gabet (2006).

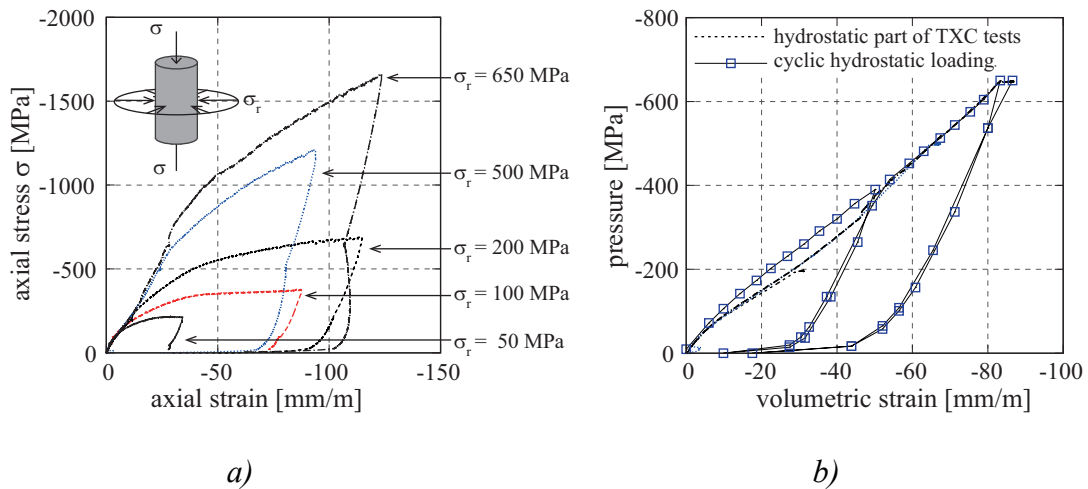


Figure 2.8 Stress-strain relationship for a) triaxial compression tests (TXC) with different confining pressures, and b) hydrostatic part of TXC-tests in a) and cyclic hydrostatic compression; results from Gabet (2006).

The volumetric compaction behaviour of concrete is often divided into three different phases, as schematically shown in Figure 2.9. These phases are:

- Initial elastic phase:
The concrete behaviour may be approximated as linear elastic, and unloading during this phase does not lead to any remaining deformations.
- Plastic compaction phase:
If the elastic threshold p_{el} is exceeded, the pressure causes damage in the cement matrix and a significant drop in the material stiffness is observed. A gradual increase of pressure leads to plastic compaction of the cement matrix and an irreversible compaction of the concrete due to pore compaction, with additional matrix damage. If unloading occurs during this phase, a reduced volume compared to the initial volume is reached. However, the gradual compaction of the material leads to increased stiffness of the material.
- Pore-free, granular compaction phase:
As additional pores are compacted during the plastic compaction phase, the concrete approaches the behaviour of a fully compacted granular, for which the structure in the cement matrix is fully damaged and all pores compacted. In this phase where pressure exceeds the threshold p_s , the compaction stiffness again becomes approximately linear elastic.

In the results from Gabet (2006) shown in Figure 2.8b the first two phases can be distinguished. The third phase is, however, not attained during these tests.

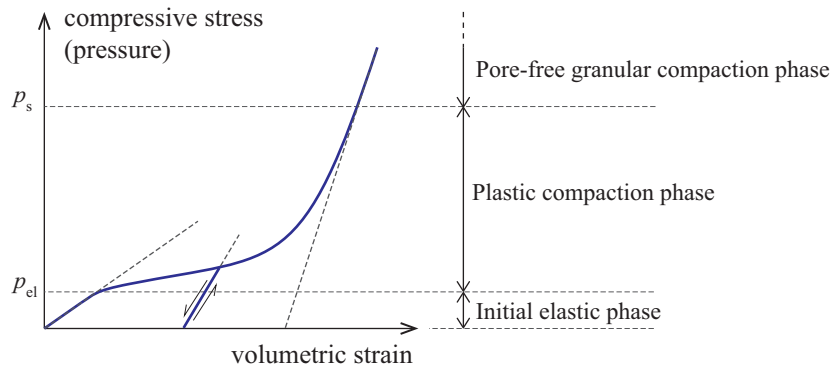


Figure 2.9 Schematic illustration of the concrete compaction curve in hydrostatic compression.

Another characteristic of concrete is the shear-induced or shear-enhanced compaction, meaning that in the presence of shear stresses, the concrete shows more compaction than in its absence. This effect can be seen when comparing data from hydrostatic compression tests with those from one-dimensional compression (uniaxial strain). Figure 2.10 shows the response from the hydrostatic part of the triaxial compression tests and a uniaxial contraction strain test in the mean stress-volumetric strain plane; from Gabet (2006).

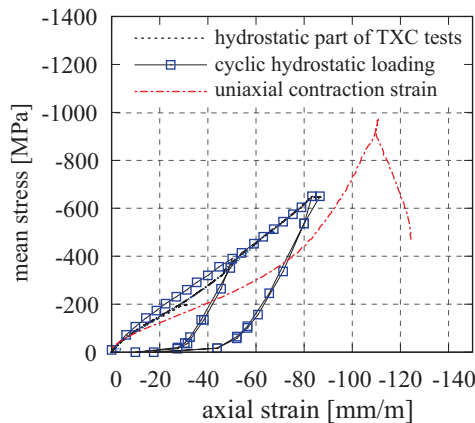


Figure 2.10 Shear induced compaction. Experimental data from hydrostatic compression and uniaxial strain, based on Gabet (2006).

2.3.2 Dynamic behaviour

At higher pressure levels than approximately 1 GPa testing of concrete material behaviour is performed by means of dynamic loading. As mentioned in Section 2.3.2, these tests are constructed to form a one-dimensional shock wave in the material, which is achieved by means of for example contact detonations or reversed flyer-plate impact tests. Further mentioned in Section 2.3.2, such compressive waves cause almost instantaneous jumps in the stress state, density and temperature of the concrete. Depending on the shock wave amplitude, different material states are reached. These states are denoted Hugoniot states. Since the increase of temperature

may only be implicitly accounted for in the evaluation of the test data, the Hugoniot states are often represented by points in a two-dimensional plane, for concrete often in terms of stress and density. The theory of shock waves, shock wave material transition and Hugoniot points are treated in Section 4.3.

Figure 2.11 shows results from contact-detonation tests (Gebbeken *et al.* 2006), and several flyer-plate impact tests (Eibl and Ockert, 1996; Gebbeken *et al.*, 2006; Grady, 1993, 1996; Hall *et al.*, 1998) in the axial stress-density plane. The data scatter, especially pronounced for high stresses, may be attributed to for example differences in concrete mixes, water content, and limitations in test-measuring and evaluation techniques.

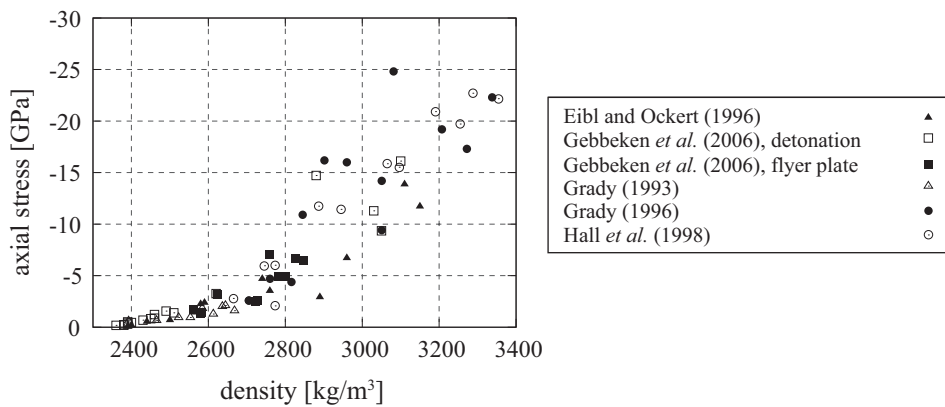


Figure 2.11 Hugoniot-data points for concrete.

The data shows non-linearity and the behaviour may be related to the three phases of compaction described in Section 2.3.1; the initial elastic phase, the plastic compaction phase, and the pore-free granular compaction phase. However, the first phase is difficult to distinguish in the figure since the elastic limit is low compared to the minimum level of stresses reached. Further, the effects of the thermal energy and strain rate on the response cannot be differentiated from material strength.

3 Blast and fragment loads and their effect on concrete structures

3.1 General

Generally seen, explosions cause two types of loading on the surroundings: blast load and fragment impact load. The fragments can be of primary or secondary kind, i.e. caused by fragmentation of a material casing the explosive medium or caused by fracture of surrounding objects or structures.

Primary fragments are created when the casing bursts after successive swelling caused by the high internal pressure build up as the explosive filling transforms into hot gas when initiated. During swelling, radial tensile cracks will form on the outside and shear cracks on the inside of the casing. As these cracks meet or propagate to a free edge, fragments are formed and start to propagate in the surrounding air away from the point of detonation; see Curran (1997). Figure 3.1 schematically shows the fragmentation process on a global and local level. As the casing fractures, the hot gas and its remaining energy is released and expands into the surrounding air causing a blast wave, i.e. a shock wave propagating in the air. Obstructing objects or structures surrounding the explosion affects the properties of the blast wave. The interaction of the blast wave with these objects may also lead to the creation of secondary fragments. Thus, the loading on a structure caused by an explosion may be very complex and is highly dependent on for example the type and amount of explosive medium, casing thickness and material, the geometry of the exploding object, the surroundings and the stand-off, i.e. the distance to the centre of detonation. As the blast wave propagates into the surroundings, the energy is spread out and the intensity of the blast wave decreases with increasing stand-off. In the same way and in combination with air resistance, the density and velocity of fragments decreases with increasing stand-off.

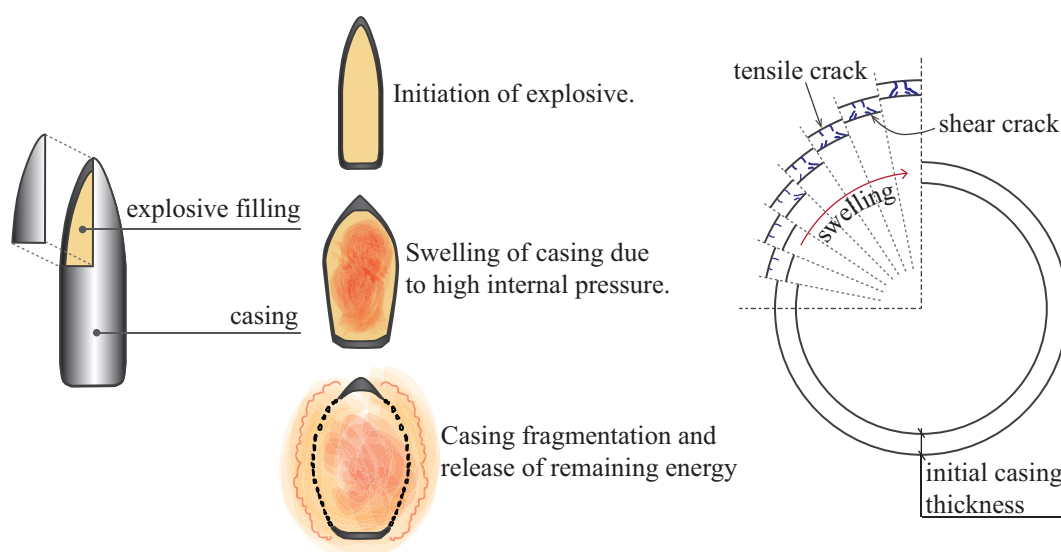


Figure 3.1 Fragmentation process of bomb casing; global (left) and local (right) point of view, respectively, partly based on Janzon (1978).

In order to define the loads for structures exposed to explosions, the striking blast wave and fragments, respectively, have to be idealised and characterised. Brief descriptions of blast and fragment load characteristics are provided in Section 3.2; for more comprehensive descriptions, see Johansson (2012) and Leppänen (2012), respectively.

Structural response due to high transient dynamic loading can differ substantially from the response caused by static loading. Principally derived from inertia and wave propagation effects; see Chapter 4. Fast loading in combination with high load amplitudes, causing material damage, thus affects the target failure mode. In general, an increased concentration and intensity of the total load leads to increased localisation of the damage. Common modes of failure in concrete structures subject to blast and/or fragment loading are described in Section 3.3.2.

3.2 Load characteristics at target

3.2.1 Blast load

Thanks to a large amount of test data from bare high-explosive detonations, the blast load characteristics from such detonations can be estimated with good accuracy. Expressions of the pressure-time relation of the loads can be found in most handbooks and design manuals within the field, e.g. Johansson (2012), Krauthammer (2006) and U.S. Army (1992). However, it is the nature of the propagating blast wave before it strikes the target together with the nature of the reflection as the target is struck that characterises the resulting load.

As seen in Figure 3.2a, the pressure profile of an idealised blast wave from a bare detonation consists of two phases; the positive and negative phase, respectively. The positive phase, characterised by an overpressure relative to the initial ambient pressure, is initiated by an almost instantaneous increase of pressure, as the blast wave front passes. The abrupt increase of pressure is followed by descending pressure. As the pressure level falls below the initial ambient pressure, the negative phase is entered. The negative pressure relative to the initial ambient level is caused by the partial vacuum created as air particles have been removed by the wave front (Johansson, 2012). The reversal of air particle flow makes the pressure level increase and the initial state of the ambient air is finally reached again.

For cased charges, where energy is consumed to fracture the casing and imparting velocity to the fragments, the blast wave parameters also depend on the geometry and material properties of the casing; as a result, the blast wave will be estimated with less accuracy than in the case of bare charges. As a blast wave strikes a surface not parallel to its direction of propagation, it is reflected, thereby changing its behaviour. In the case of normal reflection, i.e. the reflecting surface is perpendicular to the direction of the blast wave, the effect can lead to significant enhancement of the pressure, which according to Johansson and Laine (2012) may be as much as 20 times higher than the incident pressure. Thus, reflections of the blast wave on surrounding structures before the target is reached makes the resulting blast wave profile more complex than in the

case of free field propagation shown in Figure 3.2a. Thus, more rough estimations are used when determining the blast load from cased charges.

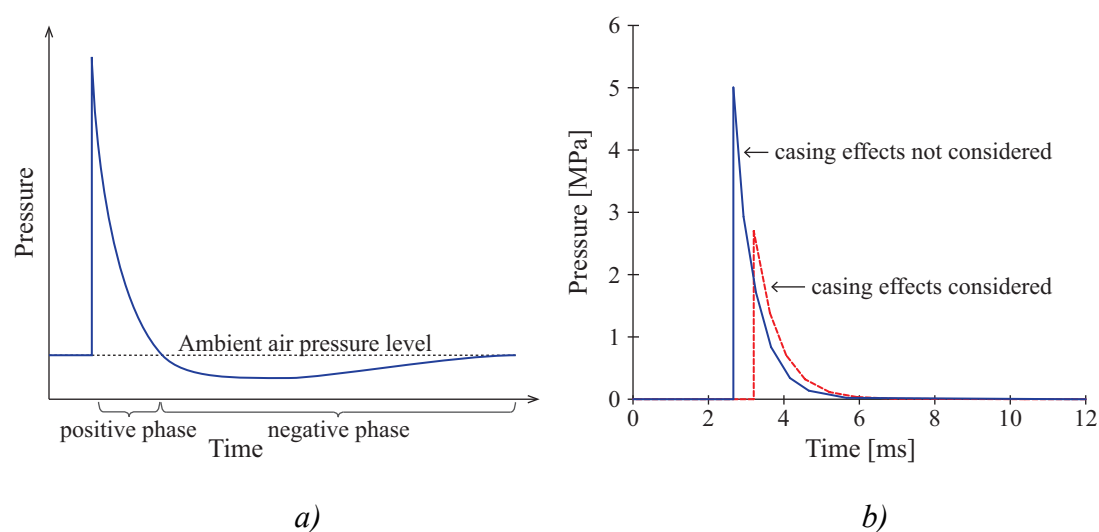


Figure 3.2 a) Idealised blast wave profile at a certain stand-off, and b) estimated blast load profiles from a 250 kg GP-bomb of 50 weight-percent TNT at a stand-off 5 metres, with and without casing effects considered.

Since the blast wave is reflected as it strikes the target, the magnitude of the pressure in the resulting load is higher than in the incident blast wave. As stated above, the resulting pressure acting on the target may be as much as 20 times higher than the incident pressure. The general shape of the blast wave profile is negligibly affected by the reflection and the duration of the positive and negative phases is generally assumed to be unaffected; Krauthammer (2006) and U.S. Army (1992). However, in design with regard to explosions, the negative phase is generally considered less important than the positive phase; thus, often only the latter is taken into consideration. The duration of the positive phase depends on the type and amount of explosive and the stand-off but is often in the range of a few to tens of milliseconds.

Figure 3.2b shows the idealised reflected loads from the blast wave on a perpendicular wall at a stand-off of five metres caused by a 250 kg General Purpose (GP) bomb of 50 weight-percent trinitrotoluene (TNT). The bomb is a fictive bomb referenced in the Swedish design manual for civil defence shelters; see e.g. Räddningsverket (1994), MSB (2011) and Leppänen (2012). The load caused by the blast wave is shown for two different assumptions; 1) the energy consumed to fracture the casing and imposing the velocity on the fragments is not considered, and 2) the weight of the explosive filling is reduced to take into account the reduced energy available to form a blast wave after imposing kinetic energy to the fragments. The former case is equal to neglecting the effect of the casing on the blast wave assuming a bare detonation of the TNT. In the latter case, the casing effect is considered to some extent but the energy consumed while breaking up the casing to form fragments is still neglected. The calculation of loads and the assumptions made are presented in Leppänen (2012).

3.2.2 Fragment load

While the blast load generally can be estimated with sufficient accuracy as a pressure-time relation, the fragment loading is much more difficult to characterise. The fragmentation process of casings is very complex and dependent on the example at hand. Hence, unless a very large number of test results are compiled and analysed generic empirical expressions for fragment characteristics cannot be developed in the same way as for bare explosions in free air. Instead analytical methods, where the exploding items are assumed to be cylindrical cased charges, are derived and confirmed by test data. Through this method, the expressions used to characterise the fragments apply in particular to cylindrical items and to items that may be reasonably approximated as either cylindrical or series of cylindrical items. The more the shape of the exploding object deviates from this, the less accurate the fragment characterisation estimations. The expressions give estimations of the fragment mass and size distribution, their initial velocities and how these velocities reduce as a function of the increasing stand-off distance. However, these characteristics cannot directly be used to characterise the load. Assumptions must still be made about e.g. the shape of the fragments and their spatial distribution.

Further, since fragments impacting a structure do not only cause a pressure on the surface of the structure, but also penetrate into the structure to cause local damage, the character of the load also depends on the material properties of the exposed structure and its ability to withstand this penetration and stop fragments. The faster a fragment is stopped, the shorter is the load duration caused by its impact; generally, load durations caused by fragment impacts are in the range of fractions of milliseconds.

Also, since the damage and failure modes differ for different fragment load scenarios the definition of the fragment loading has to be made using a worst-case scenario. Thus, it might be necessary to consider both the load effect of a large single fragment, producing a severe local damage, and a fragment cluster, producing a more uniform damage distribution on the structure, while also resulting in a greater impulse.

In conclusion, due to the great complexity the characterisation of a load caused by fragments is difficult. However, by the use of assumptions unifying the fragment characteristics and empirical relations, pressure-time relations from fragment loading caused by the fictive 250 kg GP-bomb, referred to in Section 3.2.1, are derived; see Figure 3.3. The fragment loading is assumed to derive from relatively small fragments uniformly distributed over the exposed structure; other assumptions and the derivation of the load are presented in Leppänen (2012).

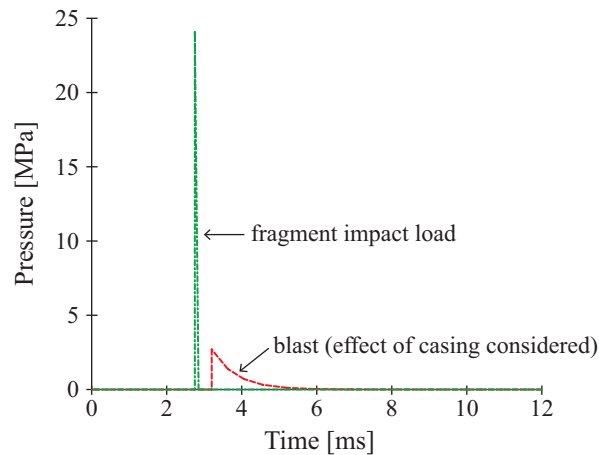


Figure 3.3 Estimated loading from uniformly distributed idealised fragment impacts (cluster) together with the estimated blast load profile from a 250 kg GP-bomb of 50 weight-percent TNT at a stand-off 5 meters.

3.2.3 Combined loading

The combined loading of blast and fragments means that the loads characterised in Sections 3.2.1 and 3.2.2, respectively, are superimposed. Thus, the exposed structure will be subjected to impulse loading from the blast load and impulse and impact loading from the fragments. Despite the high complexity involved in blast and fragment loading, some general conclusions may be drawn:

- Blast wave and fragment impact loading are dynamic loads characterised by their fast transient and high magnitude nature.
- Peak-load amplitude and load duration of both blast and fragment loading are dependent on the properties of the exploding charge and its casing. While the load amplitude decreases for both types of loading, the duration of the blast loading increases and the duration of the fragment loading decreases with increasing stand-off.
- The durations of the loads are in the range of fractions of milliseconds for fragments to tens of milliseconds for blast loads causing high strain rates on exposed structures.
- The initial speed of propagation of the blast and fragment are highly dependent on the type and amount of explosive filling, as well as the thickness and material properties of the casing.
- The relative difference in the time of arrival for the loads is dependent on the initial speed of propagation of the blast and fragments, in addition to the stand-off. The blast wave front has higher initial velocity than the fragments but a more pronounced deceleration as it propagates in the air. Thus, at a close range (within a few meters), the blast load will strike the structure before the fragments, and vice versa.

The response of the exposed structure is highly influenced by the load characteristics and in case of combined loading, the different striking time for the blast and

fragments may also be important. The combined blast and fragment loading from the 250 kg GP-bomb referred to in Sections 3.2.1 and 3.2.2 is shown in Figure 3.3. In this case, the fragment cluster arrives before the blast wave front; thus, the damage caused by the fragment impacts may weaken the structure and greatly influence the response because of the blast load. The effects on the structural response in the event of the combined loading of blast and fragment on reinforced concrete structures are further treated in the enclosed Paper II and Section 3.3.5.

3.3 Load effect on reinforced concrete structures

3.3.1 General

The response of reinforced concrete structures subjected to blast and/or fragment loading may be divided into global and local responses. A global response refers to the overall response of the structure and a global failure means that the structure is unable to withstand further loading. Since the duration of blast and fragment loading is in the range of fractions to tens of milliseconds, which is low in relation to the global structural response period, the structure may be too inert for global response. As the response is constrained to a limited part of the structure, the response is referred to as local. Even though its global response may be highly affected by local failure, the structure may still exhibit load-bearing capacity. However, global and local responses may be defined at different scales; see Figure 3.4. The work presented in this thesis is limited to structures of low complexity and rather represent structural members than entire structures. Thus, global response refers to the global response of a structural member and not to the global response of an entire structure. Similarly, local response refers to the local response of a structural member and not to the local response of an entire structure.

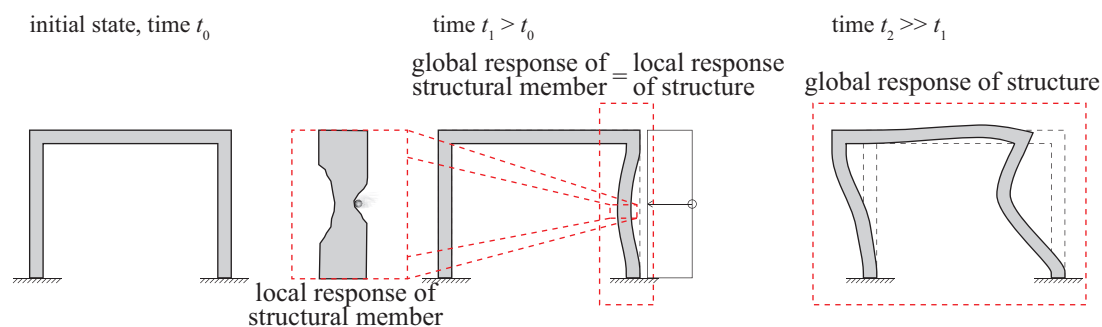


Figure 3.4 Definition of global and local response at different scales of view.

The size of the zone involved in the response is mostly depending on peak load amplitude, rate of loading, area of impact, and the ratio of masses involved in an interaction; Gebbeken *et al.* (2001). In general, blast loading at stand-offs large enough for the load to be considered uniform over the structure will cause a global response. As the stand-off decreases the load becomes more concentrated causing a more localised response. A fragment impact has a local effect on the structure but may also cause global response, especially in case of uniform fragment cluster impact.

3.3.2 Modes of failure

Global failure modes of reinforced concrete structures known from static loading are common also in case of high transient loading. These modes can be generalised to flexural and shear failure, including one or more failure mechanisms in concrete and reinforcement; see Figure 3.5. Flexural failure occurs due to concrete crushing or after the formation of plastic hinges where reinforcement yields and may fracture. Failure may also occur when in-plane deformations are large enough to make the structure slip off its supports. On the other hand, if supports provide sufficient strength and stiffness to resist in-plane displacement of the edges, the load-carrying capacity of the structure may be significantly increased due to membrane action (catenary action). In dynamic loading where inertia effects become significant, membrane action may be activated even for simply supported structures. Shear failure can, as in the case of static loading, occur due to inclined shear cracks related to flexural behaviour; hence such shear failure must be taken into account also in case of severe dynamic loading. However, direct or dynamic shear response is typical of short-duration dynamic loads and is caused by high shear inertia forces, which do not exist under static or low dynamic loading; see ASCE (1999). The direct shear is a local response localised to zones of geometric or load discontinuity but since it affects the overall behaviour of the structural element, it is here still related to global response. This failure occurs early in the structural response before any significant bending deformation takes place, and is therefore not associated with flexure. The phenomenon of direct shear and its emergence are well described by such authors as Krauthammer (2006).

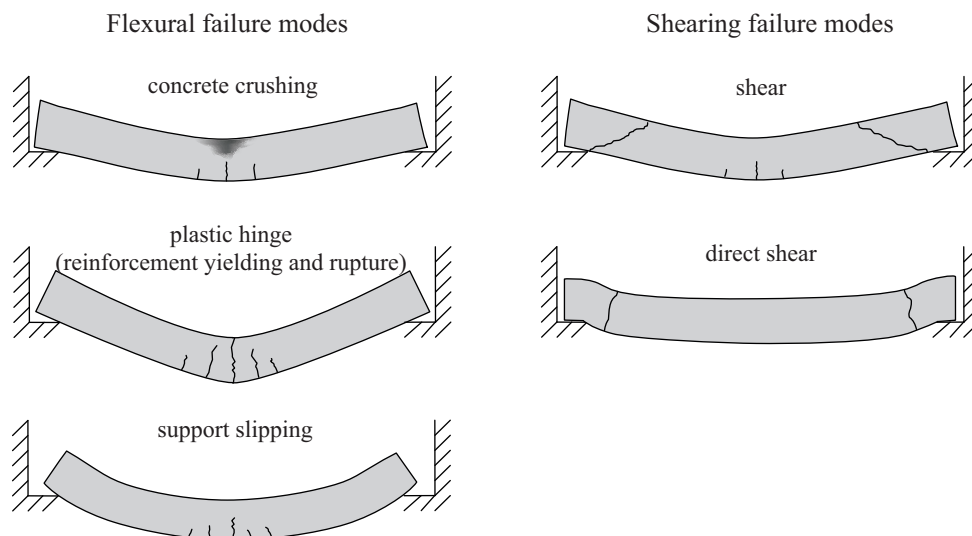


Figure 3.5 Common global failure modes under high dynamic loading of concrete structures.

Close-in detonations may cause propagation of pressure waves in the exposed structure strong enough to cause localised cratering due to the crushing of the front-face concrete and is often referred to as spalling or cratering. As the pressure wave propagates into the concrete, it loses amplitude and energy, limiting the depth of the crater. When the pressure wave reaches the rear face of the structure, it is reflected as a tensile wave on the condition that the bordering medium is of lower impedance.

This tensile wave may cause failure in the rear face region, resulting in a rear face crater, i.e. scabbing. If the front face crater and scabbing zone were merged, the cross-section is breached; see Figure 3.6a.

In case of fragment or projectile loading, the impacting body penetrates the concrete, resulting in crushing the concrete and crater formation, i.e. spalling. In the same way as for close-in detonations, the pressure wave propagating into the structure may also cause scabbing at the rear after having been reflected as a tensile wave at the rear face medium intersection. The depth of penetration of the fragment/projectile depends on its characteristics and the material properties of the target. When the depth of penetration is major in relation to the structure element thickness, plugging may occur. Plugging is the formation of a cone-like crack in front of the penetrator and the potential subsequent punching-shear plug; see Li *et al.* (2005). If the impacting body were to travel through the structural element, perforation occurs; see Figure 3.6b.

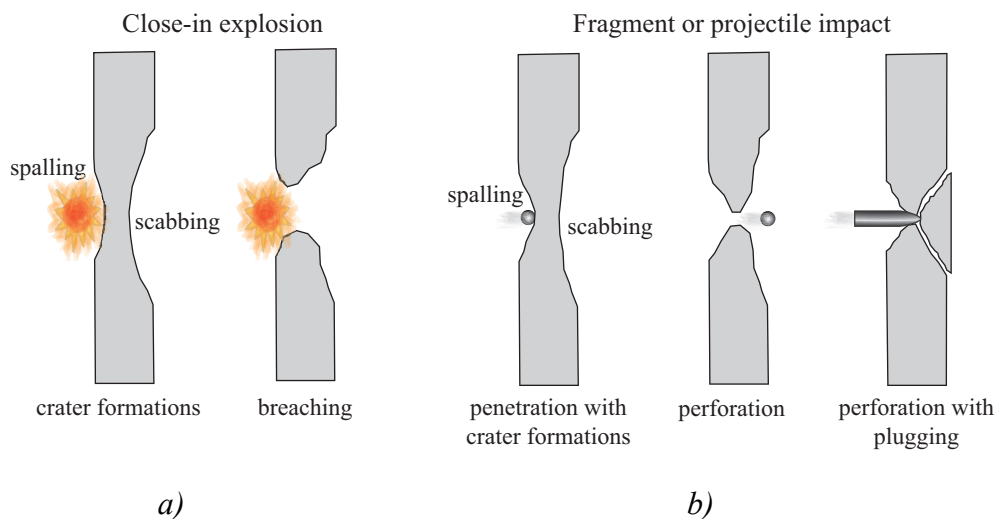


Figure 3.6 Common local failure modes of concrete in case of a) close-in explosion, and b) fragment or projectile impact.

3.3.3 Effect of reinforcement

With regard to global response, the effect of reinforcement is crucial for the energy-absorbing capacity of a concrete structural element, and thereby also its capacity to withstand blast and fragment loading and avoiding structural collapse. A properly reinforced concrete structure ought to have a ductile behaviour.

Local damage does not in general lead to structural failure, and a certain level of local damage is often allowed to occur. However, the damage must still be limited. With close-in blast loading and fragment or projectile impact, where spalling occurs on the front face and possible scabbing craters form at the rear face, the presence of reinforcement bars may limit the damage since they help holding the concrete in place. This is especially true in the case of scabbing, where the amount and placement of reinforcement are highly critical parameters; see Leppänen (2004). With projectile and fragment impacts, the penetrating body may strike the reinforcement, leading to a

decreased depth of penetration and damage of the reinforcement bar and surrounding concrete. The impact on the reinforcement may also lead to local steel rupture, as well as reduced bond between the reinforcement and the concrete further away from the impact point because of vibrations.

A numerical study of how the projectile impact resistance of concrete was affected by the presence of reinforcement and reinforcement detailing was conducted within the scope of the work presented in this thesis; see Nyström and Leppänen (2006). Numerical simulations of projectile impact on reinforced and plain concrete cylinders were carried out where the amount, spacing and dimensions of the reinforcement were varied; see Figure 3.7 and Figure 3.8. It was shown that reinforcement may influence both the depth of penetration and the front-face crater size, and that these effects decreased with a decreasing amount of reinforcement in the damage zone. The increase in impact resistance is plausibly explained by increased confinement effects from the reinforcement. Since the damage caused by a projectile is local, reinforcement bars located further away from the impact area will not influence impact response. This seems logical since the confinement effects of the reinforcement decrease with increasing distance between the projectile path and the reinforcement bar. However, the increased impact resistance due to reinforcement (if a direct hit were disregarded) requires optimised reinforcement detailing. Regarding the global response, the amount and placement of the reinforcement will still be crucial for the load-bearing capacity.

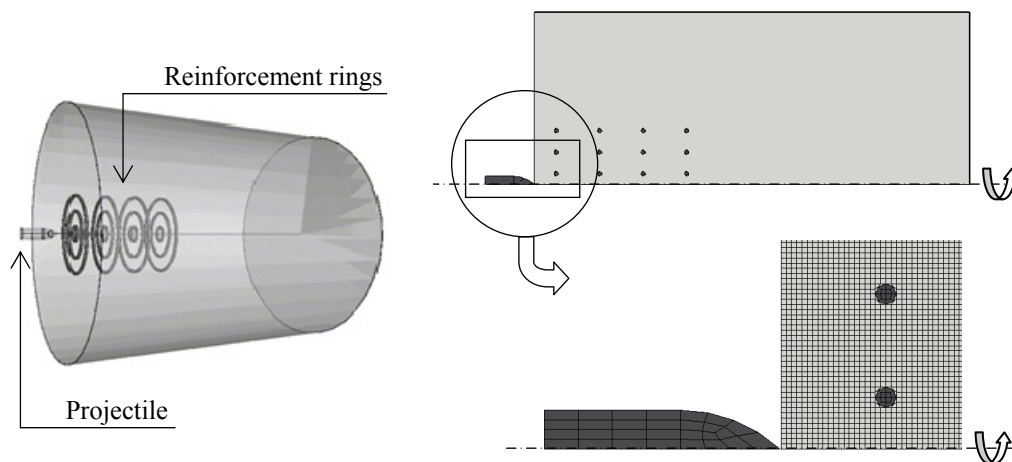


Figure 3.7 Schematic illustration of the numerical model for one of the reinforced concrete cylinders used in the study.

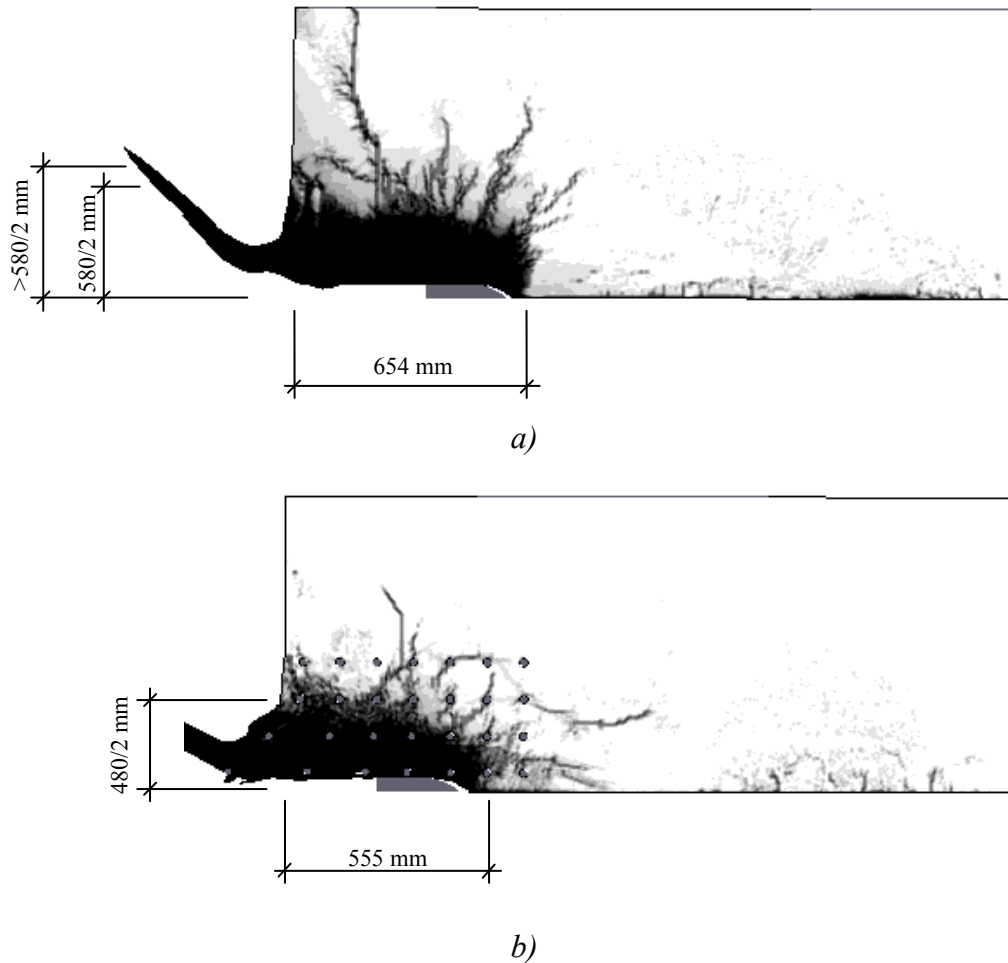


Figure 3.8 Simulation results in the case of a) plain concrete and b) reinforced concrete (4 x 7 reinforcement rings). Black indicates fully damaged concrete and white undamaged concrete.

3.3.4 Effect of steel fibres in concrete on local response

The addition of steel fibres in the concrete has been shown to improve the mechanical properties; Löfgren (2005). According to ACI 544 (1996), the most significant properties of steel-fibre reinforced concrete, compared to plain concrete, are its improved ability to absorb energy, impact resistance and flexural fatigue endurance. However, there are various factors influencing the behaviour of the fibre-reinforced concrete and, consequently, also the degree of improvement, e.g. concrete matrix quality, fibre type (material properties and geometry), bonding between the fibres and concrete matrix, in addition to distribution, orientation and concentration of fibres; see Zollo (1997).

Several experimental studies of the effect of fibres on concrete target impact resistance have been presented, e.g. Ong *et al.* (1999) and Nataraja *et al.* (2005). Since the response depended on material factors as well as test conditions, the conclusions drawn were often case sensitive and lack generality. Due to the limited possibilities to

draw generic conclusions from such studies, a numerical study of the generic effect of adding moderate dosages of steel fibres in concrete in case of projectile penetration was conducted; see enclosed Paper I. It was concluded that the addition of moderate dosages of steel fibres in concrete did not significantly influence the depth of penetration of a striking projectile since this measure only decreased negligibly in the simulations when the effect of fibres were taken into account. The size of both the spalling and possible scabbing crater decreased considerably when steel fibres were added into the concrete; see Figure 3.9. An increased amount of fibres only led to a small reduction of the spalling crater, whereas the effect on the scabbing crater was more significant – it decreased and in one case, it was even prevented.

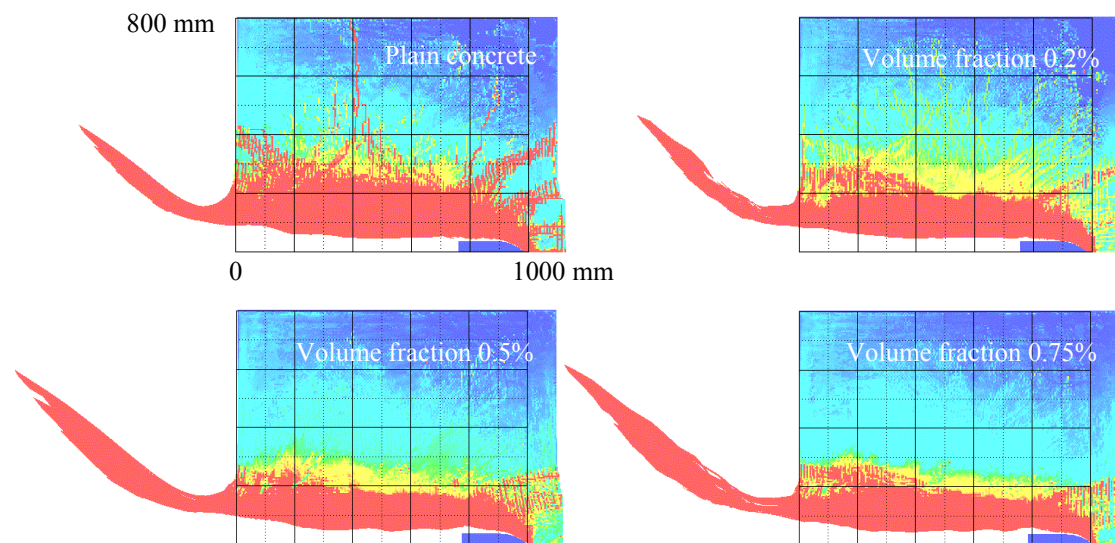


Figure 3.9 Simulation result for plain concrete and fibre-reinforced concrete with volume fractions of 0.2, 0.5 and 0.75%. Projectile impact velocity of 485 m/s. Red indicates fully damaged and blue undamaged concrete.

3.3.5 Effects of combined loading

Combined blast and fragment loading are known to produce a synergetic effect in that the combined loading results in damage greater than the sum of the damage caused by each load treated separately. This effect has been observed in numerous experiments, see Marchand *et al.* (1989, 1992) and Girhammar (1990). However, the complex nature of the loading and response, and variations in experimental set-ups and documented test results makes it difficult to draw general conclusions about the phenomena involved from these experiments.

The enclosed Paper II presents a numerical study of the synergetic effects connected with blast and fragment loading. Since complexity makes it difficult to interpret results, the loads and structure used in the numerical study was of purely academic character and did not represent an existing case in reality. However, both the definition of the structure and loads were based on the requirements of physical protection against conventional weapons for civil-defence shelters in Sweden

according to MSB (2011). The numerical models used correspond to a reinforced concrete structure subjected to three different load conditions; blast load, fragment cluster impacts, and a combination of these two. In case of combined loading, the blast wave front and fragments were assumed to strike the structure simultaneously.

Figure 3.10 shows the response of the structure at a time of maximal deflection for the three different loading cases. In case of blast loading (Figure 3.10a), the response was characterised by damage localised to a relatively low number of flexural cracks, even though the initiation of flexural cracks had occurred relatively densely along the rear face. In case of fragment loading (Figure 3.10b), besides the formation of flexural cracks, spalling cratering and scabbing crack formation occurred; see also Figure 3.11. The cracks indicated as initial flexural cracks in Figure 3.11 were formed prior to other flexural cracks. Since the spalling craters, the scabbing cracks and the initial flexural cracks were formed early in the response during the initial phase of the global deflection, the flexural behaviour and damage pattern were highly influenced and a large number of flexural cracks was formed. In the case of combined loading (Figure 3.10c), the response was highly influenced by fragment impacts and the overall damage was very similar to that achieved during fragment loading alone, albeit more severe. It was also concluded that the maximal mid-point deflection in case of combined loading was larger than the sum of mid-point deflections for blast and fragment loading treated separately; the superposition of the deflections is not applicable which indicates a synergy effect in combined loading. The large difference of top surface deformations observable in Figure 3.10b and c, may be a consequence of the concrete being held in place by the blast load.

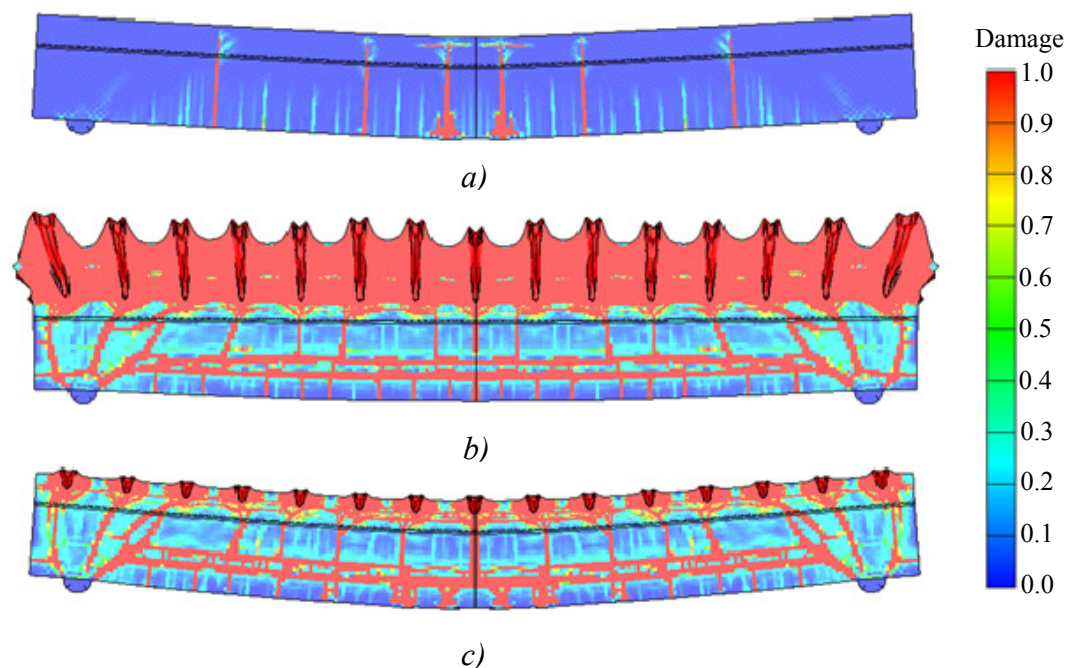


Figure 3.10 Response of reinforced concrete structure exposed to a) blast loading, b) fragment impacts and c) combined blast and fragment loading.

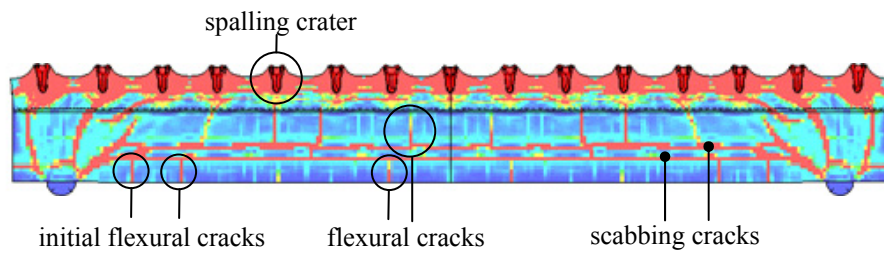


Figure 3.11 Clarification of damage modes shown for early stage response to fragment loading.

4 Dynamic aspects of wave propagation

4.1 General

Blast and fragment loadings are related to high strain rates in the exposed structure, which due to inertia and wave propagation effects may greatly influence the response both along material and structural scales. Figure 4.1 shows a categorisation of different problem aspects related to strain rates in the loaded structure. The figure is based on data from different publications: Bischoff and Perry (1991), Field *et al.* (2004), Gebbeken and Ruppert (2000), Ramesh (2008), and Zukas (2004).

In the discipline of mechanics, ‘statics’ refers to physical systems in static equilibrium where the state (e.g. load and deformation) is time independent and therefore constant. However, for many solids exposed to long-term loads creep and stress relaxation are known phenomena that affect the state of the system and make it time dependent. Quasi-static loading refers to conditions where the loading is performed at a rate fast enough not to produce effects of creep and relaxation but slow enough for dynamic effects to be negligible. For higher strain rates, the dynamic effect of inertia can no longer be ignored and the effects of structural dynamics such as vibrations may be of great concern. As the strain rate increases further, the effect of wave propagation becomes a problem i.e. assumptions from static and low dynamic mechanics may no longer be enough to describe the behaviour. It is important to note that there are no distinct borders between the different aspects, but rather overlapping zones where both views must be considered.

The strain rate in a structure exposed to transient loading is a function of time, and strain rates below peak strain rate will develop if sufficiently long time scales are considered. In case of impact and contact detonation, the peak strain rate may be as high as 10^6 s^{-1} and 10^8 s^{-1} , respectively; Ramesh (2008) and Gebbeken and Ruppert (2000). However, the strain rate decreases and most of the deformation takes place at lower strain rates. In case of blast loading, the peak strain rate is generally lower. Thus, even though the strain rate in a structure exposed to blast and fragment loading may be lower on a longer time scale, it is often related to strain rates in the range of 1 and 10^6 s^{-1} , with most of the damage occurring in the lower range.

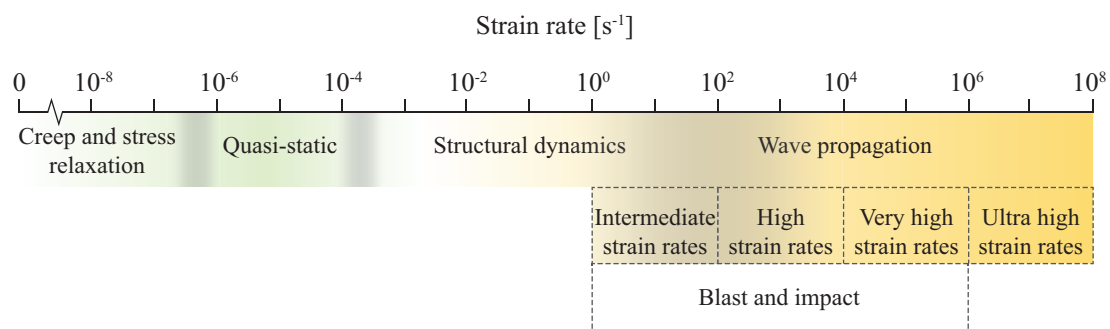


Figure 4.1 Strain rates and associated problem aspects.

4.2 Inertia and wave propagation effects

In fact, wave propagation in the material occurs for all strain rates since information on the applied load is transported through the material by stress waves. These waves propagate with the local speed of sound, which in concrete is about 3 500 m/s. In the case of quasi-static loading, the duration of the load is long compared to the time it takes for multiple wave reflections throughout the structure to take place; see Figure 4.2a. This means that the waves and their propagation do not have to be explicitly considered in this case. For shorter load durations, causing strain rates in the intermediate to high strain-rate regime, induced waves may not have the time to reach all parts of the structure before deformation is initiated in areas close to the applied load resulting in a different structural response than in the corresponding quasi-static case. This means that even though it remains a structural dynamic problem, wave propagation influences the response the effects of which might become important. In the very high and ultra-high strain-rate regimes, the loading may be so fast that most deformation takes place before the waves have reached other parts of the structure causing highly localized damage; see Figure 4.2b, where the ball impacts the beam at a high velocity. These high-rate phenomena are to be considered wave propagation problems and structural dynamics may be of secondary interest.

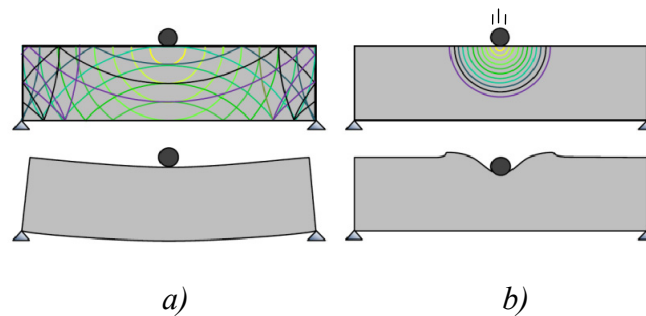


Figure 4.2 Schematic illustration of wave propagation and associated structural response for a) quasi-static loading and b) very high strain rate loading.

At a material scale, the highest strain rate-regimes lead to conditions closer to uniaxial strain rather than uniaxial stress since the material does not have the time to deform laterally, i.e. producing an inertial effect. This means that for high strain rates, the lateral stresses may be considerably high and a confining pressure may build up also for uniaxial loads, which would produce a condition of uniaxial stress in the material if the load came to be applied at a low rate. Since strain rates in the case of blast and fragment loading may reach levels in the high and very high strain-rate regimes they are related to very high confining pressures, thereby potentially exceeding material uniaxial strength by several orders of magnitude; Zukas (2004). These high pressure levels may hence cause severe damage and/or phase transformations in the material.

The stress waves propagating in a solid material may be elastic or plastic depending on the magnitude of the load and material strength. However, due to high strain rates and subsequent high pressure levels, plastic waves may transform into shock waves. These shock waves constitute compressive stress waves with extremely short rise times, propagating in the material and formed as a consequence of dispersion, an

effect arising in media with nonlinear compressive behaviour and further described in Section 4.3.2. Shock waves are likely to develop in materials with strain rate levels of above 10^5 s^{-1} ; Haddad (2000).

4.3 Shock waves

4.3.1 Introduction

A shock wave is by definition a compressing disturbance propagating in a medium faster than the speed of sound at ambient conditions. Further, it is characterised by its abrupt, nearly discontinuous, change in material characteristics: density, pressure and temperature. Due to this abruptness, the change of state is a non-equilibrium thermodynamic process which may highly influence the state reached after the shock transition. In Figure 4.3, a shock disturbance propagating into a stationary medium featuring pressure p_0 , density ρ_0 , and specific internal energy e_0 is schematically shown. The disturbance is travelling at a speed U_s which is higher than the speed of the piston, U_p , causing the disturbance. Behind the shock, the material reaches a new thermodynamic material state featuring pressure p , density ρ , and specific internal energy e . The material behind the shock disturbance also gains a particle velocity, u_p (which is equal to the velocity U_p of the piston), and the material is travelling in the same direction as the shock disturbance.

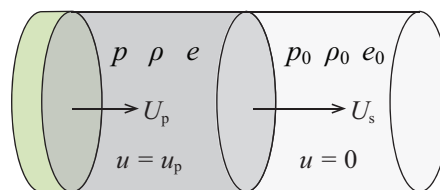


Figure 4.3 One-dimensional shock transition in medium imposed by piston.

The treatment of shock waves is not intended to be complete in this thesis, for the reader interested in a comprehensive treatment of the subject, the literature by Zel'dovich and Raizer (1966, 1967), Asay and Shahinpoor (1993), and Meyers (1994) are recommended.

4.3.2 Shock wave formation

As mentioned in Section 4.2, stress waves propagate in the material with the local speed of sound, which is proportional to the adiabatic compaction modulus, i.e. the inclination of the compaction curve. A nonlinear compaction curve, therefore, results in waves which propagate at different speeds at different levels of pressures. Shock waves are formed when faster components overtake earlier induced waves of lower propagation speed; i.e. a dispersion effect. However, since the compressibility of mediums is related to atomic and molecular interactions it is strongly dependent on

the characteristics of the medium. Fundamental distinctions can be made between the compressive behaviour of gases, liquids and solids.

In general, the average distances between particles in gases are much greater than the particle dimensions, and the interaction between the atoms (or molecules) takes place mainly through collisions. Since temperature is related to the mean translational kinetic energy of its constituent particles, the pressure in gases is of thermal origin. In fluids and solids, however, the constituent particles are sufficiently close to cause interactive forces. These forces are of dual character, attractive and repulsive. In the absence of external pressure, the attractive and repulsive forces are in balance and the constituent particles have a certain equilibrium distance. If the particles separate, the attractive (binding) forces increase and when brought together, the particles repel each other and the repulsive forces increase; Zel'dovich and Raizer (1967). Since these repulsive forces rapidly increase as the atoms are brought together, the compressibility decreases with increasing pressure, yielding a non-linear compaction curve.

Even though the cohesive forces between atoms and molecules in liquids hold the particles together, the temporary character of the bindings allows the particles to move around each other, thereby allowing the medium to flow. Fluids in general exhibit some resistance to flow, i.e. resisting shearing and tensile forces, which is a measure of fluid viscosity. However, compared to solids, the shear resistance of fluids is generally of negligible size. The binding forces between atoms and molecules in solids are rigid and as long as bindings are intact flow is prevented. The shear strength of a solid is thus depending on such factors as the interatomic and molecular type of bonding which can be one or a mixture of covalent, ionic, metallic or van der Waals bindings.

Thus, if viscosity is neglected, even though it is loaded in only one direction, the pressure in fluids is equal in all directions. However, contradictory to fluids, solid matter exhibit considerable shear strengths and a non-hydrostatic component of stress may exist which affects the conditions for shock wave formation.

Figure 4.4 shows the effect of dispersion responsible for the shock wave formation in the case of high rate uniaxial compressive loading from pressure p_0 to p_1 of an idealised fluid. The increase of pressure leads to a change of specific volume, v , from initial state v_0 to final state v_1 , where the specific volume is defined as $v = 1 / \rho$, and ρ represents the density of the medium. From left to right the figure shows: the pressure-time relation for the external load, the compaction curve of the medium in the pressure-specific volume plane, and profiles of the compression waves propagating in the medium at different times t and distances away from the external load, respectively. The compression modulus K (which is proportional to the square of the local sound speed c) is indicated as the tangent of the compaction curve for different states. In the wave profiles, the speed of different wave components is indicated by arrows. Initially, the compressive waves are propagated at the ambient wave speed related to pressure p_0 . As the pressure increases, the gradient and thus propagation speed increases and waves are initiated that propagate faster than the previously induced waves, leading to a superposition of slower wave packages by faster ones. Thus, the gradual steepening of the initial simple compression-wave profile leads to the formation of a shock wave. Due to the continuous decrease of compressibility for increasing pressure levels in idealised fluids, all simple

compression waves will steepen up to form a shock wave when the load is applied fast enough for the later induced wave packages to catch up with the previous ones before the wave has been damped, reflected or affected in other ways.

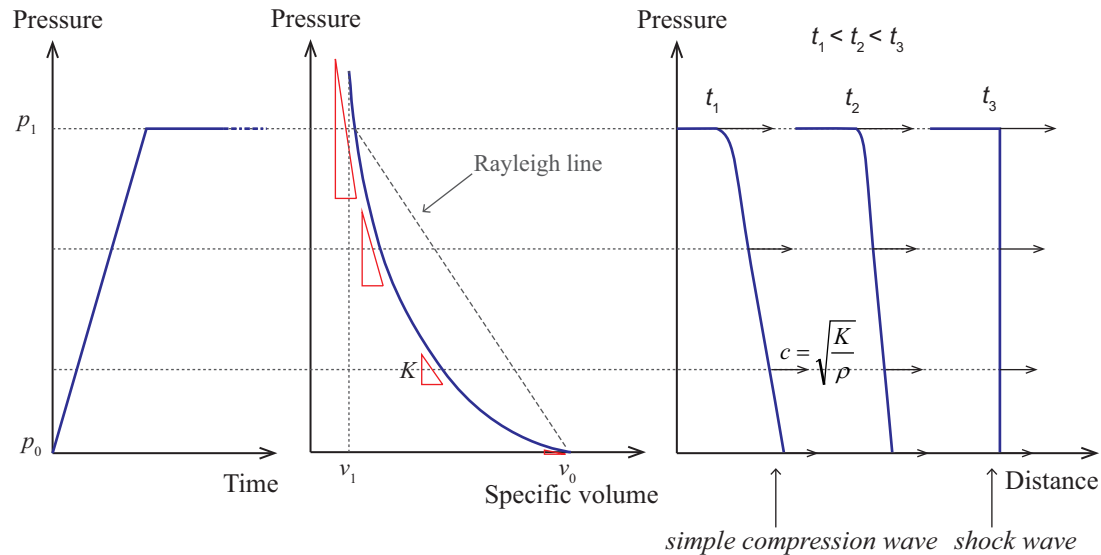


Figure 4.4 Schematic illustration of shock wave formation in idealised fluid; from left to right: loading curve, compaction curve and wave front steepening and subsequent shock front formation, partly based on Hiermaier (2008)

The line referred to as a Rayleigh line in Figure 4.4 represents the process path in the material state transition from the initial state during shock loading and is further explained in Section 4.3.3. The incline of this line is related to the propagation speed of the shock front in the same way as the compression modulus is related to the local speed of sound, i.e. the more inclined, the faster the propagation.

Due to the strength of solids and their effect on the uniaxial strain compression curve, the conditions of shock wave formation in this matter is different from that of an ideal fluid. In Figure 4.5, the influence of strength on the compaction curve for a perfectly elastic-plastic solid material (left) and the subsequent effect on shock wave formation (right) are schematically shown. As seen in the compaction curve (where the axial and volumetric stress components are shown), the influences of the deviatoric stress component are:

- The rate of stress with volume is higher in the elastic range, compared to hydrostatic conditions.
- When the elastic limit is reached (in shock loading called the Hugoniot Elastic Limit (HEL)), the stress-strain curve shows a change in slope, i.e. the stiffness is suddenly reduced.
- The sudden stiffness reduction is followed by a continuous increase of stiffness.
- For low stresses the relative influence of the deviatoric strength on total stress is considerably high, but decreases with increasing stress.

Thus, as opposed to fluids, solid materials exhibit considerable shear strengths and the non-hydrostatic part of the stress state during uniaxial strain conditions must be considered. However, for high pressure levels the rigidity of the atomic and molecular bindings is reduced due to fractures, thereby limiting shear resistance. For very high pressure levels, the deviation from isotropic compression may thus be small compared to the pressure level and hydrodynamic treatment (assuming that the solid material has no resistance to shear) may be applied also for solids; Meyers (1994).

One consequence of the deviatoric stress component and the HEL is that an elastic precursor may be formed; for materials with a considerably high HEL, the wave may consist of two discontinuities rather than one; see Figure 4.5. For pressure levels below the HEL, elastic waves will propagate in the material at the speed of sound for the initial state. Pressures above the HEL will cause the formation of a steep plastic wave front, but since the elastic portion of the wave propagates faster, an elastic precursor is formed. The shock wave will thus not only feature one steep front, but rather two. For pressures exceeding a certain pressure (indicated as σ_1 in Figure 4.5), the speed of the plastic wave front will exceed the propagation speed of the elastic part, i.e. one steep wave front is formed. The existence of an elastic precursor is often defined as the difference between a weak and a strong shock wave.

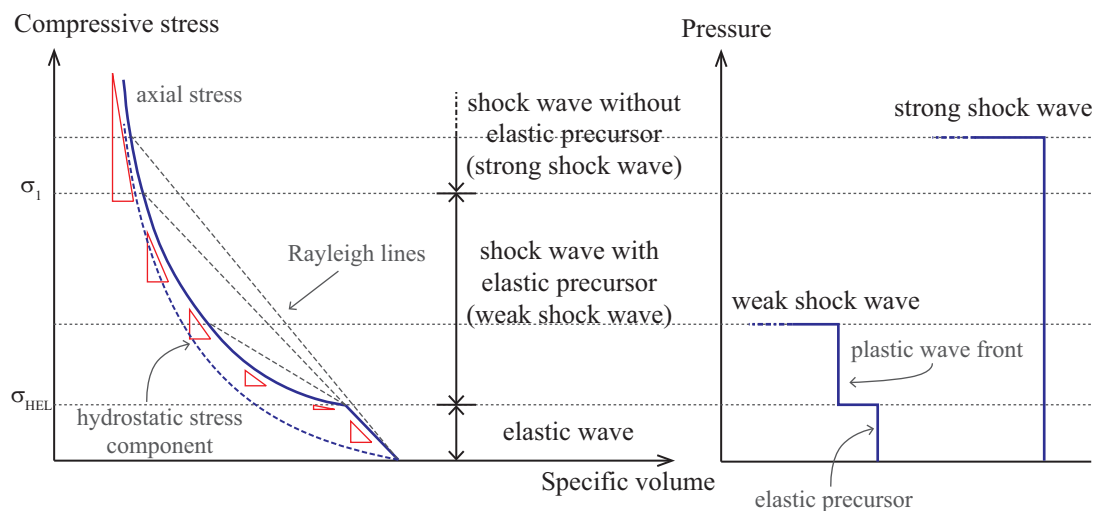


Figure 4.5 Schematic effect of shear strength on compaction curve and shock wave fronts in solid matter.

However, the variation of material characteristics in solid materials is large and the compression curve may show great complexity and differ from the idealised behaviour shown in Figure 4.5. For concrete and similar materials with inherent brittleness and porosity, there is a pressure range above the HEL across which the gradient of the compression curve does not increase and it may even decrease; see Figure 4.6. If the magnitude of the load is within this range ($\sigma_{HEL} < \sigma < \sigma_2$ in Figure 4.6), a shock wave will not form since the speed of the wave portions induced at lower pressure levels will propagate at the same speed (or even faster) than the wave portions induced at higher pressure levels. Instead, a simple elastic-plastic wave will propagate.

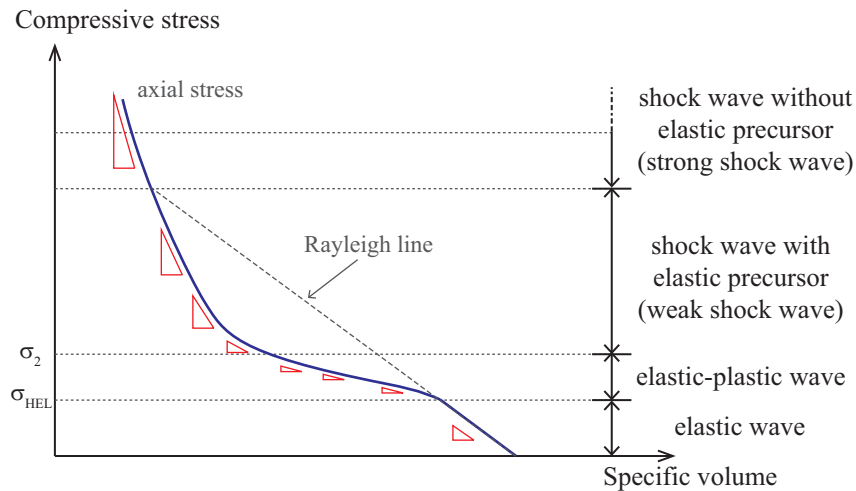


Figure 4.6 Conditions for shock wave formation in brittle porous solid.

4.3.3 Shock transition – a thermodynamic processes

As is the case involving all other state changes, shock transition is a thermodynamic process, i.e. a change in the thermodynamic state of the material due to a change of energy within the system, i.e. due to the flow of mass, heat transfer and/or performance of work. A thermodynamic state can be specified by state variables; properties that only depend on the current state and not the path to get there. Typically used state variables include pressure, volume, and temperature. However, volume and temperature are sometimes replaced by density and internal energy (or entropy), respectively, since these properties are related. Thermodynamic processes can be characterised by the constancy of a particular state variable such as pressure (isobaric process), volume (isometric process), temperature (isothermal process), entropy (isentropic process) or enthalpy (isenthalpic process). For shock transition, however, the process is only characterized by the existence of a shock wave and no thermodynamic state variables remain constant. Instead, the shock transition may be considered as adiabatic irreversible thermodynamic process:

- Adiabatic because the loading time for shocks is short in relation to the inertial material response, and the heat transfer is therefore kept minimal.
- Irreversible since the process involves dissipation of energy (i.e. a generation of entropy).

Thus, even though the passage of the wave may be considered adiabatic (no transfer of heat from or into the system), the transition is non-isentropic (part of the work applied to the system is converted into thermal energy) and the temperature increases. The increased temperature during shock transition is sometimes referred to as shock heating. However, as stated above, this heating is not attributed to a heat exchange between the shocked material and the surrounding but is rather a consequence of energy dissipation effects within the material as it is compressed.

All thermodynamic equilibrium states reachable by a medium are represented by a three-dimensional surface, including the phase transformations schematically shown

in Figure 4.7 (left). Thermodynamic processes are then represented as curves connecting the initial and final states of these transitions. Even though thermodynamic states are defined by at least three state variables, e.g. pressure, volume and temperature, thermodynamic processes are often graphically presented in two-dimensional pressure-volume graphs. Such graphs project three-dimensional curves representing the paths followed during the processes on the pressure-volume plane; see Figure 4.7 (right). The areas beneath the curves in the pressure-volume plane represent energies related to work performed during the process.

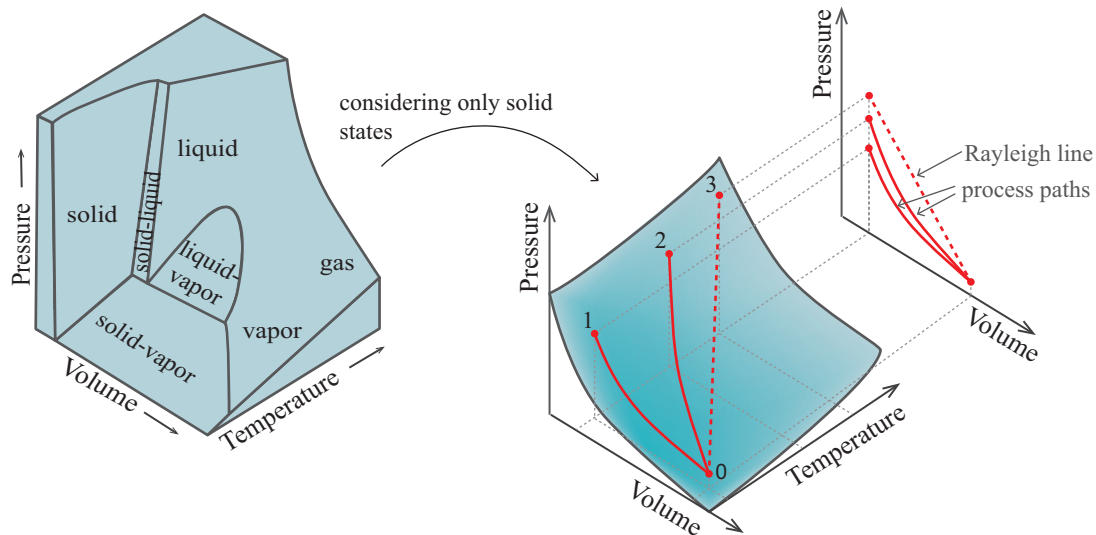


Figure 4.7 Thermodynamic equilibrium surface (left) and equilibrium surface in solid states with process paths from initial state (0) to final states (1), (2) and (3) (middle), and projection of the process paths on pressure-volume plane (right), partly based on Çengel and Boles (2006).

In quasi-static loading, the process is assumed to be slow enough to prevent inhomogeneity (e.g. temperature and pressure gradients) within the system. Thus, the states between the initial and final states are assumed to be in thermodynamic equilibrium, i.e. the path followed during the thermodynamic transition is on the equilibrium surface. Since the process is slow, heat caused by energy-dissipation mechanisms has the time to flow to the surroundings if this is not prevented, thereby causing an isothermal process (indicated by curve 01 in Figure 4.7). If this heat flow would be prevented, the temperature would increase. Thus, since the process is still slow, the process path would lie on the equilibrium surface, but since it has a higher temperature for the same volume than the isothermal process state, the pressure would be higher in this case; see curve 02 in Figure 4.7.

However, in dynamic processes the transitions are fast enough to cause inhomogeneity in the system, i.e. the system is not in thermodynamic equilibrium during the entire process, representing a non-equilibrium process. The representation of the process path between the initial and final states is, therefore, not well defined. In the case of shock wave loading, a thermodynamic equilibrium is achieved only at the initial and final states (state 0 and 3 in Figure 4.7), and the process is often represented by a straight (in Figure 4.7 dashed) line, referred to as the Rayleigh line.

Considering state transitions due to the shocks from different pressure magnitudes, from an initial state (p_0, v_0, T_0) in a material, the Hugoniot curve (also referenced as the Rankine-Hugoniot curve, or simply the Hugoniot) appears. Thus, the Hugoniot curve is the locus of all states (p, v, e) which may be obtained through the shock transition of a material from a given initial state (p_0, v_0, e_0) . It is important to note that the Hugoniot curve does not represent the path of states through which material progresses when transitioning from the initial state (p_0, v_0, e_0) to the final state (p, v, e) . Such a path, as mentioned above, is instead represented by the Rayleigh line. The meaning of the Hugoniot curve and the Rayleigh line is schematically shown in Figure 4.8.

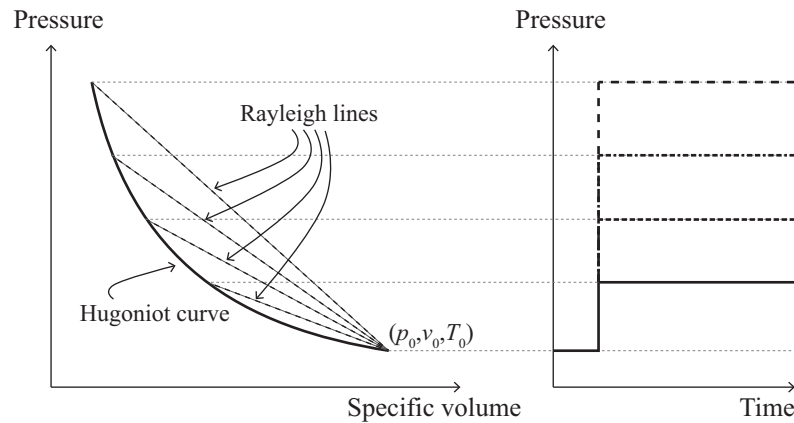


Figure 4.8 Schematic illustration of the Hugoniot curve and Rayleigh lines (left) and associated load curves (right).

4.3.4 Rankine-Hugoniot jump conditions

The conservation equations of mass, momentum and energy may be used to express relations between the state variables of the initial and final states of a thermodynamic process. In the event of a discontinuous transition between two states, as in a shock transition, these equations are called the Rankine-Hugoniot jump conditions, relating the state variables ahead of a shock front with the one behind it. The Rankine-Hugoniot jump conditions are often expressed as in equations (4.1) to (4.3); variables are described in Section 4.3.1.

$$\text{Conservation of mass:} \quad \rho_0 U_s = \rho (U_s - u_p) \quad (4.1)$$

$$\text{Conservation of momentum:} \quad p - p_0 = \rho_0 U_s u_p \quad (4.2)$$

$$\text{Conservation of energy:} \quad e - e_0 = \frac{U_s^2}{2} - \frac{(U_s - u_p)^2}{2} + \frac{p_0}{\rho_0} - \frac{p}{\rho} \quad (4.3)$$

If equations (4.1) to (4.3) were combined, the Hugoniot equation may be derived. This equation is a version of the energy equation, i.e. equation (4.3) above, but is free from any velocity terms and represents the relationship between the thermodynamic state variables alone. The Hugoniot equation is:

$$e - e_0 = \frac{1}{2}(p + p_0) \left(\frac{1}{\rho_0} - \frac{1}{\rho} \right) = \frac{1}{2}(p + p_0)(v_0 - v) \quad (4.4)$$

However, the above equations are independent of material and in order to quantify the change of state variables during the transition, characteristic material descriptions have to be known.

With a graphical representation of the Hugoniot equation, the change in specific internal energy ($e - e_0$) is represented by the area beneath the Rayleigh line; see Figure 4.9. The change in specific kinetic energy is represented by the triangular area above the Rayleigh line. If the effect of the initial pressure p_0 can be neglected, the change in specific internal energy equals the change in specific kinetic energy.

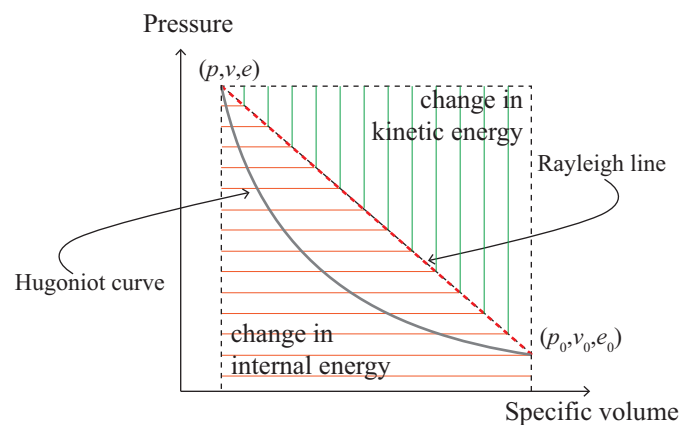


Figure 4.9 Graphical representation of the change in internal energy and kinetic energy in shock transition.

4.3.5 Release from shocked state

The release from a shocked state can be assumed to be isentropic, i.e. the decrease of temperature will be less than the increase during the shock transition. For a medium which does not undergo plastic compaction, the material state upon release back to initial pressure will be characterised by a higher temperature and thus a larger volume (dilation) due to thermal expansion, compared to the initial state; see Figure 4.10. For solids which undergo severe plastic compaction during the shock transition, thermal expansion and plastic compaction counteract each other. According to Boslough and Asay (1993), if the strains are considered minor, the release isentrope may be approximated by the Hugoniot curve of the initial state. Since the strains are large and irreversible, this is, however, not applicable in the case of plastic compaction.

It is also worth pointing out that since wave components corresponding to higher pressures will travel faster than those of lower pressures, release waves can never take on the characteristics of a shock wave .

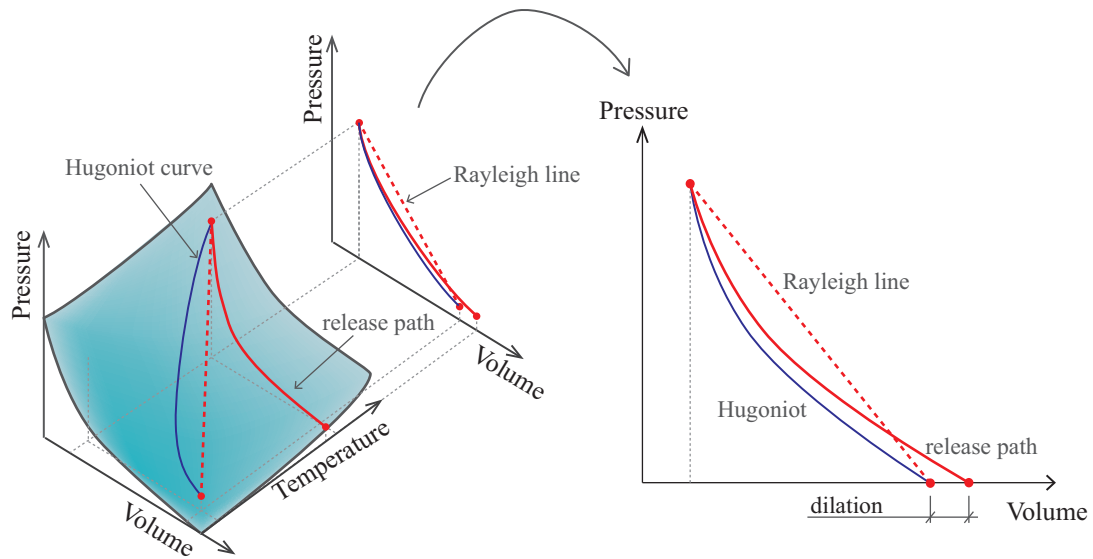


Figure 4.10 Schematic illustration of release path from shocked state, and the effect of dilation due to shock heating.

5 Numerical modelling at high dynamic loading

5.1 Introduction

Numerical simulations of high dynamic phenomena such as blast and fragment loading of structures, grow more common and nowadays constitute important additions to physical testing. The use of numerical approaches is, among other things, motivated by the opportunity to reduce the cost of parameter studies, which are important to increase the understanding of the behaviour and phenomena involved. Another advantage motivating the use of numerical simulations to study the effects of high dynamic loading is the opportunity to monitor the response through the process, which is limited in the case of testing.

As stated in Chapters 2 to 4, blast and fragment loading is related to short loading durations resulting in wave propagation effects, high stress levels, large strains, and nonlinear material behaviour. These phenomena place additional demands on the solver techniques used in numerical simulations.

A group of numerical tools used for simulations of phenomena involving high pressures caused by shock or impact is the so-called hydrocodes, also referred to as “wave propagation codes”. The denotation “hydrocode” originates from “hydrodynamic computer code” which may be explained by the fact that in the early states of these codes, only hydrodynamic material behaviour was assumed, i.e. the material of matter was assumed to behave as a fluid with no viscosity, thus, no resistance to shear forces. Under this assumption, the response of a material can be described by means of the conservation equations of mass, momentum and energy together with an “Equation of State” for the material. Later, in the development of the hydrocodes, the possibility of describing shear resistance of materials was included, to account for the behaviour of solids at low and moderate stresses. This behaviour is relevant also in the case of strong shock wave loading, e.g. in the field afar and subsequently in the close field as well.

The general approach used in hydrocodes is, therefore, to separate the stresses and strains into hydrostatic and deviatoric portions which tend to change the volume of the element and to distort it, respectively. This means that for solids, the hydrostatic behaviour is still described by an Equation of State and that an accompanying constitutive model is necessary to describe the relation between deviatoric stresses and strains. This constitutive model is sometimes referred to as the “strength model”. Models describing the material behaviour in one constitutive model, i.e. without splitting the stresses and strains into volumetric and deviatoric parts, are available in some hydrocodes. In order to describe the plastic compaction caused by isotropic (i.e. hydrostatic) compression, these models sometimes include a cap function, the effect of which is to close the yield surface against the hydrostatic axis. Even though theoretically possible, these models do not generally include thermal effects, as many Equation of States do.

5.2 Solution techniques

5.2.1 Numerical solution

In order to determine the distribution of stresses and strains in a structure, it is necessary to solve a boundary value problem, defined by partial differential equations derived from the conservation of mass, momentum, and energy, respectively, together with a set of boundary conditions. Often these calculations are far too complex for finding analytical solutions and instead numerical techniques are used to approximate the solution. However, before any solution of the boundary value problem is sought, the physical problem has to be idealised. This often includes:

- limitation and idealisation of the geometrical domain,
- idealisation of boundary conditions including for example loads, surface contacts, symmetry planes and connections to other parts of the physical domain, and
- the idealisation of material behaviour to allow for mathematical descriptions thereof, i.e. the formulation of constitutive laws for the material.

After the idealisation, the numerical solution is approached by establishing weak forms of the differential equations and by discretisation of the idealised spatial domain by a finite element, a finite difference or a finite volume method. This discretisation arrives at a system of ordinary differential equations which may be solved by numerical integration.

For static problems, the effects of dynamics are neglected and the forces of inertia and damping, respectively, are set to zero. For dynamic problems, these effects must be considered in order to produce accurate results and the solution becomes time dependent demanding time integration methods.

For non-linear dynamic problems, direct time integration methods are required to solve the boundary value problem. The direct integration methods are commonly classified into two groups: implicit and explicit methods. Implicit methods are known to yield high accuracy as equilibrium is imposed at each time step. In general, these methods are also unconditionally stable, with no limits existing on the size of the time step to fulfil the accuracy. However, these methods are costly for highly non-linear problems since they require iterations to find this equilibrium and generally also require that the inverse of the stiffness matrix is calculated for each such iteration. In explicit time integration methods, on the other hand, it is assumed that if small enough steps are taken, it is accurate enough to use the equilibrium from the last time step to solve the current time step even though this means that no strict equilibrium is imposed. Therefore this group of methods is conditionally stable, limiting the size of the time step. Consequently, an exceedingly large number of time steps may be necessary to achieve accurate results, but no iteration process is necessary to find the equilibrium. Also, in contrast to the implicit method, the inverse of the mass matrix is calculated instead of the inverse of the stiffness matrix. Therefore, an explicit time integration method is commonly used to integrate the governing equations for problems involving high geometrical and material non-linearity and short time durations.

5.2.2 Lagrange solver

Even though the average engineer probably associates numerical modelling of structural responses with Lagrangian elements – where the numerical mesh moves and distorts along with the material, there are often several other solver techniques available in hydrocodes. Among these techniques are Euler, ALE (Arbitrary Lagrange Euler) and SPH (Smooth Particle Hydrodynamics). The most obvious difference between the Lagrange and the other solver techniques mentioned is the rigid coupling between the material and the numerical mesh. Contradictory to the Lagrange solver, the numerical mesh in a Euler solver is fixed in space and the material moves in and between the mesh elements; see Figure 5.1. The ALE technique can in a simplified manner be said to use the Lagrange solver with continuous rezoning of the spatial volume and the SPH is a mesh-free solver technique.

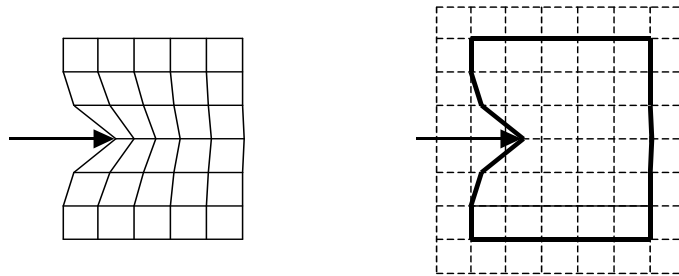


Figure 5.1 The Lagrangian description (left) and the Eulerian description (right) for material movement, from Leppänen (2004).

Only a brief description of the numerical techniques of Lagrange is provided since it was used in the numerical studies presented in enclosed Papers I, II and IV. The choice to use the Lagrange solver is in these cases based on e.g. the opportunity to follow history dependent material behaviour.

However, for a Lagrange solver, distortion of the mesh may lead to inaccurate and ineffective solutions. Since explicit time integration is used, the size of the time-step must be limited in order to achieve stable solutions; see Section 5.2.1. The maximum time-step allowed is often defined as a function of the minimum length of an element or its equivalent. For a contracting element, the time-step decreases which may cause extended computational time. In a Lagrangian mesh the positions, velocities, and material accelerations for an element are defined at the element nodes situated in element corners. Material quantities such as pressure, density, internal energy, stress and strain deviators and temperature are, on the other hand, defined by centred differencing at element-zone centres. Due to accuracy losses in the centred differencing, an element with a high aspect ratio, i.e. a large difference in the length of its sides, may lead to a loss of solution accuracy. To overcome these numerical problems, rezoning or erosion algorithms may be used. Rezoning means that the distorted mesh is remapped onto a new, more regular mesh. Erosion algorithms normally remove elements if a pre-defined strain exceeds a specified limit.

A simplified illustration of the Lagrange computational cycle with explicit time integration of the boundary value problem is shown in Figure 5.2. Each cycle starts

with updating the boundary and/or interactive forces, which are then combined with the internal forces calculated during the previous time cycle to estimate the nodal forces. The nodal accelerations are then evaluated by use of the momentum equation (i.e. equation of motion). Thus, the acceleration is calculated by means of the internal force of the previous time step. Explicit time integration, generally the central difference time integration or a modified version thereof, is used in hydrocodes to calculate nodal velocities and displacements from the assumed nodal accelerations. By direct calculation, element volume and strains (or strain rates) are calculated. One or more constitutive laws, i.e. material models, are then used to calculate stresses in the material. For nonlinear material behaviour, numerical integration is necessary for the constitutive law (local level). The integration method used at the local level may, however, be different from the method used for the boundary value problem (global level). When the stresses have been calculated, the internal forces are updated by using the momentum equation, these forces are to be used in the following time cycle. Thus, equilibrium for the momentum equation is not imposed and it is assumed that the solution is sufficiently accurate for minor time steps.

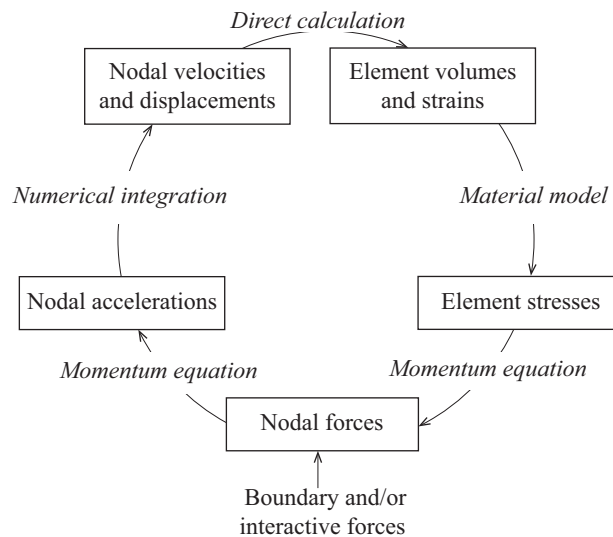


Figure 5.2 Lagrange computational cycle; based on AUTODYN (2005).

5.2.3 Material modelling

Numerical solutions to boundary value problems in stress analyses require mathematical descriptions of the material behaviour, often referred to as constitutive laws or material models. Correct approximations of the material behaviour under the applicable loading conditions are essential to ensure the quality of the numerical representations of the real behaviour. Accordingly, the material models used for the analyses must be accurate enough within the applicable loading conditions to capture crucial phenomena in the material.

As mentioned in Section 5.1 a general approach to material modelling used in hydrocodes is to divide the total stress tensor $\boldsymbol{\sigma}$ into a volumetric part $\boldsymbol{\delta}\sigma_v$ and a deviatoric part \mathbf{s} , respectively, as:

$$\boldsymbol{\sigma} = \boldsymbol{\delta}\sigma_v + \mathbf{s} \quad (5.1)$$

Two different constitutive laws are then used to describe the material behaviour; an Equation of State and a strength model, describing the volumetric and deviatoric behaviours, respectively. The Equation of State is thus a mathematical representation of the thermodynamic equilibrium states that can be reached in a material. There are many different forms of Equation of States proposed in the literature, which are applicable in different situations. Generally they relate the thermodynamic state variables of the material, i.e. the pressure p , density ρ (or specific volume v , or compaction μ), and temperature T (or specific internal energy e). Heat conduction and other effects that require the variable temperature is not always of interest nor relevant to the analysis. The Equation of State is, therefore, often defined as a function of the specific volume, or density, or compaction, and the specific internal energy;

$$p = p(v, e), \text{ or } p = p(\rho, e), \text{ or } p = p(\mu, e) \quad (5.2)$$

in which

$$p = -\sigma_v \quad (5.3)$$

and

$$v = \frac{1}{\rho} \quad \text{and} \quad \mu = \frac{\rho}{\rho_0} - 1 \quad (5.4)$$

The forms of Equation of States shown in equation (5.2) are called incomplete, in contrast to those involving the temperature. As stated in Section 4.3, the processes involving shock transition are so fast that there is no time for heat conduction effects to develop which is why incomplete Equation of States may be used in these situations.

An Equation of State for a solid material is often too complex to be analytically derived, at least for high pressures. Thus, it is common to construct the Equation of State by means of an empirically determined Hugoniot curve, i.e. a reference Hugoniot. Since the energy distribution within the experiment is unknown, it is impossible to construct a full three-dimensional Equation of State empirically. However, by using the conservation equation for energy, or the Hugoniot equation (see Section 4.3.4) the change of internal energy may be implicitly considered, and a Hugoniot curve in the three-dimensional thermodynamic space is achieved. An assumption of the equilibrium states surrounding the determined Hugoniot curve allows for a theoretical extension and the derivation of a three-dimensional equilibrium surface. The Grüneisen parameter Γ (sometimes referred to as Grüneisen gamma) provides such an extension used in e.g. the Mie-Grüneisen Equation of State:

$$p = p_{\text{ref}} + \Gamma(v)\rho(e - e_{\text{ref}}) \quad (5.5)$$

where p_{ref} is a reference curve for which the relation between the reference pressure and the specific volume is given, i.e. $p_{\text{ref}} = p_{\text{ref}}(v)$ and e_{ref} is an estimated value of the internal energy at the initial state, i.e. $e_{\text{ref}} = e(p_0, v_0, T_0)$.

However, as stated in Section 4.3.2, the pressure in an idealised fluid is of pure thermal origin while in a solid, it is mainly dependent on interatomic (or molecular) forces. Thus, the variation of pressure in a fluid is described by the variation of specific internal energy, while its contribution to the pressure in a solid does not become considerable until higher pressure levels are reached. Thus, the Equation of States for solids are sometimes reduced to $p = p(v)$. Practically, the hydrostatic behaviour of the material is given explicitly via the material input parameters and the only variation from this behaviour may be if the hydrostatic pressure were assumed to be a function of the temperature.

In general, there are several forms of Equations of States available in hydrocodes; the suitable form differs according to different materials and phenomena. In Appendix A, brief descriptions of the Linear, Polynomial, Mie-Grüneisen and P - α Equation of States are given. The Polynomial and Mie-Grüneisen Equation of States are widely used for the mathematical description of the volumetric behaviour of solids in high dynamic loading. For porous materials where considerable plastic pore compaction may occur, the general P - α Equation of State (Herrmann, 1969) is often used to take into account the effects of the porosity.

For solid materials, where in contrast to fluids the shear strength is considerable, the Equation of State has to be accomplished by a strength model. Such a model describes the material resistance to distortion and thus the size of the deviatoric stress tensor \mathbf{s} . Commonly used theories in strength modelling include the plasticity and damage mechanics or combinations thereof. A fundamental assumption in the classical theory of plasticity is that plastic deformation is isometric, i.e. volume is preserved. According to Khan and Huang (1995) and Lubliner (2008), this assumption was made after experimental observations which established that even at exceedingly high hydrostatic pressure, volume change is only reversible, thus indicating only elastic volume change. Thus, following this theory, the yield surface should be open towards the hydrostatic axis.

Nevertheless, since materials undergoing irreversible compaction do not fit under this assumption, this is a subject of discussion. While plasticity is related to inelastic deformation due to dislocation processes in the microscopic theory of materials, it may be interpreted as any type of permanent deformation of the material in macroscopic continuum mechanics. Thus, from a macroscopic point of view, plasticity theory is applicable in describing irreversible volume changes and the yield surface may be closed towards the hydrostatic axis. Accepting this point of view would allow the volumetric behaviour to be described by moving the yield surface along the hydrostatic axis, the approach in so-called cap models. In these models, the total stress tensor is calculated by means of one constitutive model alone, and a cap is used on the yield surface to close it towards the hydrostatic axis. The movement of the yield surface is then described by a hardening law. Even though it is theoretically possible, cap models do not generally consider the influence of temperature explicitly.

Damage to the material can be described in different ways but in general terms, it is described by a damage parameter D used to scale the effective stress and goes from

$D = 0$ (undamaged material) to $D = 1$ (fully damaged material). In the case in which the total stress tensor is divided into a volumetric and a deviatoric part, equation (5.6) is used to calculate the stress. In a cap model, however, the common approach is described in equation (5.7). In these equations, $\boldsymbol{\sigma}$ and $\bar{\boldsymbol{\sigma}}$ are the nominal and effective stress tensors, σ_v and $\bar{\sigma}_v$ are the nominal and effective volumetric stresses, D is the damage parameter and $\bar{\mathbf{s}}$ is the effective deviatoric stress tensor.

$$\boldsymbol{\sigma} = \delta \sigma_v + (1 - D) \bar{\mathbf{s}} \quad (5.6)$$

$$\boldsymbol{\sigma} = (1 - D) \bar{\boldsymbol{\sigma}} = (1 - D) \delta \bar{\sigma}_v + (1 - D) \bar{\mathbf{s}} \quad (5.7)$$

5.2.4 Large strain and stress theory

Since phenomena involved in high transient dynamic loading are related to high stress levels and large strains, the otherwise common approximation of infinitesimal strain theory and engineering stresses are no longer valid which is why the theory of large strains and true stress must be used. In numerical solver tools developed to model the behaviour of large strain and high stress phenomena, the true measures of strains and stresses are used, i.e. $\varepsilon_{\text{true}}$ and σ_{true} . However, since experimental data are often presented in engineering measures ($\varepsilon_{\text{engineering}}$ and $\sigma_{\text{engineering}}$), conversion may be necessary to provide correct material model input data and make fair evaluations of the validity of the model. The conversion between engineering and true strains and stresses are shown in equation (5.8) and (5.9), respectively; for derivation of the equations, see Appendix B.

$$\varepsilon_{\text{true}} = \ln(\varepsilon_{\text{engineering}} + 1) \quad (5.8)$$

$$\sigma_{\text{true}} = \sigma_{\text{engineering}} (1 + \varepsilon_{\text{engineering}}) \quad (5.9)$$

5.3 Material models for concrete

5.3.1 Background

The fidelity of the numerical results is highly dependent on the ability of the material models to realistically describe the behaviour of the material under blast and impact loading. A number of material models for concrete subjected to high dynamic loading have been developed over the years. These models often use one or more features from well-known concrete material models developed for simulations with static or low transient loading, e.g. Drucker and Prager (1952), William and Warkne (1975), Ottosen (1979), Osborn (1982), and Chen (2007), which are adapted and complemented to take into account material behaviours connected to high transient loading. The model proposed by Chen was published in 1982, but here it refers to the republication of the original work.

Even though concrete generally is considered to be a brittle material, allowing relatively minor deformations before failure, the plastic portion of this deformation is relatively large compared to the elastic portion, at least for compressive stress states. If the concrete were also laterally confined, the plastic deformations prior to failure were further increased. Thus, theory of plasticity, by which irreversible deformations can be described, is useful for describing the hardening behaviour. However, when concrete reaches its ultimate strength, it shows softening with decreased capacity to carry loads with increasing deformations. During this softening, the unloading stiffness of concrete is also reduced. This behaviour cannot be described by a plasticity model which is why it is often accomplished by a damage mechanics model. Thus, theories of plasticity and damage mechanics are often combined to describe the behaviour of concrete and most concrete material models developed for high dynamic loading generally take into account pressure hardening, strain hardening and strain rate dependence. However, the level of complexity, robustness and generality differs between the models. The simplest models often have the advantage of requiring a smaller number of model-input parameters, but are limited to special load cases where the complexity is low. The more complex material models are to a higher extent capable of describing the varying concrete material behaviours under different and more complex loading conditions, but at the cost of requiring a higher number of model parameters.

One of the earliest complex material models for dynamically loaded concrete is the Johnson-Holmquist-Cook (JHC) concrete model developed in 1993; Johnson *et al.* (1993). Soon thereafter, Malvar *et al.* (1994) developed a concrete material model for DYNA3D. This model has experienced several stages of modifications, leading to three different versions of the model (Malvar *et al.* 1994, 1997, and Magallanes *et al.* 2010), of which the third version is available in LS-DYNA (2012) as the Concrete Damage Model (material type #72). This model is sometimes referred to as the Karagozian and Case (K&C) Concrete Model.

Towards the end of the 1990's, two new concrete material models for hydrocode simulations were developed separately by Riedel (2000) and Ruppert and Gebbeken (2000). Both models were implemented in AUTODYN, but only the former was implemented in the commercial version of the program where it was named the RHT model. Since version 971 R5.1, LS-DYNA also includes the RHT model (as material type #272); LS-DYNA (2012) and Borrvall and Riedel (2011).

Several modifications of the RHT model have been proposed since the implementation in AUTODYN. Schuler (2004) and Leppänen (2004) worked simultaneously on enhancements to the tensile softening law in the RHT model, and in the latter reference also the function describing the strain rate effect on the tensile strength was changed to a more realistic one. In 2010, Zhenguang and Yong (2010) proposed modifications of the residual strength surface used in the RHT model. They also proposed modifications of the tensile softening law and the strain rate dependency of tensile strength but these seem to be the same as was already proposed by Leppänen (2004).

The Ruppert-Gebbeken model has been a source of inspiration for further enhanced models. In 2004, Greulich (2004) developed the RGGP model for concrete, similar to the Ruppert-Gebbeken model, but more generalised to also be able to describe the behaviour of concrete with low or moderate dosages of steel fibres.

Hartmann *et al.* (2010) developed an enhanced material model called the HPG model for concrete which combines modelling approaches from several previously mentioned material models, including the JHC, K&C, RHT and RGGP models. The HPG model also provides new formulations for dynamic strength increase, as well as damage and degradation of material strength with damage.

All above mentioned models used for simulations of high dynamic events are constructed in such a way that the stress tensor is divided into a hydrostatic and a deviatoric part. Examples of another approach described in Section 5.2.3, i.e. cap models, are the Geological CAP model (material type #25), the Schwer Murray Cap model (material type #145), and the Continuous Surface Cap Model (CSCM) (material type #159), all implemented in LS-DYNA; see Schwer and Murray (1994), Murray (2007) and LS-DYNA (2012). The two latter cap models in LS-DYNA are modifications of the former. Even if possible, the contraction and expansion of the yield surface in these cap models is not related to the internal energy (or temperature), i.e. the hydrostatic pressure is not a function of the thermal energy, as is often the case when an Equation of State is used.

However, of the previously mentioned enhanced material models developed for concrete subjected to high dynamic loading, only the K&C, the RHT, and the various cap models are implemented in the commercial versions of the hydrocodes LS-DYNA and/or AUTODYN which means that the availability of the other models is limited for program users. Furthermore, these material models are often based on a large number of parameters, which are not always directly linked to physical quantities and are, therefore, difficult to determine. For some material models, however, default values of input-parameters are provided, with the user only having to specify a limited number of the input parameters required. However, since input parameters may influence several physical phenomena, it is difficult to enhance the models for taking into account new loading conditions and material properties.

Clearly, many existing material models for concrete provide good results for the loading cases for which they were developed. Nevertheless, their lack of versatility raises the demand for constitutive models for the dynamic failure of concrete, which are easy to extend and are based on input parameters of physical significance. In the work presented in Papers I and II, the RHT model was used to simulate the response of concrete due to impact or/and blast load. Limitations to modify and adapt the model to new material and loading conditions were observed. With these factors in mind, a “new” model was developed. The theoretical build-up of the RHT model is provided in Section 5.3.2; for further details on the model, Riedel (2000) and Riedel *et al.* (2009) are recommended. A detailed description of the “new” model, the CDPM2, is provided in Chapter 6 and appended Papers III and IV.

5.3.2 RHT model

5.3.2.1 Introduction

The RHT model is based on the concept of dividing the total stress tensor into a volumetric and a deviatoric part, respectively. These parts are then calculated by means of two different constitutive relations; an Equation of State and a strength

model (see Section 5.2.3), with the RHT model representing the latter. However, even though the Equation of State is not defined in the RHT model, it is often associated with the use of a P - α Equation of State, with a Polynomial or Mie-Grüneisen Equation of State for the description of the compaction behaviour of the non-porous, matrix material; see Appendix A.

In the RHT model, theories of plasticity and damage mechanics are combined to calculate the deviatoric stress tensor \mathbf{s} . The model is, however, described in terms of the pressure p , the equivalent stress σ_{eq} , and the Lode angle θ , defined according to:

$$p = -\frac{I_1}{3} \quad (5.10)$$

$$\sigma_{\text{eq}} = \sqrt{3J_2} \quad (5.11)$$

$$\theta = \frac{1}{3} \arccos\left(\frac{3\sqrt{3}}{2} \frac{J_3}{J_2^{3/2}}\right) \quad (5.12)$$

where I_1 , J_2 and J_3 represent the first invariant of the stress tensor $\boldsymbol{\sigma}$, and the second and third invariants of the deviatoric stress tensor \mathbf{s} , as:

$$I_1 = \boldsymbol{\sigma} : \boldsymbol{\delta} \quad (5.13)$$

$$J_2 = \frac{1}{2} \mathbf{s} : \mathbf{s} \quad (5.14)$$

$$J_3 = \frac{1}{3} \mathbf{s}^3 : \boldsymbol{\delta} \quad (5.15)$$

These are then related to the principal deviatoric stress tensor according to:

$$\begin{bmatrix} s_1 \\ s_2 \\ s_3 \end{bmatrix} = \frac{2}{3} \sigma_{\text{eq}} \begin{bmatrix} \cos(\theta) \\ \cos(\theta - \frac{2\pi}{3}) \\ \cos(\theta + \frac{2\pi}{3}) \end{bmatrix} \quad (5.16)$$

The equivalent stress is calculated based on the effective equivalent stress $\bar{\sigma}_{\text{eq}}$ and a scalar damage parameter D , ranging from 0 (undamaged material) to 1 (fully damaged material), and $\bar{\sigma}_{\text{eq,residual}}$ which represents a residual (frictional) stress capacity in the fully damaged material; see equation (5.17). The effective equivalent stress is calculated by the plasticity part of the model and the damage parameter by the damage part of the model.

$$\sigma_{\text{eq}} = (1 - D)\bar{\sigma}_{\text{eq}} + D\bar{\sigma}_{\text{eq,residual}} \quad (5.17)$$

The plasticity part of the model is defined to give an initial elastic phase and linear yield-surface hardening before damage is initiated. The yield surface is pressure dependent and takes into account triaxiality (i.e. reduced strength on shear and tensile meridians compared to the compressive meridian) and strain rate dependence. By the option to use a smooth cap function, the yielding surfaces prior to damage initiation

may be closed towards the hydrostatic axis. The strain driven damage model is used to initiate damage and describe the linear evolution of damage for increasing plastic strains. The damage model describes the increased post-peak ductility for increasingly confining pressures.

Brief descriptions of the theoretical build-up of the plasticity and the damage part of the model are provided in Sections 5.3.2.2 and 5.3.2.3, respectively. However, the structure of the description differs from the common one (in e.g. Riedel, 2000 and Riedel *et al.* 2009), which is more focused on the three limit surfaces schematically shown in Figure 5.3 (left), than on the description in a more classical sense of the different model constituents. In Section 5.3.2.4, some known limitations of the RHT model are discussed.

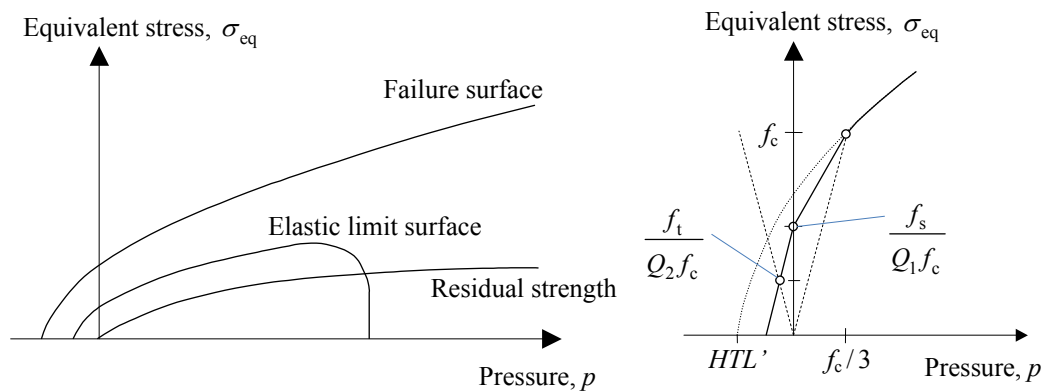


Figure 5.3 Schematically shown surfaces used in the RHT constitutive model (left), from Leppänen (2004), and behaviour of the failure surface for low hydrostatic pressures (right), based on Riedel (2000).

5.3.2.2 Plasticity part

The main components of the plasticity part are the yield function, the flow rule, the hardening law, and the evolution law of the hardening variable.

Yield function

The yield function:

$$f_p(\bar{\sigma}_{eq}, \bar{p}, \bar{\theta}, \dot{\epsilon}, \kappa_p) = \bar{\sigma}_{eq} - Y_{fail}(\bar{p}, \bar{\theta}, \dot{\epsilon})q(\kappa_p) \quad (5.18)$$

depends on the effective stress (through $\bar{\sigma}_{eq}$, \bar{p} and $\bar{\theta}$), the failure surface Y_{fail} , and a dimensionless variable q , which describes the evolution of the yield surface during hardening by means of the hardening variable κ_p . The failure surface, in equation (5.18) is described by means of the pressure sensitive compressive meridian Y_{TXC} representing the limit states under stress conditions of $\sigma_1 < \sigma_2 = \sigma_3$, the Rubin function $R_3(\bar{\theta})$, and a factor $F_{rate}(\dot{\epsilon})$ representing the dynamic increase factor at the strain rate $\dot{\epsilon}$.

$$Y_{\text{fail}}(\bar{p}, \bar{\theta}, \dot{\varepsilon}) = Y_{\text{TXC}}(\bar{p}) R_3(\bar{\theta}) F_{\text{rate}}(\dot{\varepsilon}) \quad (5.19)$$

The compressive meridian on the failure surface, $Y_{\text{TXC}}(\bar{p})$, is described by means of a power function:

$$Y_{\text{TXC}}^*(\bar{p}^*) = A(\bar{p}^* - HTL'^*)^N \quad (5.20)$$

where $*$ indicates that the values are normalised with respect to the uniaxial compressive strength f_c . However, since this function does not represent the behaviour of concrete for low and negative pressure levels ($\bar{p}^* < 1/3$), a piecewise linear function is used to describe the compressive meridian in this pressure range; see Figure 5.3 (right). In this figure, the meaning of the auxiliary variable HTL' , which is used just to provide continuity to the point of ultimate compressive strength is illustrated as well. This variable can be calculated as:

$$HTL'^* = \frac{1}{3} - \sqrt[N]{\frac{1}{A}} \quad (5.21)$$

To create the three-dimensional failure surface, the compressive meridian is rotated around the hydrostatic axis under the influence of the Rubin function $R_3(\bar{\theta})$ describing the variation of strength in relation to the strength of the compressive meridian, i.e. the shape of the deviatoric section. The Rubin function is:

$$R_3(\bar{\theta}) = \frac{2(1 - Q_2^2)\cos \bar{\theta} + (2Q_2 - 1)\sqrt{4(1 - Q_2^2)\cos^2 \bar{\theta} + 5Q_2^2 - 4Q_2}}{4(1 - Q_2^2)\cos^2 \bar{\theta} + (1 - Q_2^2)^2} \quad (5.22)$$

where:

$$0.5 \leq Q_2 = Q_{2,0} + B_Q \bar{p}^* \leq 1.0 \quad (5.23)$$

F_{rate} in equation (5.19) represents the ratio of the dynamic and static strength, for the strain rate $\dot{\varepsilon}$. This ratio, i.e. the dynamic increase factor, is calculated according to CEB (1988), but only the expression normally used for lower strain rate regimes is used in the model. Thus, the model only describes the moderate increase of strength and not the strong increase seen in material testing at higher strain rate levels (see Section 2.2.2). However, the strength increase is differentiated for tension and compression, and F_{rate} is calculated according to:

$$F_{\text{rate}} = \begin{cases} \left(\frac{\dot{\varepsilon}}{\dot{\varepsilon}_0}\right)^{\alpha_{\text{RHT}}} & \text{with } \dot{\varepsilon}_0 = 30 \cdot 10^{-6}, \alpha_{\text{RHT}} = \frac{1}{5 + \frac{3}{4} f_c} \quad \text{for } \bar{p} > \frac{f_c}{3} \\ \left(\frac{\dot{\varepsilon}}{\dot{\varepsilon}_0}\right)^{\delta_{\text{RHT}}} & \text{with } \dot{\varepsilon}_0 = 3 \cdot 10^{-6}, \delta_{\text{RHT}} = \frac{1}{10 + \frac{1}{2} f_c} \quad \text{for } \bar{p} < \frac{-f_t}{3} \end{cases} \quad (5.24)$$

In between the pressures $f_c/3$ and $-f_t/3$ the function F_{rate} is linearly interpolated.

Flow rule

The flow rule used in the RHT model is non-associative in the meridional plane, and associated in the deviatoric plane so that plastic strain increments are calculated by radial return. Thus, the plastic equivalent strain increase is calculated as the difference between the trial effective equivalent stress $\bar{\sigma}_{eq}^{tr}$, and the effective equivalent stress after plastic return, and the shear modulus G as:

$$\Delta \varepsilon_{eq}^{pl} = \frac{\bar{\sigma}_{eq}^{tr} - \bar{\sigma}_{eq}}{3G} \quad (5.25)$$

and the total plastic equivalent strain can be expressed as:

$$\varepsilon_{eq}^{pl} = \frac{\bar{\sigma}_{eq} - Y_{elastic}}{3G} \quad (5.26)$$

where $Y_{elastic}$ is the initial yield surface defined below.

Hardening law

The variable q in equation (5.18) is a function of the hardening variable κ_p and describes the evolution of the yield surface during hardening according to:

$$q(\kappa_p) = \begin{cases} \frac{Y_{elastic} + \kappa_p (Y_{fail} - Y_{elastic})}{Y_{fail}} & \text{if } \kappa_p < 1 \\ 1 & \text{if } \kappa_p \geq 1 \end{cases} \quad (5.27)$$

Thus, for $\kappa_p \geq 1$ the yield surface, described by the yield function in equation (5.18) will equal the failure surface Y_{fail} . For $\kappa_p = 0$, the failure surface would equal the initial yield surface, $Y_{elastic}$, limiting the elastic behaviour of the material. The elastic limit surface, expressed in equation (5.28), is scaled from the failure surface via a factor $F_{elastic}$, representing the elastic stress normalised with the ultimate stress as shown in equation (5.29). In between these pressure levels, linear interpolation is used to calculate $F_{elastic}$. The elastic limit surface may also be closed towards the hydrostatic axis by use of a factor F_{cap} which describes a smooth cap surface through the function shown in equation (5.30), where p_{el} is related to the elastic limit defined in the Equation of State and p_s is the pressure for which all pores have collapsed.

$$Y_{elastic}(\bar{p}, \bar{\theta}, \dot{\varepsilon}) = Y_{fail}(\bar{p}, \bar{\theta}, \dot{\varepsilon}) F_{elastic}(\bar{p}) F_{cap}(\bar{p}) \quad (5.28)$$

$$F_{elastic}(\bar{p}) = \begin{cases} \frac{f_{t,elastic}}{f_t} & \text{for } \bar{p} < \frac{-f_{t,elastic}}{3f_t} \\ \frac{f_{c,elastic}}{f_c} & \text{for } \bar{p} > \frac{f_{c,elastic}}{3f_c} \end{cases} \quad (5.29)$$

$$F_{\text{cap}}(\bar{p}) = \begin{cases} 1 & \text{for } \bar{p} \leq \bar{p}_s = \frac{f_c}{3} \\ \sqrt{1 - \frac{\bar{p} - \bar{p}_s}{\bar{p}_0 - \bar{p}_s}} & \text{for } \bar{p}_s < \bar{p} < \bar{p}_0 \\ 0 & \text{for } \bar{p} \geq \bar{p}_0 = \bar{p}_{\text{el}} \end{cases} \quad (5.30)$$

Hardening variable

The hardening variable is defined as:

$$\dot{\kappa}_p = \frac{\dot{\varepsilon}_{\text{eq}}^{\text{pl}}}{\varepsilon_{\text{eq}}^{\text{pl,hard}}} \quad (5.31)$$

where $\varepsilon_{\text{eq}}^{\text{pl}}$ is the increase of equivalent plastic strain defined in equation (5.26), and $\varepsilon_{\text{eq}}^{\text{pl,hard}}$ is a measure of the plastic strain at peak shear strength, defined in equations (5.32). In this equation G is the elastic shear modulus and $G/G_{\text{elasto-plastic}}$ is an input parameter defining the ratio of elastic and elasto-plastic shear modulus. The geometrical meaning of $\varepsilon_{\text{eq}}^{\text{pl,hard}}$, G , and $G_{\text{elasto-plastic}}$ are shown in Figure 5.4.

$$\varepsilon_{\text{eq}}^{\text{pl,hard}} = \frac{Y_{\text{fail}} - Y_{\text{elastic}}}{3G} \left(\frac{G}{G_{\text{elasto-plastic}}} \right) \quad (5.32)$$

This yields a linear hardening from the initial yield surface Y_{elastic} to the final yield surface Y_{fail} .

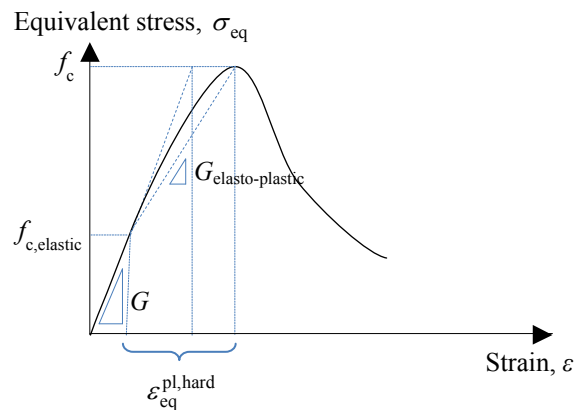


Figure 5.4 Geometrical meaning of $\varepsilon_{\text{eq}}^{\text{pl,hard}}$, G and $G_{\text{elasto-plastic}}$ in uniaxial compression, based on Riedel (2000).

5.3.2.3 Damage part

The strain driven damage model is based on the damage formulation in the Johnson-Holmquist-Cook model (Johnson *et al.*, 1993) and is used to initiate damage and calculate the damage parameter D . Damage is initiated as the plastic equivalent strain $\varepsilon_{\text{eq}}^{\text{pl}}$ equals $\varepsilon_{\text{eq}}^{\text{pl,hard}}$, i.e. when the yield surface is equal to the failure surface. The evolution of the damage in incremental form is:

$$D = \sum \frac{\Delta \varepsilon_{\text{eq}}^{\text{pl}}}{\varepsilon_{\text{eq}}^{\text{pl,fail}}(\bar{p})} \quad (5.33)$$

where $\varepsilon_{\text{eq}}^{\text{pl,fail}}(\bar{p})$ is the ultimate strain and a function of pressure, with increased ductility for increasing pressure; see equation (5.34). However, the value of the ultimate strain is limited to a minimum value $efmin$, given as an input to the model.

$$\varepsilon_{\text{eq}}^{\text{pl,fail}}(\bar{p}) = D_1 (p^* - HTL^*)^{D_2} \geq efmin \quad (5.34)$$

The residual surface Y_{fric} , with which the residual equivalent strength $\bar{\sigma}_{\text{eq,residual}}$ of the fully damaged material ($D = 1$) is described, is described as:

$$Y_{\text{fric}}(\bar{p}) = B \bar{p}^M \quad (5.35)$$

This surface is, as opposed to the yield surfaces, not dependent on the strain rate or the Lode angle.

5.3.2.4 Limitations

The RHT model uses a linear softening curve but according to Jirásek (2006) a linear softening curve can only be used for rough approximations, motivating modification of the RHT model to more accurately describe this behaviour. Again referring to Jirásek (2006), the Hordijk-Reinhard expression (also described in e.g. van Mier 1984) provides the best fit to experimental results but is relatively complicated. This fact may justify the use of a simpler relation, such as an exponential or bi-linear crack-softening law, which still usually gives results with good accuracy.

A hydrodynamic tensile-failure model is used by default in the RHT material model, i.e. if the value of the hydrodynamic pressure in a cell would fall below a specified limit, tensile failure is assumed to occur. However, a fracture energy cannot be specified for this model and since the failure strain, at which no more stresses can be transferred, is constrained from being smaller than $efmin$, the fracture energy may be underestimated for large elements; see Nyström (2008). It is also not possible to use a modified crack-softening description of this tensile-failure model. In AUTODYN it is possible to use a principal stress tensile-failure model together with the RHT strength model, thereby providing the possibilities of specifying the fracture energy and of modifying the tensile failure behaviour. However, the use of a principal stress tensile-failure model entails that the strain-rate dependence of the tensile strength defined in the RHT strength model is no longer activated. Within the numerical study described

in Paper I, trials were made to reintroduce this strain-rate dependence by employing a user-subroutine. However, these trials failed due to the emergence of stability problems, see Paper I and Nyström (2008).

Leppänen (2004) developed a modified crack-softening behaviour in the RHT material model and used the bi-linear softening curve proposed by Gylltoft (1983). Leppänen (2004) also modified the tensile strain-rate dependence of the RHT model to better fit experimental data found in the literature. The modified strain-rate dependence was introduced in a user-subroutine, which, as previously mentioned, was not possible in the study presented in Paper I. The routine for sub-routines in AUTODYN had changed in the version 11.0, and might explain the difference in success.

Another modification of the RHT material model, contemporaneous with Leppänen's (2004) modification, was developed by Schuler (2004), and included a more refined damage model for the description of crack softening than the original version. A modified strain-rate dependence was used for the tensile strength, and a power function was used to describe the shape of the descending crack-softening curve which also took into account the strain-rate dependence of the fracture energy. However, this modification has not yet been implemented in the commercial versions of AUTODYN and LSDYNA.

6 The Concrete Damage Plasticity Model 2

6.1 Development process

As seen in Section 5.3.1, there are several material models developed to describe the behaviour of concrete exposed to high dynamic loading. Some of these models are implemented in the standard material library in one, or more, commercial finite element codes. In general, these models are sufficient to describe the behaviour of the type of concrete and the loading conditions for which they have been developed. The user is often able to make modifications of the material model behaviour through user subroutines to improve the model or to adapt it to different material characteristics and/or loading conditions. However, the use of these subroutines rather means that a part of the behaviour calculated by the original material model is conditionally overwritten by the behaviour described in the user subroutine than the original model being modified. If these conditions are not met, the original model description is used and the behaviour described in the user subroutine neglected. Since these conditions are built into the program the user cannot change them, which limits the possibility to improve and adapt the original model.

For example, in Paper I the RHT model in AUTODYN was used to study the effect of adding steel fibres on the damage caused by projectile impact and in Paper II, the same model was used to study the behaviour of a blast and fragment loaded structure. Both studies invoked the need to modify the description of the tensile behaviour in the RHT model; in the former to take into account the improved softening behaviour due to the fibres and in the latter to improve the description of the tensile behaviour since it is poorly described in the original model. However, in neither case, it was possible to combine the modifications with a correctly described strain rate dependence of the tensile strength which, even though qualitative conclusions could be drawn, limited the quantitative results of these studies. The limitations in material-model modification observed in the work presented in Papers I and II have been described in Nyström (2008).

The limited opportunity to improve and adapt the material models for concrete available to the user raised the need to implement a complete material model in a user subroutine. Such implementation opens up the possibility to modify the behaviour of the model at any moment. However, the process from choosing the model to be implemented to using it for numerical simulation is more or less demanding. The amount of work associated depends on e.g. which model is being implemented and how well this model has already been established and tested. The development process can generally be divided into six important steps:

- specifying the needs and requirements of the model
- defining the theoretical build-up
- implementing the model in a suitable program
- verifying the implementation
- validate the behaviour of the model
- review the requirements and check if fulfilled

After the specification of needs and requirements, the theoretical build-up of the model is to be defined. If there is an existing material model which fulfils the needs and requirements this model may be implemented as it is. However, often one or more parts of the model has to be modified, or a mix of different models are used to fulfil the needs and requirements, and the theoretical build-up of the “new” model has to be defined before implementation is possible. Implementation is followed by verification and validation, referring to the work related to checking that the model has been correctly implemented, and finally the task of evaluating how well the model describes real behaviour. The validation of the model may also be divided into two parts: validation at a material level and validation at a structural level. Simplified, it can be stated that validation at a material level can be made by means of simulations of a single or a few elements the results of which are compared to experimental results. Validation at a structural level refers to the validation of the structural response.

The last step of reviewing the requirements for the model and checking on whether these are being fulfilled can be seen as an evaluation of the model. If the model does not fulfil the requirements, modifications and/or extensions of the theoretical description may be necessary and included in the implementation which should be followed by additional verification and validation steps. All the previously mentioned steps are of great importance. Nevertheless, it is not uncommon that only a limited part of the work related to this process is presented in descriptions of newly developed models or modifications of existing models. These descriptions are often limited to a presentation of the theoretical build-up and to a validation at structural levels.

However, in this chapter the developing process of the Concrete Damage Plasticity Model 2 (CDPM2) is presented, which is schematically shown in Figure 6.1. Based on the need described above, the requirements of a “new” material model has been specified, which have then been used to define the theoretical description. The theoretical build-up of the “new” model was made by Grassl (2011), with continuous feed-back from the reference group of the project and the present author. The “new” model was named CDPM2, since it is a modification and extension of the first version, CDPM1 developed by Grassl and Jirásek (2006). The constitutive model was implemented in the object-oriented finite element package OOFEM (Patzák and Bittnar, 2001). Verification of the implementation and validation during quasi-static loading conditions were performed on material, as well as structural level, as detailed in Paper III. However, in order to benefit from the possibilities of using large strain and stress theories and advanced contact interface algorithms, the model was also implemented in the advanced general purpose finite element package LS-DYNA (2012). This implementation was made by DYNAmore Nordic AB with contributions from the present author, who also conducted the verification of this implementation. To verify the implementations in OOFEM and LS-DYNA, parts of the model were also implemented in MATLAB. The verification of the implementation in LS-DYNA was followed by a validation study of the CDPM2 for dynamic loading at material level, and these results were then used to evaluate the model based on the initially defined requirements. It was found that certain modifications of the theoretical description should be made to fulfil the requirements also for high strain rates and high pressure levels, something that was not part of the present work.

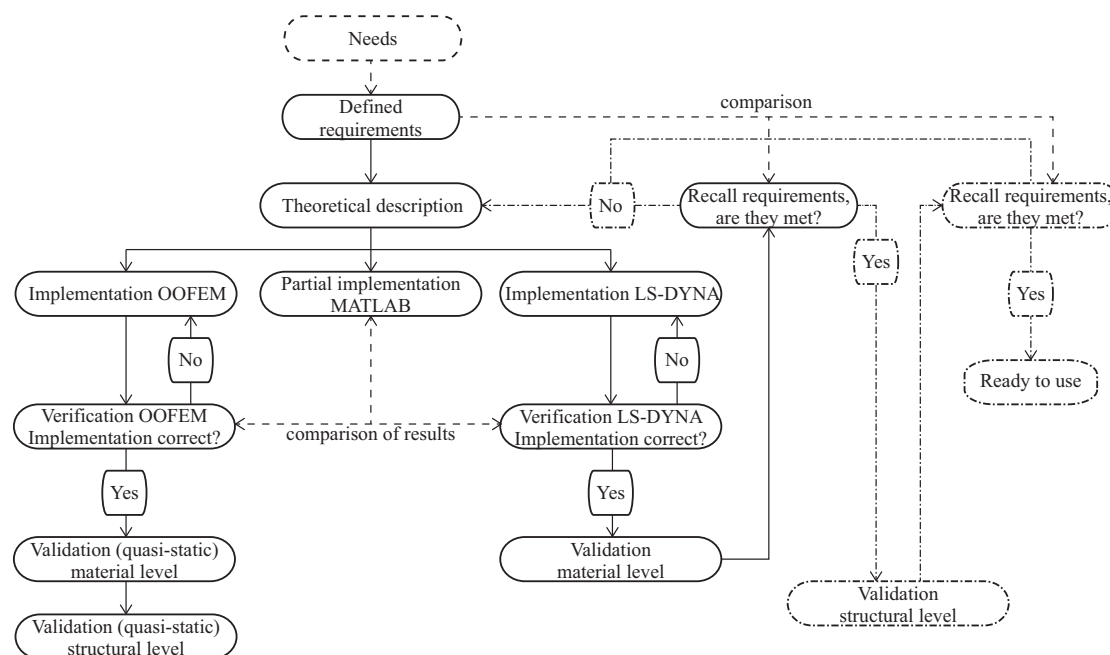


Figure 6.1 Schematic illustration of the development process of the CDPM2; dash-dotted lines indicate steps that are not performed yet, but are proposed for future work.

6.2 Needs and requirements

Objectives can only be met if necessary resources are available – if they are not, a need is created. An objective of the work presented in this thesis is to “observe and understand different phenomena involved in blast and fragment loading of reinforced concrete structures”, which is approached by the use of numerical simulations; see Chapter 1. Thus, the objective can only be met if the constitutive models used are capable of describing characteristic behaviours in a general way or that the model allows for modifications to take different behaviour into account. As mentioned in Section 6.1, this was not fulfilled for the concrete material model previously used and the need of such a constitutive model was raised during the progress of the work.

Specifying needs and requirements constitutes the base of the developing process. Correctly specified requirements simplify and shorten the rest of the process. However, for the CDPM2, some basic requirements of the model was defined before the more specific requirements, on which material behaviour the model should describe were specified. This resulted in four key words:

- Simple
- Clear
- General
- Robust

Even though the response related to high dynamic loading of concrete involves complex material behaviour, the constitutive model should be kept as simple as possible. The structure should be transparent in that the influence of different material parameters on the behaviour should be clear. It is also desirable to use a low number

of material parameters and that these should have a clear physical meaning or be at least related to parameters that have a physical meaning. It should also be possible to determine relevant input parameters from the literature. The documentation of the model should be comprehensive and advantages, as well as disadvantages, should be clearly stated and described. The model should describe the important characteristics of concrete subjected to multiaxial and rate-dependent loading and should be general enough to be used for different classes of concrete. Further, it should be possible to modify the behaviour to describe the response of fibre-reinforced concrete and other similar materials. The failure description in the model should be mesh independent, and input parameters should not depend on element size. Further, the model should show numerical stability and robustness. Since the model is to be used to estimate the response of structures, the numerical cost of describing the concrete material behaviour must be limited so as to avoid unrealistic simulation run times. It is difficult to meet these sometimes conflicting requirements, and it was seen more as an aim than an objective to fulfil them. However, these key words have been kept in mind throughout the developing process.

Next, the more specific requirements on what the constitutive model should be able to describe were to be specified. Thus, the characteristic material behaviour important to describe the response to high dynamic loading was to be identified and a mutual order of priority was compiled; see Figure 6.2. The closer to the base a material characteristic appears in the pyramid, the more important was this behaviour considered to be for the description of the response under these loading conditions. The material behaviour of concrete for static and dynamic loading was briefly described in Chapter 2. Since high dynamic loading is related to high pressure levels and high strain rates, the nonlinear material compaction response and the pressure sensitive strength of the model was considered crucial to describe the response of concrete. Further, a correctly described post-peak softening behaviour is important in order to correctly describe the dissipation of energy due to failure. The residual strength of concrete damaged in confined compression is considered important if the model were to describe the behaviour during multiple wave reflections in a structure. Even though the material characteristics appearing further up in the pyramid are important if a detailed description of the material response is desired, they are not crucial for the general behaviour and had a lower priority.

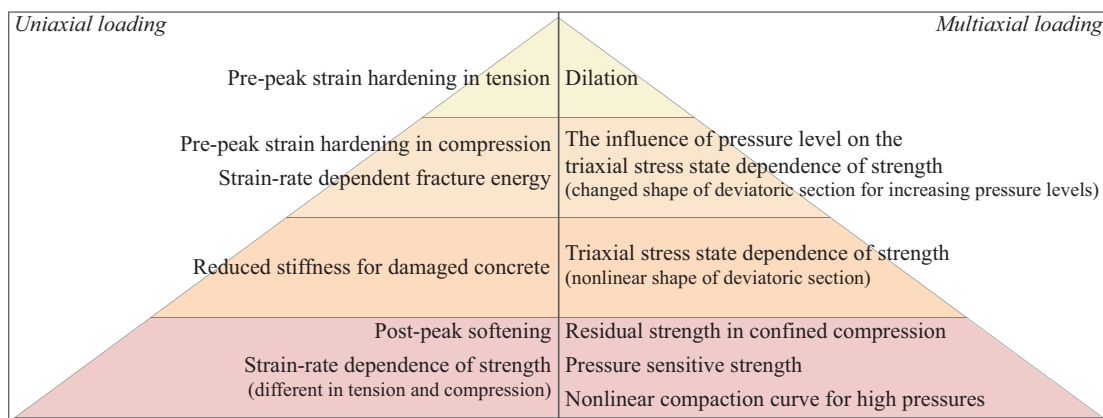


Figure 6.2 Concrete material characteristics and their mutual order of priority in the model description.

6.3 Theoretical description

As mentioned in Section 6.1, the theoretical description of the CDPM2 is based on the prior model, the CDPM1. Since a detailed description of the interaction between the concrete constituents are of secondary interest, this model is defined in the framework of continuum mechanics at a macroscopic scale. The CDPM1 is defined by combining the theories of plasticity and isotropic damage mechanics albeit in a static framework. Strain rate dependence in the CDPM2 is taken into account by delaying the initiation of damage. This delay required that the perfectly plastic response in the static nominal post-peak regime described in the CDPM1 was replaced by plastic hardening. To increase the generality and make it possible to model e.g. fibre reinforced concrete, the single damage parameter in the CDPM1 is replaced by two, one parameter for the tensile portion of the stress tensor and another for the compressive. Besides the strain rate dependence, the CDPM2 describes:

- pre-peak strain hardening (in compression and tension)
- pressure sensitive peak strength
- triaxial stress state dependence of strength (and its pressure dependence)
- post-peak softening
- reduced stiffness in post-peak regime
- realistically described dilation in compression

A comprehensive description of the CDPM2 model is found in the appended Paper III; however, this is limited to the static behaviour. The extension to strain-rate dependence is treated in Paper IV.

The model requires sixteen input parameters in the case of bilinear softening behaviour and fourteen if linear softening is desired; see Table 6.1. Observe that the numbering of parameters in the table does not represent the order they are provided as input to OOFEM and LS-DYNA. The first five parameters (no. 1 to 5) have a clear physical meaning and can be determined from uniaxial compressive tests, uniaxial tensile tests, and three-point bending tests. If limited or no experimental data are available, these parameters can be estimated by use of e.g. the CEB-FIP Model Code 1990 (CEB, 1993). The following five parameters (no. 6 to 10) do have a less clear physical meaning, but are closely related to physical properties and can also be determined from tests or by expressions from recommended references. Since they lack clear physical meaning, the six remaining parameters (no. 11 to 16) are normally more difficult to determine. However, default values are given for these parameters and there is normally no need to adjust them for every set of analysis. These six material parameters are all related to the description of plastic hardening, four of which (A_h , B_h , C_h and D_h) are related to the strain at peak stress in quasi-static loading under uniaxial tension, uniaxial compression and triaxial compression. The dilation constant D_f is related to the amount of dilation in the softening regime for uniaxial compression and represents a constant ratio between the lateral and axial plastic strain increments. The calibration of A_h , B_h , C_h , D_h , and/or D_f is thus possible if relevant experimental data are available. However, this is believed to be necessary only if high accuracy of strain at peak stress and/or dilation were desired and was considered important for the outcome of the results. The hardening modulus, H_p , affects the

amount of plastic strain both before and after the static failure surface is reached. In the case of static loading, calibration of this parameter can be made by the use of experimental data. However, since it affects the behaviour for all load cases, this calibration must be done with care. In dynamic loading, the value of the hardening parameter is critical for the description of the strain at peak strength, which also limits the possibility of calibration; see Paper IV. The different model parameters and their meaning are described in Papers III and IV.

Table 6.1 Model input parameters for the CDPM2.

No.	Input parameter		No.	Input parameter	
1	E	Young's modulus	9	e	eccentricity factor
2	ν	Poisson's ratio	10	q_{h0}	initial hardening parameter
3	f_t	uniaxial tensile strength	11	H_p	hardening modulus
4	f_c	uniaxial compressive strength	12	A_h	hardening ductility measure
5	w_f	ultimate crack opening	13	B_h	hardening ductility measure
6	w_{f1}	crack opening threshold ^a	14	C_h	hardening ductility measure
7	σ_{t1}	damage stress threshold ^a	15	D_h	hardening ductility measure
8	A_s	damage ductility measure	16	D_f	dilation constant

a. used in case of bilinear softening curve

6.4 Implementation

The global boundary value problem is determined by the numerical solution techniques used within the numerical solver. Both OOFEM and LS-DYNA allow for the choice of implicit and explicit solvers. However, in the results presented in Paper III, the static solver was used in OOFEM, and implicit time integration. In the simulations performed with LS-DYNA, presented in Paper IV, the explicit solver was used. Even though this means that different methods of time integration was used while solving the boundary value problem (global level), the technique used to integrate the constitutive laws (local level) was the same in the two cases, in which an implicit time integration scheme was used.

If assumed that all quantities have been evaluated up to time t , and the time increment Δt and the incremental strain vector for this time increment, ${}^{t+\Delta t}\Delta\boldsymbol{\varepsilon}$, are given, the nominal stress can be calculated. In the following, the superscript $t + \Delta t$ is dropped in order to simplify the notation, the superscript t is, however, left to indicate quantities evaluated at time t . Thus, where the time at which the quantity has been evaluated is not indicated, this refers to the time $t + \Delta t$. The flow chart for the algorithm of the constitutive law shown in Figure 6.3, is explained below.

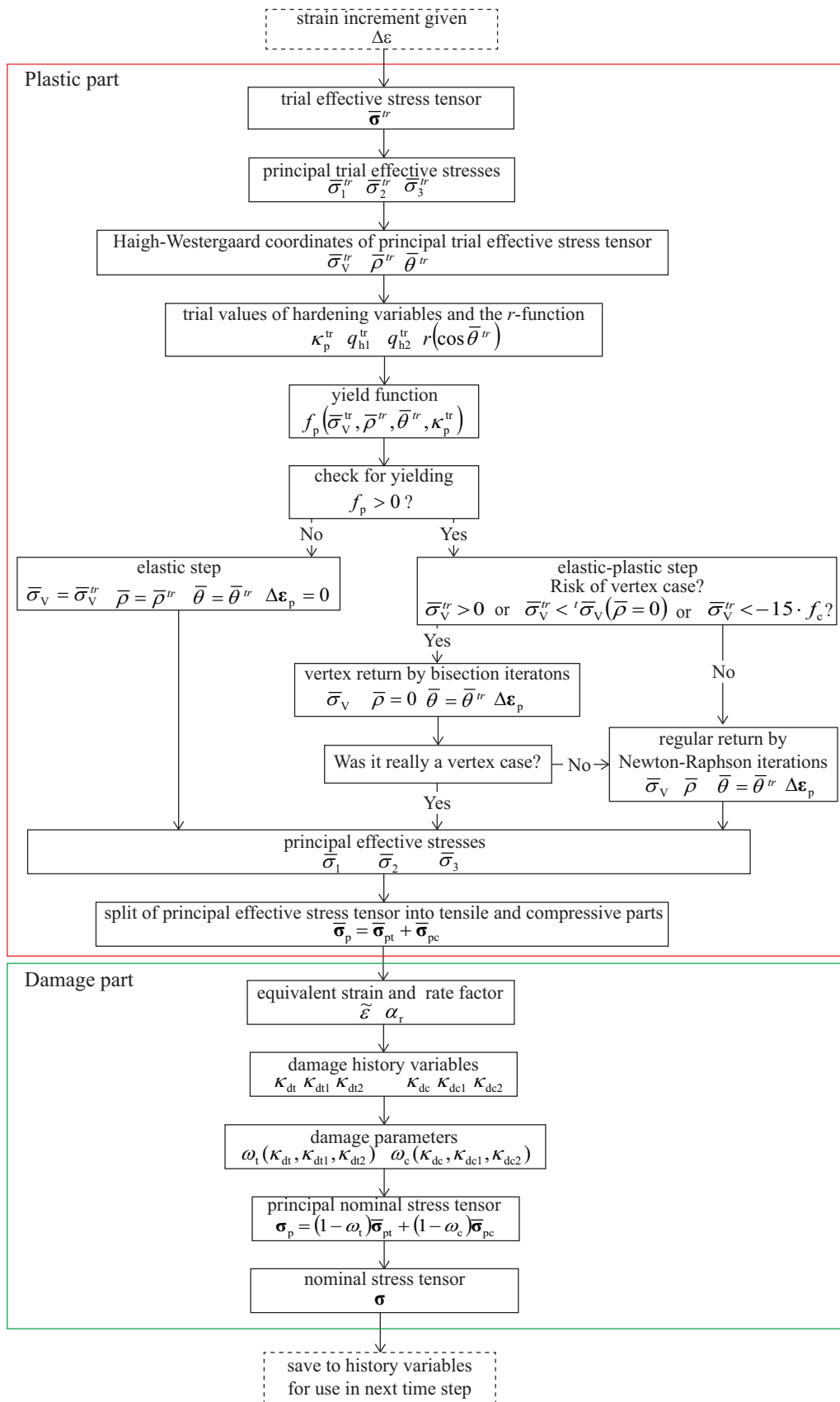


Figure 6.3 Flow chart for the CDPM2 algorithm.

The integration scheme is divided into two subsequent steps corresponding to the plastic and damage parts of the model. In the plastic part, the effective stress, $\bar{\sigma}$, and the plastic strain, ϵ_p , at the current time are calculated and in the damage part, the two damage parameters, ω_t and ω_c , and the nominal stress, σ , are calculated. The plastic part begins with calculating the trial effective stress vector $\bar{\sigma}^r$ from the given strain increment by assuming an elastic stress increment according to:

$$\bar{\sigma}^r = {}^t\bar{\sigma} + \mathbf{D}_e : \Delta\epsilon \quad (6.1)$$

where ${}^t\bar{\sigma}$ is the effective stress vector evaluated at time t , and \mathbf{D}_e is the elastic stiffness matrix.

Since the plasticity part of the model is described in terms of the cylindrical coordinates in the principal effective stress space first, the trial principal effective stresses and their directions are calculated, and thereafter the Haigh-Westergaard coordinates. The principal effective stresses are represented by the eigenvalues and eigenvectors of the effective stress tensor, respectively, which are sorted in ascending order.

Since an elastic stress increment is assumed, there is no plastic strain increment and the trial values of the hardening variable κ_p , as well as the dimensionless variables q_{h1} and q_{h2} , remain unaffected from previous time step. However, since q_{h1} and q_{h2} are not stored as history variables, these variables are recalculated. After calculation of the trial value of the elliptic function, $r(\cos\bar{\theta}^r)$, the yield function, $f_p(\bar{\sigma}_v^r, \bar{\rho}^r, \bar{\theta}^r, \kappa_p^r)$, is calculated and checked if yielding might occur. If $f_p(\bar{\sigma}_v^r, \bar{\rho}^r, \bar{\theta}^r, \kappa_p^r) \leq 0$, the assumption of an elastic stress increment is correct and the trial values are valid. If yielding occurs, i.e. if $f_p(\bar{\sigma}_v^r, \bar{\rho}^r, \bar{\theta}^r, \kappa_p^r) > 0$, the trial stress is erroneous and plastic return has to be performed.

The flow directions at intersection points of the yield surface and the hydrostatic axis are not unique and special treatment of these vertex cases are necessary. If the trial effective volumetric stress becomes larger than zero, or if it falls below the intersection point of the yield surface at time t , or below $-15 \cdot f_c$, a vertex return is performed. This is done on the assumption that the final stress state lies on the hydrostatic axis ($\bar{\rho} = 0$). The effective volumetric stress fulfilling the yield criterion $f_p(\bar{\sigma}_v, \bar{\rho} = 0, \bar{\theta} = 0, \kappa_p) = 0$ is thereafter determined by the bisection iterative method. Finally, it is checked that it really was a vertex case and that regular plastic return was not applicable. Thus, if the absolute value of the ratio of deviatoric and volumetric plastic flow as calculated in the vertex return is larger than the corresponding ratio calculated from the plastic potential it is not a real vertex case. If the ratio from the vertex case is smaller, the assumption is abandoned and a regular return is performed.

A regular plastic return is performed for the cases which are not classified as vertex. The set of four nonlinear equations, equations (6.2) to (6.5), is solved by the Newton-Raphson method. The unknowns, i.e. the effective volumetric stress $\bar{\sigma}_v$, the norm of the deviatoric effective stress $\bar{\rho}$, the hardening variable κ_p , and the increment of the plastic multiplier $\Delta\lambda$, for the current time $t + \Delta t$ are thus calculated by means of

iterations, starting from the initial guess values $\bar{\sigma}_v = \bar{\sigma}_v^{tr}$, $\bar{\rho} = \bar{\rho}^{tr}$, $\Delta\lambda = 0$ and $\kappa_p = {}^t\kappa_p$. The Lode angle for the trial effective stress tensor, $\bar{\sigma}^{tr}$, and the actual effective stress tensor, $\bar{\sigma}$, is the same ($\bar{\theta} = \bar{\theta}^{tr}$) since the plastic potential g_p , only depends on the stress invariants $\bar{\sigma}_v$ and $\bar{\rho}$, but not on the Lode angle; Grassl and Jirásek (2006). In addition, the gradient of the plastic potential, $\mathbf{m} = \partial g_p / \partial \bar{\sigma}$, and its invariants m_v and m_D have the same Lode angle. The parameters K and G in equations (6.2) and (6.3), represent the elastic bulk modulus and elastic shear modulus, respectively. The variable x_h in equation (6.4) is a hardening ductility measure taking into account the increased ductility in compression and increasing confinement levels compared to the response to tensile loading. It is worth pointing out that the total strain tensor is solved explicitly already on the global level and is not affected by the iterations.

$$\bar{\sigma}_v = \bar{\sigma}_v^{tr} - K\Delta\lambda m_v \quad (6.2)$$

$$\bar{\rho} = \bar{\rho}^{tr} - 2G\Delta\lambda m_D \quad (6.3)$$

$$\kappa_p = {}^t\kappa_p + \frac{\Delta\lambda \|\mathbf{m}\|}{x_h (\bar{\sigma}_v)} (2 \cos \bar{\theta})^2 \quad (6.4)$$

$$f_p(\bar{\sigma}_v, \bar{\rho}, \bar{\theta}, \kappa_p) = 0 \quad (6.5)$$

When the plastic return is performed, the principal effective stresses are updated according to equation (6.6). These stresses are then sorted in ascending order and constitute the principal effective stress tensor, $\bar{\sigma}_p$. Since damage is separated into tension and compression, the principal effective stress tensor is split into a tensile and a compressive part, $\bar{\sigma}_{pt}$ and $\bar{\sigma}_{pc}$, respectively, where $\bar{\sigma}_{pt,i} = \max(0, \bar{\sigma}_{p,i})$ and $\bar{\sigma}_{pc,i} = \max(0, -\bar{\sigma}_{p,i})$, with $i = 1, 2, 3$.

$$\begin{pmatrix} \bar{\sigma}_1 \\ \bar{\sigma}_2 \\ \bar{\sigma}_3 \end{pmatrix} = \bar{\sigma}_v \begin{pmatrix} 1 \\ 1 \\ 1 \end{pmatrix} + \sqrt{\frac{2}{3}} \bar{\rho} \begin{pmatrix} \cos(\bar{\theta}) \\ \cos(\bar{\theta} - 2\pi/3) \\ \cos(\bar{\theta} + 2\pi/3) \end{pmatrix} \quad (6.6)$$

With the actual effective stress state and plastic strains known, the damage part of the constitutive law is entered in order to check for damage and calculate the nominal stress state. This part of the model, which is based on the theory of strain driven isotropic damage mechanics, uses measures of the equivalent strain, $\tilde{\epsilon}$, and the plastic strain vector, $\boldsymbol{\epsilon}_p$, to calculate the two damage parameters. The plastic strain vector is known from the plasticity part of the model, but the equivalent strain is yet to be calculated. Further, the strain rate affects the initiation and evolution of damage and the dynamic increase factor, which in the model is represented by the rate factor α_r , is calculated. The strain rate used in the calculation of the rate factor is calculated as the change of strain in the relevant principal direction divided by the time increment Δt . Since the strain rate dependence is different in tension and compression, the relevant principal direction corresponds to the one giving the maximum and

minimum strain, respectively. However, as damage is initiated, the rate factor is locked and does not alter in subsequent steps to avoid effects of strain localisation on the rate factor, as described in e.g. Leppänen (2004).

The damage variables in tension and compression, ω_t and ω_c , respectively, are calculated by means of the six damage history variables, i.e. $\omega_t = g_{dt}(\kappa_{dt}, \kappa_{dt1}, \kappa_{dt2})$ and $\omega_c = g_{dc}(\kappa_{dc}, \kappa_{dc1}, \kappa_{dc2})$. Since damage in the model cannot heal, these damage variables cannot decrease. Further, besides the equivalent strain, the plastic strain, and the rate factor, the damage variables are calculated by means of the damage ductility measure x_s , and variable α_c , distinguishing between tensile and compressive stresses. The damage history variables used to determine the tensile damage variable are calculated according to:

$$\kappa_{dt} = \begin{cases} \tilde{\varepsilon}_t = \frac{\tilde{\varepsilon}}{\alpha_r} & \text{if } \tilde{\varepsilon}_t \geq {}^t\kappa_{dt} \\ {}^t\kappa_{dt} & \text{else} \end{cases} \quad (6.7)$$

$$\kappa_{dt1} = \begin{cases} {}^t\kappa_{dt1} + \frac{\|\Delta \boldsymbol{\varepsilon}_p\|}{\alpha_r x_s} & \text{if } \kappa_{dt} \geq \varepsilon_0 \\ {}^t\kappa_{dt1} & \text{else} \end{cases} \quad (6.8)$$

$$\kappa_{dt2} = {}^t\kappa_{dt2} + \frac{(\kappa_{dt} - {}^t\kappa_{dt})}{x_s} \quad (6.9)$$

where $\varepsilon_0 = f_t/E$ is a threshold representing the elastic strain at ultimate strength in quasi-static uniaxial tension, since E is the Young's modulus and f_t is the strength under this stress condition. The damage history variables used to determine the compressive damage variable are similarly calculated:

$$\kappa_{dc} = \begin{cases} \tilde{\varepsilon}_c = \alpha_c \frac{\tilde{\varepsilon}}{\alpha_r} & \text{if } \tilde{\varepsilon}_c \geq {}^t\kappa_{dc} \\ {}^t\kappa_{dc} & \text{else} \end{cases} \quad (6.10)$$

$$\kappa_{dc1} = \begin{cases} {}^t\kappa_{dc1} + \alpha_c \beta_c \frac{\|\Delta \boldsymbol{\varepsilon}_p\|}{\alpha_r x_s} & \text{if } \kappa_{dc} \geq \varepsilon_0 \\ {}^t\kappa_{dc1} & \text{else} \end{cases} \quad (6.11)$$

$$\kappa_{dc2} = {}^t\kappa_{dc2} + \frac{(\kappa_{dc} - {}^t\kappa_{dc})}{x_s} \quad (6.12)$$

where β_c is a factor providing a smooth transition from pure damage to damage-plasticity softening processes, which may occur during cyclic loading.

When the damage parameters have been calculated, the principal nominal stress vector is calculated according to equation (6.13), and then rotated back to the original coordinate system.

$$\boldsymbol{\sigma} = (1 - \omega_t)\bar{\boldsymbol{\sigma}}_t + (1 - \omega_c)\bar{\boldsymbol{\sigma}}_c \quad (6.13)$$

6.5 Verification

The verification of the implementation in OOFEM was made by single element simulations of quasi-static experiments including:

- uniaxial tension (cyclic loading)
- uniaxial compression (cyclic loading)
- bi- and triaxial compression
- hydrostatic compression

The above experiments have been reported in the literature, see Paper III. Thus, the verification process also constituted validation of the model at a material level for these loading conditions. Simulations of the general behaviour in the following were also conducted:

- cyclic loading (tension-compression-tension)
- uniaxial tension and compression at various strain rates

However, all verification simulations for the OOFEM implementation were performed with the static solver in OOFEM and the maximum achieved compressive stress level in the experiments used for validation was approximately 800 MPa.

The verification of the model implementation in LS-DYNA was performed by conducting simulations of the same experiments used in the verification and validation in OOFEM and then comparing the results from these with the results from the OOFEM simulations. Since LS-DYNA uses true stresses and strains while OOFEM uses engineering measures, small variations from the behaviour in OOFEM were expected. However, where larger variations were observed, they were investigated. By comparing different parameters calculated according to the two implementations the error could be localised and corrected. In a few cases, the part of interest of the model was implemented in MATLAB to facilitate the error search. For example; since the results from the LS-DYNA simulation showed a great divergence from the results of OOFEM in the case of hydrostatic compression, the part of the model describing this behaviour was implemented in MATLAB. Since the Lode angle was not defined in hydrostatic loading, its value was pending between 0 and 60 degrees in the OOFEM simulation while it was set to 0 in the LS-DYNA implementation. The implementation in OOFEM was adjusted to set the Lode angle equal to 0 degrees in the case of hydrostatic conditions.

Since a static solver was used to verify the implementation in OOFEM, no effects of inertia and propagating waves were modelled. In the simulations performed by the use of LS-DYNA, an explicit solver was used and inertia effects could be observed for

faster loading. Figure 6.4a shows an example of verification simulations from OOFEM and LS-DYNA in uniaxial compression. For the LS-DYNA simulation involving faster rate of loading ($t_{\max} = 0.05$ ms), an elastic wave was created in the element, which was not observed at the lower rate of loading ($t_{\max} = 2.00$ ms).

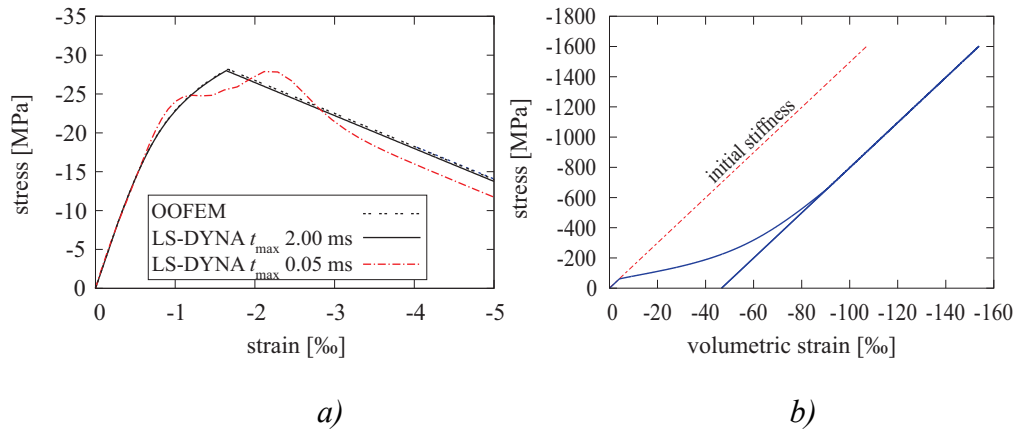


Figure 6.4 Verification simulations in a) OOFEM and LS-DYNA for uniaxial compression, and b) LS-DYNA for hydrostatic compression.

In the verification process of the implementation in LS-DYNA the element size, the loading time and the final deformation were varied. The implementation in LS-DYNA was also verified by the simulation of hydrostatic compression for high pressure levels; Figure 6.4b.

6.6 Validation

As mentioned in Section 0; since experiments were simulated in the verification of the implementation in OOFEM was combined with validation. Further, the behaviour of the model in 2D simulations of a three point bending test and a four point shear test has been validated; Paper III. However, these simulations were limited to quasi-static conditions. Since high dynamic loading may be related to high strain rates, the build-up of high confining pressures, uniaxial strain conditions and even shock wave propagation, the model had to be validated for these cases as well. Appended Paper IV presents the evaluation study of the model behaviour for high dynamic loading. Results from single element simulations of the following were compared to experimental results reported in the literature:

- uniaxial compression at different strain rates (up to $1\,000\text{ s}^{-1}$)
- uniaxial tension at different strain rates (up to $1\,000\text{ s}^{-1}$)
- quasi-static hydrostatic compression (minimum stress level of -650 MPa)
- quasi-static compression in uniaxial strain (minimum stress level of approximately -1 500 MPa).

Since the level of confining pressures in quasi-static testing is limited, testing at very high pressure levels are conducted by means of impact and detonations, involving

shock wave propagation in the concrete sample; see Section 2.3.2. To validate the model behaviour under these conditions, the ability of the model to describe shock wave formation was studied. Further, results from simulations of reverse flyer-plate-impact tests were compared to results reported in Gebbeken *et al.* (2006) and Grady (1996).

In quasi-static loading, the CDPM2 has provided a response in good agreement with experimental results for a wide range of loading, from uniaxial tension to confined compression; Paper III. Further, the model has shown mesh independent load-displacement curves for tensile fracture dominated problems. However, local results in the form of damage patterns were mesh-dependent; see Paper III. The evaluation of the ability of the model to describe the material response in the case of dynamic loading showed some model weaknesses that may limit the material description at high strain rates and pressure levels; Paper IV. The gradual increase of elastic stiffness during plastic pore compaction is not described in the present version of the model. Further, the strain-rate dependence of compressive strength and fracture energy overestimate the effect of strain rate. This behaviour may lead to overestimations of material strength and the energy required to reach total material fracture. However, the response of the model in the case of flyer-plate impact simulations showed good agreement with experimental results.

No simulations for validation of the model have been conducted at structural levels for dynamic loading, since these results were considered to be irrelevant due to the previously mentioned weaknesses. However, modifications of the CDPM2 to better describe the increased elastic stiffness at high pressure levels and strain-rate dependence is believed to improve the dynamic response.

6.7 Evaluation

Evaluation of the model and its ability to describe the relevant behaviours in case of high dynamic loading is made by reviewing the requirements (presented in Section 6.2) to see if these requirements have been met, and to evaluate the findings from the validation studies discussed in Section 6.6.

It is difficult to objectively evaluate whether the general requirements of the model characterised by the four key words: simple, clear, general and robust, have been met or not. However, even though the model parameters are relative numerous, only a part of these has to be given for every set of analysis. The material parameters that should be given for every new set of analyses have, or are at least related to parameters with, a clear physical meaning, see Section 6.3. A comprehensive description of the model is available, which also presents a validation of the model for static and dynamic loading conditions and describes advantages, as well as disadvantages of the model. The ability of the model to describe the behaviour for multiaxial and time-dependent loading is good in many aspects, without being fully satisfactory at high strain rates and high pressure levels, as further described below. The generality of the model is good, with flexibility to describe the behaviours of concrete with different characteristics by means of input parameters and softening curves. However, to use different shapes of the softening curves in tension and compression, the current implementation has to be modified to adapt the description of parameter A_s . The

parameter A_s relates the inclinations of the softening branch in the stress-strain curves in uniaxial tension and uniaxial compression. Further, some generality is missing with respect to the effect of initial density and water content, which according to the literature have clear effects on the response at high confining pressure levels. The stability and robustness of the model is good and have not caused any problems to the work performed. Since the simulations at a structural level are limited to two cases of quasi-static loading, the study of mesh dependency is limited. However, these simulations show mesh-independency at a global level. The influence of mesh size can be further investigated as more simulations at a structural level are conducted.

In general the specific requirements on what the model should be able to describe are also well met since the model describes all material characteristics specified in the requirements except the residual strength in confined compression, see Figure 6.2. This material characteristic can, however, be taken into account explicitly by the softening curve in compression. The validation of the model with experimental results from the literature has shown that the model is capable of describing the response for a wide range of loading, from uniaxial tension to confined compression and dynamic impacts. However, in some cases the behaviour is somewhat incorrectly described.

Even though the shape of the nonlinear compaction curve in hydrostatic compression captures the three characteristic phases, the elastic stiffness remains equal to the initial stiffness. The gradual increase of the stiffness during plastic compaction is thus not captured. This practically means that the model yields a weaker behaviour for high pressure levels than observed in experiments. Further, it may cause an underestimation of the dissipated energy due to plastic compaction of the material. It also affects the possibility of describing the formation of strong shock waves since this requires that the bulk modulus at high pressure levels exceeds the initial value. The validation study for dynamic loading has shown that the numerical model is capable of describing the structural inertia effects causing the sharp increase of strength in uniaxial compression at high strain rates. Thus, this part of the dynamic increase curve used when calculating the rate factor in compression α_{rc} should be removed for solid elements. The relation describing the dynamic increase of compressive strength should thus only take into account the moderate increase attributed to viscosity effects. Further, the strain rate effect of the fracture energy is erroneously described, resulting in too high a value for high strain rate levels.

The model does not take into account any temperature dependence. In the case of shock wave loading, the temperature may increase and cause a considerable thermal pressure component. However, in the experimental techniques used to evaluate the stress reached during shock wave transition, the effect of temperature, strain rate and static material behaviour cannot be differentiated. Thus, the temperature dependence in such cases is difficult to characterise. In the model, this behaviour is instead assumed to be implicitly accounted for.

As stated above, the response of the model shows good agreement with experimental results for a wide range of loading, static as well as dynamic. The incorrect description of the elastic stiffness during plastic compaction, and the erroneous description of strain rate dependence of fracture energy and the compressive strength mean that the results achieved by the CDPM2 in simulations of high dynamic loading may be misleading. Thus, it is recommended that the descriptions of these behaviours in the model are modified before the model is used for such simulations. However,

simulations involving dynamic events with high compressive stress levels (up to about 5 GPa), are believed to yield accurate results. For simulations of events with low, or negative pressure levels involving material failure, the capability to yield accurate results is limited to relatively low strain rates.

7 Conclusions

7.1 General conclusions

The area of blast and fragment loading of concrete structures involves phenomena not yet well understood. A numerical approach, together with literature reviews and theoretical investigations, have been used to increase the knowledge of this area. Three numerical studies have been conducted within the scope of the work presented, involving investigations of the effect of reinforcement on the projectile impact, the relative effect of the impact resistance when adding steel fibres to concrete, and the combined effects of blast and fragment loading.

The reinforcement in a concrete structure is necessary in order to ensure ductile behaviour and thereby an energy-absorbing capacity, but may also increase the resistance against local damage. However, an increased projectile resistance, i.e. decreased depth of penetration, can only be achieved with, for this case, suitable reinforcement detailing, since the reinforcement must be located in the damage zone in order to have an effect. Furthermore, since the confinement effect of the reinforcement, pointed out as a plausible explanation for the increased projectile resistance, decreases with increasing distance, the distance between the projectile path and the reinforcement bars is a crucial factor. Suitably positioned reinforcement bars do, however, generally reduce the scabbing and spalling effects.

The addition of moderate dosages of steel fibres in the concrete does not significantly influence the depth of penetration of a striking projectile while the size of both the spalling and possible scabbing crater decreases. An increased amount of fibres only lead to a small reduction of the spalling crater, whereas the effect on the scabbing crater is more significant – it decreases and may even be prevented.

Most damage caused by a multi-fragment impact on a wall element occurs within fractions of a millisecond and may consist of local damage on the front face, i.e. craters, scabbing cracks at the rear and initial flexural cracks close to supports. In the case of blast loading, the number of flexural cracks to which elongation of the reinforcement is localised, is lower than for fragment loading, which may have a positive effect on the energy-absorbing capacity. The early appearance of damage caused by the fragments and the larger number of flexural cracks indicate that the load-bearing capacity and mid-point deflection of the element in the case of combined, simultaneous loading are highly influenced by the fragment impact. For combined loading, a synergy effect is observed; the sum of the mid-point deflections for blast and fragment loading treated separately is smaller than the mid-point deflection for combined loading.

Due to limitations in material models available in commercial programs for simulations of high dynamic events, and the limited opportunities to improve and adapt these models, the CDPM2 (Concrete Damage-Plasticity Model, version 2) was developed and implemented in one such program, i.e. LS-DYNA. The response described by the CDPM2 showed good agreement with experimental data of the material behaviour for a wide range of loading conditions, static as well as dynamic. The model describes pre-peak hardening, pressure sensitive strength, and post-peak softening with reduced unloading stiffness. Further, the increased pre-peak ductility

for compressive states with increasing confinement is correctly described. For high compressive loads, the three phases; linear elasticity, plastic pore compaction and the approximately linear behaviour during compaction of the pore-free material are described. By use of a non-associated flow rule, the model also correctly describes dilation in the case of compression with no or low confining pressures. The dependence of the strength on the triaxial stress state, i.e. the non-circular shape of the failure surface in the deviatoric section, is described by the model. For increasing pressure levels, the shape becomes more circular in accordance with the real behaviour of concrete. Contradictory to the common approach in hydrocodes, the CDPM2 does not require an explicitly described Equation of State since this behaviour is calculated by the model and thus implicitly accounted for.

Further, the model is able to describe the strain-rate dependence of uniaxial tension and compression, respectively. However, in the case of solid elements where the three-dimensional effect of inertia and confining effects can be described by the model, the expression used to define the dependence of the strain rate for compressive loading in the model should be modified so as not to include the sharp increase of strength for strain rates above 30 s^{-1} . In addition, the description of damage accumulation should be modified to achieve an improved description of the strain rate dependence of the fracture energy, which is overestimated in the current version of the model. The CDPM2 uses extrapolation of the curves describing the strain rate dependence in tension and compression, respectively, above the strain rates for which they have been validated. This extrapolation may lead to overestimated strength at high strain rates and it should, therefore, be considered to modify the descriptions at high strain rates to limit this increase of strength.

In the case of shock wave transition, the model describes a weaker response than was been observed in experiments for stress levels below about - 5 GPa, a consequence of the description of the elastic stiffness which in the model remains constant also during plastic compaction, while it increases in reality. Thus, an improved description of the elastic stiffness during compaction would further improve the capability of the model to describe the concrete material behaviour under high dynamic loading. The description of damage in the case of compressive loading with high confining pressures should be further investigated since the current description leads to a weaker response than may be expected in these cases.

Thus, in order to further increase the capability of the model to describe the behaviour of concrete subjected to high dynamic loading, the descriptions of the damage accumulation and elastic stiffness during plastic compaction should be modified. Even though some principles for possible modifications have been presented, implementation and further evaluation of these modifications have not been part of the work presented in this thesis.

7.2 Suggestions for future research

It is believed that the CDPM2 can be used in future applied numerical studies of the response of concrete structures in the case of blast and fragment loading. However, the current version of the CDPM2 should first be somewhat modified to more correctly describe the behaviour of concrete in the case of high dynamic loading.

Thereafter, the model should be evaluated at a material and thereafter at a structural level. Once the model has been validated at both a material and a structural level the model can be used for applied studies.

In both Papers I and II, the limited possibility of adapting and modifying the RHT model in AUTODYN to take into account the effects of fibres, and improving the description of tensile failure have made it difficult to arrive at conclusions of qualitative character. With the CDPM2, these restraints are believed to be solved and these simulations may be conducted with the new model to attain quantitative results.

The effects of combined blast and fragment loading should be further studied to extend the understanding for the different phenomena involved. In Paper II the fragment loading was highly idealised and it was assumed that the fragments were uniformly distributed over the structure. A future study might preferably involve variations of the fragment loading where the distribution of fragments over the structure was varied and the effect of this would be observed. Further, in the study presented the reinforcement was modelled as beam elements with full interaction with surrounding concrete elements. It may thus be of interest to also study the effect of reinforcement modelling on the structural response. The reinforcement may be modelled as solid elements, and interface elements may be used to describe the bond strength between the elements representing reinforcement bars and surrounding concrete, respectively.

The use of different types of concrete to optimise the design of protective structures, e.g. normal, fibre-reinforced, and high strength concrete, is also of interest for future studies. Such a study may involve investigations of how the various types of concrete may be used in different areas of a structure to best use their specific material characteristics. Moreover, damage of protective structures may be of different degrees and causes. However, if the protective capability were considered to be lowered to such a degree that the requirements would no longer be fulfilled, repair of the damage may be required. Potential solutions for safe repairs of protective structures are, therefore, a proposed subject for future research, and may also involve the use of different types of concrete and special reinforcement detailing.

Numerical modelling is a useful tool to study the response of reinforced concrete structures subjected to blast and fragment impacts. However, since this method represents a mathematical approximation of the real behaviour, limited by different assumptions and idealisations, its capability to describe physical behaviour should be under constant evaluation. Often this requires validation by experimental results. If relevant experiments have not been reported in the open literature, it may be necessary to conduct such experiments. Further, improvements of the numerical techniques or models apart from those pointed out here may also be required.

8 References

- ACI 544 (1996): *State-of-the-Art Report on fibre Reinforced Concrete*. ACI Committee 544 Report 544.1R-96, American Concrete Institute, Detroit, USA.
- Asay, J. R. and Shahinpoor, M. (1993): *High-pressure shock compression of solids*, Springer-Verlag, New York, NY, USA.
- ASCE (1999): *Structural Design for Physical Security – State of the Practice*. Task committee: Conrath, E.J. *et al.*, American Society of Civil Engineers.
- AUTODYN (2005): *AUTODYN Theory Manual, Revision 4.3*. Century Dynamics Inc., Concord, CA, USA.
- Bai, W., Cui, Y., Wang, Q., Guan, J., and Zhang J. (2012): Study on Damage Evolution Mechanism of Concrete under Uniaxial Tension. *Applied Mechanics and Materials*, Vol. 238 2012, pp. 46-50.
- Bischoff P. H. and Perry, S. H. (1991): Compressive behaviour of concrete at high strain rates. *Materials and Structures*, Vol. 24, pp. 425-450.
- Borrvall, T. and Riedel, W. (2011): The RHT concrete model in LS-DYNA. *8th European LS-DYNA users conference*, May, 2011, Strasbourg, France. (<http://dynalook.com>)
- Boslough, M. B. and Asay, J. R. (1993): Basic principles of shock transition. *High-pressure shock compression of solids*, Springer-Verlag, New York, NY, USA, pp. 7-42.
- Brara, A. and Klepaczko, J. R. (2007): Fracture energy of concrete at high loading rates in tension. *International Journal of Impact Engineering*, Vol. 34, No. 3, pp. 424-435.
- CEB (1988): Concrete structures under impact and impulsive loading. CEB Bulletin d'Information No. 187, Lausanne, Switzerland.
- CEB (1993) CEB-FIP Model Code 1990, Design Code. Thomas Telford, Lausanne, Switzerland.
- Çengel, Y. and Boles, M.A., (2006): *Thermodynamics: An engineering approach (5th edition)*. McGraw-Hill, Boston, MA, USA.
- Chen, W. F. (2007): *Plasticity in reinforced concrete*. J. Ross Publishing, Inc., Fort Lauderdale, FL, USA. (Unabridged republication of the work originally published by McGraw-Hill, New York, 1982.)
- Curran, D. R. (1997): Simple fragment size and shape distribution formulae for explosively fragmenting munitions. *International Journal of Impact Engineering*, Vol. 20, 1997, pp. 197-208.

- Drucker, D. C. and Prager, W. (1952): Soil mechanics and plasticity analysis or limit design. *Quarterly of Applied Mathematics*, Vol. 10, pp. 157-165.
- Eibl, J. and Ockert, J. (1996): Problems concerning constitutive laws for shock waves in concrete. *Proceedings of the Specialty Symposium on Structures Response to Impact and Blast – Theory, Experiments & Practice*, Tel Aviv, Israel, pp. 174-183.
- Field, J. E., Walley, S. M., Proud, W. G., Goldrein, H. T. and Siviour, C. R. (2004): Review of experimental techniques for high strain rate deformation and shock studies. *International Journal of Impact Engineering*, Vol. 30, pp. 725-775.
- Gabet, T. (2006): *Comportement triaxial du béton sous fortes contraintes: Influence du trajet de chargement*. Doctoral Thesis. Joseph Fourier University, Grenoble, France.
- Gebbeken, N., Greulich and Pietzsc A. (2001): Performance of concrete based building materials against blast impact. *Proceedings of the fib-Symposium, concrete and Environment*, 3-5 October 2001, Berlin, Germany.
- Gebbeken, N., Greulich, S., and Pietzsch A. (2006): Hugoniot properties for concrete determined by full-scale detonation experiments and flyer-plate-impact tests. *International Journal of Impact Engineering*, Vol. 32, pp. 2017-2031.
- Gebbeken, N. and Ruppert, M. (2000): A new material model for concrete in high-dynamic hydrocode simulations. *Archive of Applied Mechanics*, Vol. 70, pp. 463-478.
- Girhammar, U. A. (1990): *Brief review of combined blast and fragment loading effects*. Report C7:90. National Fortification Administration, Eskilstuna, Sweden.
- Grady, D. E. (1993): Impact Compression Properties of Concrete. *Proceedings of the Sixth International Symposium on Interaction of Nonnuclear Munitions with Structures*, May 3-7 1993, Panama City Beach, Florida, USA, pp. 172-175.
- Grady, D. E. (1996): *Shock Equation of State Properties of Concrete i Structures under Shock and Impact IV*. (Edited by N. Jones *et al.*), Computational Mechanics Publications, Southampton, UK, pp. 405-414.
- Grassl, P. (2011): *CDPM2: A damage-plastic approach to model the dynamic failure of concrete*. Research Report GUCE2011PG02, School of Engineering, University of Glasgow, Glasgow, United Kingdom.
- Grassl, P. and Jirásek, M. (2006): Damage-plastic model for concrete failure. *International Journal of Solids and Structures*, Vol. 43, pp. 7166–7196.
- Greulich, S. (2004): *Zur numerischen Simulation von Stahlbeton- und Faserbetonstrukturen unter Detonationsbeanspruchung..* Doctoral Thesis. Fakultät für Bauingenieur- und Vermessungswesen, der Universität der Bundeswehr München, Munich, Germany.

- Gylltoft, K. (1983): *Fracture Mechanics Models for Fatigue in Concrete Structures*. Doctoral Thesis. Division of Structural Engineering, Luleå University of Technology, Luleå, Sweden, No. 1983:25:D.
- Haddad, Y. M. (2000): *Mechanical behavior of engineering materials, Volume 2: Dynamic and intelligent material systems*. Kluwer Academic Publishers, Dordrecht, Netherlands.
- Hall, C. A., Chhabildas, L. C. and Reinhart, W. D. (1998): Shock Hugoniot and release states in concrete mixtures with different aggregate sizes from 3 to 23 GPa. *AIP Conference Proceeding*, Vol. 429, American Institute of Physics, pp. 119-122.
- Hansson, H. (2002): Modelling of concrete perforation. *Proceedings of the 7th International conference on Structures Under Shock and Impact*, SUSI VII, May 2002, Montreal, Canada, pp.79-90.
- Hartmann, T., Pietzsch, A. and Gebbeken, N. (2010): A hydrocode material model for concrete. *International Journal of Protective Structures*, Vol. 1, No 4, pp.443-468.
- Herrmann, W. (1969): Constitutive equation for the dynamic compaction of ductile porous materials. *Journal of Applied Physics*, Vol. 40, pp.2490-2499.
- Hiermaier, S.J. (2008): *Structures under crash and impact: Continuum mechanics, discretization and experimental characterisation*. Springer Science + Business Media, LLC, New York, NY, USA.
- Hillerborg, A. (1985): Theoretical basis of a method to determine the fracture energy G_f of concrete. *Materials and Structures*, Vol. 18, pp. 291-296.
- Imran, I. (1994) *Applications of non-associated plasticity in modelling the mechanical response of concrete*. PhD thesis, University of Toronto, Toronto, Canada.
- Imran, I. and Pantazopoulou, S. J. (1969): Experimental study of plain concrete under triaxial stress. *ACI Materials Journal*, Vol. 93, pp.589-601.
- Jirásek, M. (2006): *Modelling of Localized Inelastic Deformation*. Lecture notes. Czech Technical University, Prague, Czechia.
- Johansson, M. (2000): *Structural Behaviour in Concrete Frame Corners of Civil Defence Shelters, Non-linear Finite Element Analyses and Experiments*. Doctoral Thesis. Department of Structural Engineering, Division of Concrete Structures, Chalmers University of Technology, Publication no. 00:2, Göteborg, Sweden.
- Johansson, M. (2012): *Luftstötuvåg*. (Blast wave. In Swedish), MSB, Publication no. MSB448, Karlstad, Sweden.
- Johansson, M. and Laine, L. (2012): *Bebyggelsens motståndsförmåga mot extrem dynamisk belastning, Delrapport 1: Last av luftstötuvåg* (The capacity of buildings to resist severe dynamic loading, Part 1: Blast wave loading, In Swedish). MSB, Karlstad, Sweden.

- Johnson, G. R., Holmquist, T. J. and Cook, W. H. (1993): A computational constitutive model for concrete subjected to large strains, high strain rates, and high pressures. *Proceedings of the 14th International Symposium on Ballistics*, 26-29 September, 1993, Québec, Canada, pp. 591-600.
- Khan A. S. and Huan S. (1995): *Continuum Theory of Plasticity*. John Wiley & Sons, Inc., USA.
- Krauthammer, T. (2006): *Modern Protective Structures, Design, analysis and evaluation*. Course notes. The Pennsylvania State University, Pennstate, PA, USA.
- Kupfer, H., Hilsdorf, H. K., and Rüschi, H. (1969): Behavior of concrete under biaxial stresses. *Journal of the American Concrete Institute*, Vol. 66, No. 8, pp.656-666.
- Leppänen, J. (2003): Numerical simulation of projectile penetration in concrete. *Nordic Concrete Research*, Vol. 30, pp. 84-103.
- Leppänen, J. (2004): *Concrete Structures Subjected to Fragment Impacts – Dynamic Behaviour and Material Modelling*. Doctoral Thesis. Department of Structural Engineering and Mechanics, Division of Concrete Structures, Chalmers University of Technology, Publication no. 04:4, Göteborg, Sweden.
- Leppänen, J. (2006): Concrete subjected to projectile and fragments impacts: Modelling of crack softening and strain rate dependency in tension. *International Journal of Impact Engineering*, Vol. 32, pp. 1828-1841.
- Leppänen, J. (2012): *Splitterverkan*. (Fragment load effect. In Swedish), MSB, Publication no. MSB345, Karlstad, Sweden.
- Li, Q. M., Reid, S. R., Wen, H. M. and Telford, A. R. (2005): Local impact effects of hard missiles on concrete targets. *International Journal of Impact Engineering*, Vol. 32, 2005, pp. 224-284.
- Linse, D. and Aschl, H. (1976): *Versuche zum Verhalten von Beton unter mehrachsiger Beanspruchung*. Research report, Technical University Munich, Germany.
- LS-DYNA (2012): *Keyword user's manual version 971*. Vol.1 and 2, Livermore Technology Software Corporation, Livermore, California, USA.
- Lubliner, J. (2008): *Plasticity theory*. Dover Publications Inc. Mineola, NY, USA.
- Löfgren, I. (2005): *Fibre-reinforced Concrete for Industrial Construction – a fracture mechanics approach to material testing and structural analysis*. Doctoral Thesis. Department of Civil and Environmental Engineering, Division of Structural Engineering, Chalmers University of Technology, Göteborg, Sweden.
- Magallanes, J. M., Wu, Y., Malvar, J. and Crawford, J. E. (2010): Recent improvements to release III of the K&C concrete model. *11th International LS-DYNA users conference*, June, 2010, Detroit, USA.

- Magnusson, J. and Hansson, H. (2005): *Simuleringar av explosionsbelastade betongbalkar – en principstudie*. (Numerical simulations of concrete beams – a principal study, in Swedish) National Defense Research Establishment (FOI), FOI Report 1686—SE, Tumba, Sweden.
- Malvar, L. J., Crawford, J. E. and Wesevich, J. W. (1994): *A new concrete material model for DYNA3D*. Report no. TM 94-14, Karagozian and Case, Glendale, CA, USA.
- Malvar, L. J., Crawford, J. E., Wesevich, J. W. and Simons, D. (1997): A plasticity concrete material model for DYNA3D. *International Journal of Impact Engineering*, Vol. 19, No. 9-10, pp. 847-893.
- Malvar, L. J. and Ross, C. A. (1998): Review of Strain Rate Effects for Concrete in Tension. *ACI Materials Journal*, Vol. 95, No. 6, pp. 735-739.
- Marchans, K. A., Nash, P. T. and Cox, P. A. (1989): Synergism in combined blast and fragment loadings: Can it be defined?. *Proceedings of the Special Conference of Structures for Enhanced Safety and Physical Security*, 8-10 March 1989, Arlington, VA, USA, American Society of Civil Engineers, New York, NY, USA, pp. 106-117.
- Marchand, K. A., Vargas, M. M. and Nixon, J. D. (1992): *The synergistic effects of combined blast and fragment loadings*. Southwest Research Institute, San Antonio, TX, USA.
- Meyers, M. A. (1994): *Dynamic behaviour of materials*. John Wiley & Sons, Inc., New York, USA.
- Mills, L. L. and Zimmerman, R. M. (1970): Compressive strength of plain concrete under multiaxial loading conditions. *ACI Journal*, Vol. 67, pp. 802-807.
- MSB (2011): *Skyddsrum SR09. Med tillägg 2011*. (Shelter Regulations SR09. With supplements 2011, in Swedish). (Edited by Ekengren B).MSB, Karlstad, Sweden.
- Murray, Y. D. (2007): *User's Manual for LS-DYNA Concrete Material Model 159*. U.S. Department of Transportation, Federal Highway Administration, Report No. FHWAHRT-05-062, Georgetown Pike McLean, VA, USA.
- Nataraja, M. C., Nagaraj, T. S. and Basavaraja, S. B., (2005): Reproportioning of steel fibre reinforced concrete mixes and their impact resistance. *Cement and Concrete Research*, Vol. 35, pp. 2350-2359.
- Nyström, U. (2008): *Concrete structures subjected to blast and fragment impacts: Numerical simulations of reinforced and fibre-reinforced concrete*. Doctoral Thesis. Department of Civil and Environmental Engineering, Division of Structural Engineering, Concrete Structures, Chalmers University of Technology, Publication no. Lic 2008:4, Göteborg, Sweden.
- Nyström, U. and Leppänen, J. (2006): Numerical Studies of Projectile Impacts on Reinforced Concrete. *Proceedings of the 2nd International Conference on Design*

- and Analysis of Protective Structures 2006*, 13-15 November, 2006, Singapore, pp. 310-319.
- Ong, K. C. G., Basheerkhan, M. and Paramasivam, P., (1999): Resistance of fibre concrete slabs to low velocity projectile impact. *Cement and Concrete Research*, Vol. 21, pp. 391-401.
- Osborn, J. J, Matuska, D. A. and Durrett, R. E. (1982): *Hull user guide for three-dimensional linking with EPIC3*. Report no. ARBRL-CR-00484, Orlando Technology, Inc., Shalimar, FL, USA.
- Ottosen, N. S. (1979): Constitutive model for short-time loading of concrete. *Journal of the Engineering Mechanics Division*, Vol. 105, No. 1, pp. 127-141.
- Patzák, B. and Bittnar, Z. (2001): Design of object oriented finite element code. *Advances in Engineering Software*, Vol. 32, No. 10-11, 2001, pp. 759-767.
- Ramesh, K. T. (2008): High rates and impact experiments. *Springer handbook of experimental solid mechanics*, Springer, New York, NY, USA, pp. 929-959.
- Riedel, W. (2000): *Beton unter dynamischen Lasten, Meso- und makromechanische Modelle und ihre Parameter*. Doctoral Thesis. Fakultät für Bauingenieur- und Vermessungswesen, der Universität der Bundeswehr München, Munich, Germany.
- Riedel, W., Kawai, N. and Kondo, K. (2009): Numerical assessment for impact strength measurements in concrete materials. *International Journal of Impact Engineering*, Vol. 36, pp. 283-293.
- Rossi, P., van Mier, G. M., Toutlemonde, F., Le Maou, F., and Boulay C. (1994): Effect of loading rate on the strength of concrete subjected to uniaxial tension. *Materials and Structures*, Vol. 27, pp. 260-264.
- Räddningsverket (1994): *Shelter Regulations SR-English Edition*. Swedish Rescue Services Agency, Karlstad, Sweden.
- Scholz, U., Nechvatal, D., Aschl, H., Linse, D., Stöckl, S., Grasser, E., and Kupfer, H. (1995): *Versuche zum Verhalten von Beton unter dreiachsiger kurzzeitbeanspruchung*. Heft 447, Deutscher Ausschuss für Stahlbeton, Heft 447, Berlin, Germany, pp.7-63.
- Schuler, H. (2004): *Experimentelle und numerische Untersuchungen zur Schädigung von stoßbeanspruchtem Beton*. Doctoral Thesis. Fakultät für Bauingenieur- und Vermessungswesen, der Universität der Bundeswehr, Munich, Germany.
- Schwer, L. E. and Murray, Y. D. (1994): A three-invariant smooth cap model with mixed hardening. *International Journal for Numerical and Analytical Methods in Geomechanics*, Vol. 18, No. 10, pp. 657-688.
- Smith, S. H. (1987): On fundamental aspects of concrete behavior. Master's thesis, University of Colorado, Boulder, Colorado, USA.

- Tham, C. Y. (2006): Numerical and empirical approach in predicting the penetration of a concrete target by an ogive-nosed projectile. *Finite Elements in Analysis and Design*, Vol. 42, pp. 1258-1268.
- U.S. Army (1992): *Fundamentals of Protective Design for Conventional Weapons*. Technical Manual TM 5-855-1.
- van Mier, J. G. M. (1984): *Strain-softening of concrete under multiaxial loading conditions*. Doctoral Thesis. Technische hogeschool Eindhoven, The Netherlands, 348 pp.
- Vu, X. H., Malecot, Y., Daudeville, L. and Bozaud, E. (2009): Experimental analysis of concrete behavior under high confinement: Effect of the saturation ratio. *International Journal of Solids and Structures*, Vol. 46, pp. 1105-1120.
- Weerheijm, J. (1992): *Concrete under impact tensile loading and lateral compression*. Doctoral Thesis, Delft University of Technology, Delft, Netherlands.
- Weerheijm, J., and van Doormaal J. C. A. M. (2007): Tensile failure of concrete at high loading rates: New test data on strength and fracture energy from instrumented spalling tests. *International Journal of Impact Engineering*, Vol. 34, pp. 609–626.
- William, K. J. and Warnke, E. P. (1975): Constitutive model for the triaxial behavior of concrete. *Proceedings of the International Association for Bridge and Structural Engineering: Seminar on Concrete Structures Subjected to Triaxial Stress*, Bergamo, Italy, Vol. 19, pp. 174–186.
- Williams E. M., Akers, S. A., and Reed P. A. (2006): *Laboratory Characterization of SAM-35 Concrete*. Geotechnical and Structures Laboratory, U.S. Army Engineer Research and Development Center, Publication no. ERDC/GSL TR-06-15, Vicksburg, MS, USA.
- Yan, D. and Lin, G., (2006): Dynamic properties of concrete in direct tension. *Cement and Concrete Research*, Vol. 36, pp. 1371-1378.
- Zel'dovich, Ya. B. and Raizer, Yu. P. (1966): *Physics of shock waves and high-temperature hydrodynamic phenomena*. Vol. 1. Academic Press, Inc., New York, USA.
- Zel'dovich, Ya. B. and Raizer, Yu. P. (1967): *Physics of shock waves and high-temperature hydrodynamic phenomena*. Vol. 2. Academic Press, Inc., New York, USA.
- Zhenguo, T. and Yong, L. (2010): Modifications of the RHT material model for improved numerical simulation of dynamic response of concrete. *International Journal of Impact Engineering*, Vol. 37, pp. 1072-1082.
- Zollo, R. F. (1997): Fibre-reinforced concrete: an Overview after 30 Years of Development. *Cement and Concrete Composites*, Vol. 19, No. 2, pp. 107-122.
- Zukas, J. A. (2004): *Introduction to hydrocodes*. Elsevier, Amsterdam, Netherlands.

Appendix A Equation of States for solids

Brief descriptions of the Linear, Polynomial, Mie-Grüneisen, and Herrmann's $P-\alpha$, Equations of States are given in this appendix. More comprehensive descriptions are given in e.g. AUTODYN (2005), LS-DYNA (2012), and Meyers (1994).

A.1 Linear

As the name suggests, this Equation of State is a linear relation between the pressure p , and specific volume v , (or pressure and density ρ , or pressure and compaction μ); see Figure A.1. It is described by means of the (adiabatic) bulk modulus K according to:

$$p = K \left(\frac{-\Delta v}{v} \right) = K \left(\frac{\rho - \rho_0}{\rho_0} \right) = K\mu \quad (\text{A.1})$$

Since the pressure does not depend on the specific internal energy (or temperature) it assumes isothermal processes.

Due to the linearity of this Equation of State, it cannot be used to describe plastic compaction and the formation of shock waves due to dispersion effects. Further, due the isothermal assumption, energy dissipation due to shock heating is not considered. It is therefore to be used under conditions where these effects do not have to be considered, e.g. in the region of initial elastic deformation for porous materials or for metals where the compaction curve under certain circumstances may be approximated as linear.

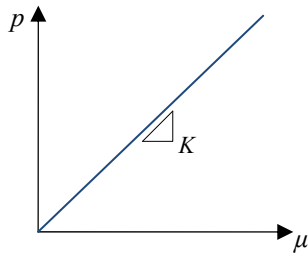


Figure A.1 Linear Equation of State.

A.2 Polynomial

A commonly used Polynomial Equation of State is:

$$p = K_1\mu + K_2\mu^2 + K_3\mu^3 + (B_0 + B_1\mu)\rho_0 e \quad (\text{A.2})$$

where μ is the compaction, K_1 , K_2 and K_3 are polynomial constants, B_0 and B_1 are constants to describe the variation of pressure with the specific internal energy e , and ρ_0 is the initial density of the material.

The first three terms in equation (A.2) represent a cubic description of a pressure-compaction curve for a reference specific internal energy of $e = 0$, and the last term describes the variation of the pressure in the neighbourhood of this reference line; see Figure A.2. The pressure changes linearly with the specific internal energy along isochors (if both B_0 and B_1 are nonzero), but depending on the choice of the constants B_0 and B_1 the magnitude of the change in pressure due to specific internal energy may vary with the compaction. The following cases can be distinguished (see also Figure A.2):

- $B_0 = B_1 = 0$

Pressure is independent of specific internal energy.

$$p = K_1\mu + K_2\mu^2 + K_3\mu^3 \quad (\text{A.3})$$

- $B_0 \neq 0, B_1 = 0$

Pressure varies linearly with specific internal energy, but this increase is independent of the density, i.e. the increase of pressure along isochors (constant volume) is constant.

$$p = K_1\mu + K_2\mu^2 + K_3\mu^3 + B_0\rho_0e \quad (\text{A.4})$$

- $B_0 \neq 0, B_1 \neq 0$

Pressure varies linearly with specific internal energy, and the increase of pressure along isochors varies linearly with the density.

- $B_0 = B_1 \neq 0$

$$p = K_1\mu + K_2\mu^2 + K_3\mu^3 + B_0\rho e \quad (\text{A.5})$$

- $B_0 \neq B_1 \neq 0$

$$p = K_1\mu + K_2\mu^2 + K_3\mu^3 + B_0\rho_0e + B_1(\rho - \rho_0)e \quad (\text{A.6})$$

The influence of the constants B_0 and B_1 on the pressure is schematically shown in Figure A.2. However, in this figure the density is used as the volumetric measure instead of the compaction used in equation (A.2). These are related according to:

$$\mu = \frac{\rho}{\rho_0} - 1 \quad (\text{A.7})$$

Often the Polynomial Equation of State is fitted to an experimentally determined Hugoniot curve. Since $e = 0$ is assumed when defining the material constants K_1 , K_2 , and K_3 in equation (A.2), the equation has to be adapted if the Hugoniot curve is to be used as reference curve. The polynomial formulation is then changed to:

$$p = K_1\mu + K_2\mu^2 + K_3\mu^3 + (B_0 + B_1\mu)\rho_0(e - e_H) \quad (\text{A.8})$$

where e_H is the specific internal energy for the Hugoniot curve.

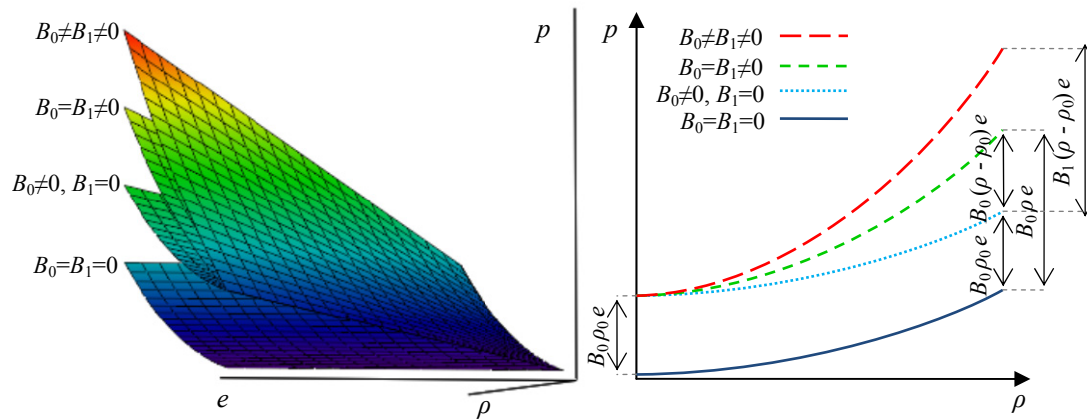


Figure A.2 Influences of parameters B_0 and B_1 in Polynomial Equation of State.

A.3 Mie-Grüneisen

In the same way as in the Polynomial Equation of State, described in the previous section, a reference curve p_{ref} (e.g. the “cold curve”, p_{cold} , with $e_{\text{ref}} = 0$ or the Hugoniot curve, p_{H} , with $e_{\text{ref}} = e_{\text{H}}$) is used together with an assumption of the equilibrium states in the surrounding of this curve; see equation (A.9). The variation of the pressure with respect to the specific internal energy is in the Mie-Grüneisen Equation of State described by the so-called Grüneisen parameter, Γ . This parameter was derived after theoretical studies of the macroscopic material behaviour as a function of distance-dependent inter-atomic forces. In a macroscopic approach the Grüneisen parameter can be defined as a measure of the change in pressure produced by a change in system total internal energy under condition of constant volume; see equation (A.10).

$$p = p_{\text{ref}} + \frac{\Gamma(v)}{v}(e - e_{\text{ref}}) = p_{\text{ref}} + \Gamma(v)\rho(e - e_{\text{ref}}) \quad (\text{A.9})$$

$$\Gamma(v) \equiv v \left(\frac{\partial p}{\partial e} \right)_v \quad (\text{A.10})$$

The second term in equation (A.9) is related to the thermal energy, and the Grüneisen parameter may be related to the physical material parameters:

- adiabatic bulk modulus, K
- thermal volume expansion coefficient, α_{therm}
- specific heat capacity at constant pressure, c_p

as:

$$\Gamma(v) = v \frac{K \alpha}{c_p} \quad (\text{A.11})$$

The dynamic value of the Grüneisen is often assumed to be:

$$\Gamma\rho = \Gamma_0\rho_0 \quad (\text{A.12})$$

where index 0 refer to ambient condition (at room temperature). Under this assumption, equation (A.9) can be rewritten as:

$$p = p_{\text{ref}} + \Gamma_0\rho_0(e - e_{\text{ref}}) \quad (\text{A.13})$$

If a polynomial (cubic) fit to a reference pressure curve is assumed equation (A.13) equals equation (A.5) if:

$$\Gamma_0 = (B_0 - B_1\mu) \quad (\text{A.14})$$

A.4 Herrmann's $P-\alpha$

Herrmann (1969) formulated an Equation of State for compressed porous materials by relating its response to the response of the non-porous states of the same material. This is done by introducing a factor α_{por} in the Equation of State. This factor is representing the porosity of the material as:

$$\alpha_{\text{por}} = \frac{v}{v_s} = \frac{\rho_s}{\rho} \quad (\text{A.15})$$

where v is the specific volume of the material and v_s is the specific volume of the solid (none porous) material and ρ and ρ_s are the related densities. The Equation of State for the porous material is then:

$$p = f\left(\frac{v}{\alpha_{\text{por}}}, e\right) \quad (\text{A.16})$$

where the function f is the same as in the Equation of State for the fully compacted material, $p=f(v_s, e)$. This function can be any other Equation of State, e.g. the Polynomial or Mie-Grüneisen, described in Sections A.2 and A.3, respectively.

In order to complete the $P-\alpha$ Equation of State the porosity factor has to be defined. Theoretically the porosity factor is a function of both the pressure and the specific internal energy, i.e.:

$$\alpha_{\text{por}} = g(p, e) \quad (\text{A.17})$$

However, for practical reasons (i.e. lack of data) it is often defined as a function of pressure only:

$$\alpha_{\text{por}} = g(p) \quad (\text{A.18})$$

Basically, arbitrary functions $g(p)$ may be chosen, but these must fulfil some mathematical requirements, i.e.:

$$\begin{aligned}
 p = 0 & \quad \alpha_{\text{por}} = \alpha_{\text{por,init}} & \quad \frac{d\alpha_{\text{por}}}{dp} = \alpha'_{\text{por,init}} \\
 0 < p < p_s & \quad \alpha_{\text{por,init}} > \alpha_{\text{por}} > 1 & \quad \frac{d\alpha_{\text{por}}}{dp} < 0 \\
 p = p_s & \quad \alpha_{\text{por}} = 1 & \quad \frac{d\alpha_{\text{por}}}{dp} = 0
 \end{aligned} \tag{A.19}$$

where $\alpha_{\text{por,init}}$ is the initial value of the porosity factor and p_s is the pressure for which all pores have collapsed; see Figure A.3.

Since the behaviour of ductile porous materials often is close to linear elastic for low hydrostatic pressures, but highly nonlinear for pressures exceeding a plastic threshold p_{el} , α_{por} is often divided into two different regimes; elastic $\alpha_{\text{por,e}}$, and plastic $\alpha_{\text{por,p}}$.

$$\alpha_{\text{por}}(p) = \begin{cases} \alpha_{\text{por,e}}(p) & \text{for } \alpha_{\text{por,init}} \geq \alpha_{\text{por}} \geq \alpha_{\text{por,el}} \\ \alpha_{\text{por,p}}(p) & \text{for } \alpha_{\text{por,el}} \geq \alpha_{\text{por}} \geq 1 \\ 1 & \text{for } \alpha_{\text{por}} \leq 1 \end{cases} \tag{A.20}$$

In the initial elastic region the porosity parameter is:

$$\alpha_{\text{por,e}}(p) = \alpha_{\text{por,el}} + (\alpha_{\text{por,init}} - \alpha_{\text{por,el}}) \left(\frac{p_{\text{el}} - p}{p_{\text{el}}} \right) \tag{A.21}$$

where $\alpha_{\text{por,init}}$, $\alpha_{\text{por,el}}$ and p_{el} are defined in Figure A.3. The porosity factor $\alpha_{\text{por,el}}$, representing the plastic threshold, is:

$$\alpha_{\text{por,el}} = \alpha_{\text{por,init}} + p_{\text{el}} \frac{d\alpha_{\text{por,e}}(p)}{dp} \tag{A.22}$$

and $d\alpha_{\text{por,e}}(p)/dp$ can be expressed by means of the bulk sound speed in the virgin porous material (c_e) and the solid material (c_0), respectively, and the bulk modulus of the pore free solid material (K_0):

$$\frac{d\alpha_{\text{por,e}}(p)}{dp} = \frac{c_e K_0}{\alpha_{\text{por,el}} (c_e^2 - \alpha_{\text{por,el}} c_0^2)} \tag{A.23}$$

Often a polynomial expression is used to define the porosity parameter in the plastic region, i.e:

$$\alpha_{\text{por,p}}(p) = \alpha_0 + \alpha_1 p + \alpha_2 p^2 + \alpha_3 p^3 + \dots + \alpha_n p^n \tag{A.24}$$

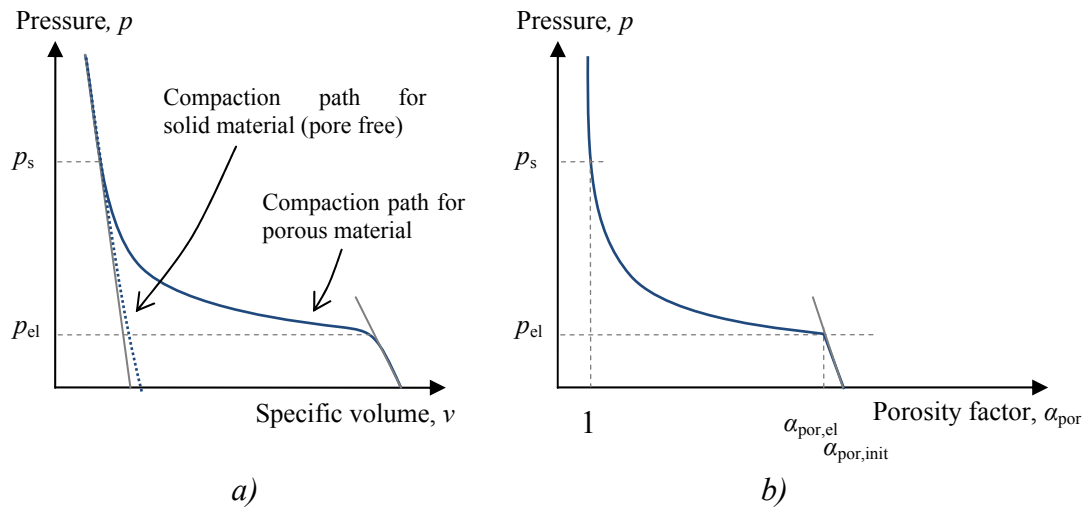


Figure A.3 Schematic illustrations of a) compaction behaviour of solid and porous material, respectively, and b) the $P-\alpha$ model.

Appendix B Conversion to true strains and stresses

A strain increment for a one-dimensional case may be expressed as:

$$d\varepsilon = \frac{dL}{L} \quad (\text{B.1})$$

where $d\varepsilon$ and dL are infinitesimal changes of strain ε and specimen length L , respectively. By integrating this expression from the initial length L_0 to the final length L_{final} the true strain, $\varepsilon_{\text{true}}$, achieved during the deformation dL is expressed:

$$\varepsilon_{\text{true}} = \int_{L_0}^{L_{\text{final}}} \frac{dL}{L} = \ln(L) \Big|_{L_0}^{L_{\text{final}}} = \ln\left(\frac{L_{\text{final}}}{L_0}\right) \quad (\text{B.2})$$

In small strain theory it is assumed that the final length is approximately equal to the initial length and the (engineering) strain, $\varepsilon_{\text{engineering}}$ is calculated as:

$$\varepsilon_{\text{engineering}} = \frac{1}{L_0} \int_{L_0}^{L_{\text{final}}} dL = \frac{1}{L_0} L \Big|_{L_0}^{L_{\text{final}}} = \frac{L_{\text{final}} - L_0}{L_0} \quad (\text{B.3})$$

Thus, the conversion from engineering strain to true strain is:

$$\varepsilon_{\text{true}} = \ln(\varepsilon_{\text{engineering}} + 1) \quad (\text{B.4})$$

Stress is defined as force F divided by the actual area A on which it acts; the true stress (or Cauchy stress), σ_{true} can thus in a one-dimensional case be expressed as:

$$\sigma_{\text{true}} = \frac{F}{A} \quad (\text{B.5})$$

In the theory of infinitesimal strains the actual area A is assumed to be approximately equal to the initial area A_0 and the engineering stress, $\sigma_{\text{engineering}}$ is thus:

$$\sigma_{\text{engineering}} = \frac{F}{A_0} \quad (\text{B.6})$$

However, contradictory to strain, the conversion from engineering to true values of stress cannot be made without assumptions (or knowledge) about the transverse response during deformation. If it is assumed that volume is preserved, i.e. that $LA = L_0A_0$, the conversion from engineering stress to true stress is described as:

$$\sigma_{\text{true}} = \frac{F}{A_0} \frac{L}{L_0} = \sigma_{\text{engineering}} (1 + \varepsilon_{\text{engineering}}) \quad (\text{B.7})$$